DISS ETH 20838

Structural and Functional Characterisation of the Cobalamin Transport Protein Haptocorrin

A dissertation submitted to

ETH ZURICH

for the degree of

DOCTOR OF SCIENCES

Presented by

EVELYNE FURGER

MSc ETH Pharm. Sci.

Born 25.04.1981

Citizen of Silenen UR

Accepted on the recommendation of

Prof. Dr. Roger Schibli, examiner

Prof. Dr. Ebba Nexø, co-examiner

Prof. Dr. Simon M. Ametamey, co-examiner

2012

To my parents

Acknowledgements

I would like to express my gratitude to all those who supported me to complete this thesis.

First and foremost, I owe my deepest gratitude to my supervisor Dr. Eliane Fischer whose help, encouragement and stimulating enthusiasm helped me through all the times of the dissertation. Furthermore, I want to thank all my colleagues from the Center of Radiopharmaceutical Sciences at the ETH Zurich and the Paul Scherrer Institute in Villigen for all their help, support and the nice time we spent together inside and outside the lab.

I would like to thank Prof. Roger Schibli for giving me the opportunity to perform my doctorate in his group and Prof. Ebba Nexø and Prof. Simon M. Ametamey for being in the committee as co-referees.

Finally, I want to express my heartfelt gratitude to my parents Eduard and Marianna, Carmen, Patricia, Thomas, Nicole and all my friends for their never-ending support and care.

Contents

Summary

Vitamin B12 (Cobalamin, Cbl) is a vital cofactor in many metabolic processes. For Cbl assimilation and maintenance of Cbl homeostasis, humans have evolved a sophisticated pathway consisting of a series of transport proteins and receptors.

Three homologous proteins are responsible for transport in the extracellular fluid: Intrinsic factor (IF), transcobalamin (TC) and haptocorrin (HC). IF is the transport protein that regulates the absorption of Cbl in the gastrointestinal part via the receptor complex cubam. TC is responsible for the cellular uptake of Cbl, facilitated by the TC-receptors: CD320 and megalin. Besides HC's role of transporting Cbl down the upper gastrointestinal tract, its role in blood circulation is still unclear. Interestingly, in contrast to the other transport proteins, HC binds to a variety of Cbl analogues.

With the publication of the crystal structures of TC and IF, structural aspects of Cbl binding to its transport proteins could be elucidated. However, structural information of HC, the least specific of the transport proteins, is still missing.

To address the role of HC in Cbl transport, especially with regard to structural aspects of Cbl analogue binding, we expressed recombinant HC (rhHC) in human embryonic kidney cells with a final yield of 6 mg (90 nmol) per litre cell supernatant. rhHC behaved similarly to native HC with respect to its spectral properties and ability to recognise Cbl and its baseless analogue cobinamide (Cbi).

Next, we established recombinant expression of three other Cbl transport protein variants, namely recombinant TC (rhTC), recombinant mouse TC (rmTC) and a glyco-variant of rhHC (rhHC*) suitable for crystallisation studies. All three proteins were obtained at 2-10 mg/L culture supernatant and based on glycosylation studies and UV-absorbance spectroscopy they compare well to the native proteins and could therefore be used for future studies.

The expression of a rhHC* that could easily been deglycosylated, allowed us to crystallise HC in complex with cyano-Cbl (CNCbl) and Cbi. Crystals were obtained and the structures were solved to 2.35 and 3.0 Å resolution respectively. We could identify the three unique residues Asn120, Asn373 and Arg357 as key players for stabilising Cbl analogues, including Cbi. Due to the lack of the nucleotide moiety at the lower axial side of Cbi, the *e*-propionamide side chain shows two different conformations: the "normal" and the "flip-in" conformation.

While Asn120 and Asn373 form hydrogen bonds to the *e*- and the *f*-propionamide side chains, Arg357 provides a hydrogen bond to either the oxygen of the ribose when a "normal" Cbl is binding and moreover it can stabilise the "flip-in" conformation of Cbi. These findings extend the insight into the complexity of Cbl binding to the transport proteins and are therefore valuable for an optimised and rational design of new Cbl derivatives.

Cbl derivatives need at least to bind to one transport protein to be retained in the body. Therefore sufficient knowledge about the interactions with the specific protein carriers is of major importance. Cbl binds to all three transport proteins with a K_d of approximately 10^{-15} M, whereas accurate determination of such high affinity constants is difficult.

We therefore introduce differential scanning fluorimetry (DSF) for the determination of Cbl derivatives ability to bind to the Cbl transport proteins. DSF offers a fast and easy way to measure ligand-induced protein stability, because the melting temperature T_m of the protein increases upon ligand binding. We screened a series of novel Cbl derivatives and ranked their binding potential to Cbl transport proteins according to their ability to increase T_m.

Tumour cells over-express receptors for Cbl uptake. Several strategies to use Cbl as a vehicle for targeted delivery of imaging or cytotoxic agents have been proven successful *in vitro*. But studies with radiolabelled Cbl derivatives in mice and in humans struggled with high delivery to vital organs such as the liver or the kidneys.

Recently, a promising *in vivo* study with a Cbl derivative, ^{99m}Tc-PAMA(4)-Cbl, that would not bind to TC showed high tumour uptake together with decreased uptake in liver and kidneys in mice. It was speculated that HC mediates the observed tumour uptake.

Based on these promising results, we investigated the uptake mechanism in tumour cells *in vivo* and *in vitro*. Biodistribution studies in tumour bearing mice with the murine cell line B16F1 and the human cell lines CLS-1 and HCC827 confirmed the observed tumour uptake. However, it was shown to be HC-independent, because no evident difference between HC-producing and non-producing tumour cell lines was recognised *in vivo*. In fact, the presence of HC blocked uptake of Cbl derivatives. Furthermore, *in vitro* cell uptake of ^{99m}Tc-PAMA(4)-Cbl was low (around 2% internalised cpm/0.3 mg protein) and seemed to be transport protein independent in the case of B16F1. Interestingly uptake of ^{99m}Tc-R-PAMA(4)-Cbl, a Cbl derivative that binds to TC, was achieved in the absence of transport proteins in both cell lines and uptake was decreased by addition of Cbi. While uptake in B16F1 seemed again

transport protein independent, uptake of this radiotracer into HCC827 was further increased in the presence of TC and mTC, and could not be blocked with Cbi. Altogether these findings point to an alternative uptake mechanism for Cbl derivatives into tumour cells and should be investigated further for a conclusive answer to the elusive uptake of Cbl derivatives in tumour cells.

Zusammenfassung

Vitamin B12 (Cobalamin, Cbl) ist ein wichtiger Cofaktor in vielen metabolischen Prozessen. Um die Assimilation und die Aufrechterhaltung der Cbl Homöostase zu gewährleisten, existiert im Menschen ein hoch komplexes System, basierend auf dem Zusammenspiel verschiedener Transportproteine und Rezeptoren.

Drei homologe Proteine sind für den Transport von Cbl in der extrazellulären Flüssigkeit verantwortlich: Der intrinsische Faktor (IF), Transcobalamin (TC) und Haptocorrin (HC). IF reguliert die Absorption von Cbl im gastrointestinalen Trakt. TC ist für die zelluläre Aufnahme von Cbl verantwortlich, die durch die TC-Rezeptoren: CD320 und Megalin zustande kommt. HC transportiert Cbl in den gastrointestinalen Trakt, jedoch ist seine Aufgabe in der Blutzirkulation immer noch ungeklärt. Interessanterweise bindet HC, im Gegensatz zu den anderen Transportproteinen, an eine Vielzahl von Cbl-Analogen.

Durch die Veröffentlichung der Kristallstrukturen von TC und IF konnten strukturelle Aspekte der Bindung zwischen Cbl und den Transportproteinen aufgeklärt werden. Strukturelle Informationen zu HC, dem am wenigsten spezifischen Transportprotein, sind bisher keine vorhanden.

Um die Rolle von HC im Cbl Transport zu studieren, vor allem auch im Hinblick auf strukturelle Aspekte der Bindung zu Cbl-Analogen, wurde rekombinantes HC (rhHC) mit einer Ausbeute von 6 mg (90 nmol) pro Liter Zellüberstand, in humanen embryonalen Nierenzellen exprimiert. Aufgrund seiner spektralen Eigenschaften und seiner Fähigkeit Cbl und das basenlose Cbl-Analog Cobinamid (Cbi) zu binden, entsprach rhHC dem nativen HC grösstenteils.

In einem nächsten Schritt etablierten wir die rekombinante Expression von drei anderen Cbl Transportproteinen: rekombinantes TC (rhTC), rekombinantes Maus-TC (rmTC) und eine Glycovariante von rhHC (rhHC*), die vorteilhaft für Kristallisationsstudien ist. Alle drei Proteine wurden mit einer Ausbeute zwischen 2-10 mg/L Zellüberstand erhalten. Glykosylierungsanalysen und UV-Absorptionsspektren stimmten mit denen der nativen Proteine überein.

Die Expression von rhHC*, das einfach zu deglykosylieren ist, ermöglichte es uns HC zusammen mit Cyano-Cbl (CNCbl) und Cbi zu kristallisieren. Mit den erhaltenen Kristallen

konnte die Struktur mit einer Auflösung von 2.35 respektive 3.0 Å gelöst werden. Die drei für HC unikalen Seitenketten Asn120, Asn373 und Arg357 wurden dabei als Hauptfaktoren der Cbl-Analog Stabilisierung, inklusive Cbi, identifiziert. Aufgrund der fehlenden Nukleotideinheit auf der Unterseite von Cbi, kann die *e*-Propionamid-Seitenkette zwei verschiedene Konformationen eingehen: die „normale“ und die „flip-in“ Konformation. Während Asn120 und Asn373 Wasserstoffbrücken zu den *e*- und *f*-Propionamid-Seitenketten ausbilden, ist es für Arg357 möglich durch eine Wasserstoffbrücke zum Sauerstoff der Ribose ein „normales“ Cbl, doch darüber hinaus auch die „flip-in“ Konformation von Cbi zu stabilisieren. Diese Forschungsergebnisse erweitern den Blick auf die Komplexität der Cbl Bindung zu den Transportproteinen und ermöglichen dadurch eine optimierte und rationale Entwicklung neuer Cbl Derivate.

Cbl Derivate müssen an mindestens ein Transportprotein im menschlichen Körper binden, sonst werden sie sofort wieder ausgeschieden. Darum ist es äusserst wichtig, Kenntnisse über die Interaktionen mit den spezifischen Proteintransportern zu haben. Cbl bindet an alle drei Transportproteine mit einer K_d von etwa 10^{-15} M, wobei die akkurate Bestimmung einer so hohen Affinitätskonstante sehr schwierig ist.

Aus diesem Grund stellen wir die dynamische Differenzfluorometrie (DSF) vor, als eine Methode zur Bestimmung der Fähigkeit der Cbl Derivate an die verschiedenen Transportproteine zu binden. Mit DSF kann, aufgrund der Erhöhung der Schmelztemperatur T_m eines Proteins durch die Bindung eines Liganden, schnell und einfach die ligand-induzierte Proteinstabilität bestimmt werden. Eine Reihe von neuen Cbl Derivaten wurde mithilfe dieser Methode gemessen und konnte anschliessend entsprechend ihrer Bindungspotentiale zu den Transportproteinen, basierend auf der Fähigkeit T_m zu erhöhen, beurteilt werden.

Auf Tumorzellen sind die Rezeptoren für die Cbl Aufnahme überexprimiert. In verschiedenen *in vitro* Versuchen konnte die Strategie Cbl als Vehikel für die zielgerichtete Aufnahme von bildgebenden oder zytotoxischen Agenzien erfolgreich umgesetzt werden. Studien mit radiomarkierten Cbl-Derivaten in Mäusen und Menschen zeigten jedoch immer auch eine hohe Aufnahme in lebenswichtigen Organen wie der Leber oder den Nieren.

Eine kürzlich veröffentlichte *in vivo* Studie mit dem Cbl Derivat ^{99m}Tc-PAMA(4)-Cbl, das nicht mehr an TC bindet, zeigte Akkumulation im Tumorgewebe zusammen mit einer

verminderten Aufnahme in der Leber und den Nieren der Mäuse. Aufgrund dessen wurde über eine mögliche Rolle von HC als Mediator der Tumoraufnahme spekuliert.

Basierend auf diesen vielversprechenden Resultaten, untersuchten wir den Aufnahmemechanismus von Tumorzellen *in vivo* und *in vitro*. Mit Biodistributionsstudien in Tumormäusen mit der murinen Zelllinie B16F1 und der humanen Zelllinie HCC827 konnte die beschriebene Tumoraufnahme bestätigt werden. Jedoch wurde widerlegt, dass HC als Mediator der Tumoraufnahme fungiert, da *in vivo* kein ersichtlicher Unterschied zwischen der HC-produzierenden und der nicht-produzierenden Tumorzelllinie erkannt werden konnte. Tatsächlich blockierte die Anwesenheit von HC die Aufnahme von Cbl Derivaten in Tumorzellen. Darüber hinaus war die *in vitro* Aufnahme von ^{99m}Tc-PAMA(4)-Cbl eher gering (ca. 2% internalisierte cpm/0.3mg Protein) und im Falle von B16F1 mutmasslich Transportprotein unabhängig. Interessanterweise zeigte ^{99m}Tc-R-PAMA(4)-Cbl, ein Cbl Derivat, das auch an TC bindet, in beiden Zellinien in Abwesenheit der Transportproteine eine Aufnahme, die durch Zugabe von Cbi geblockt werden konnte. Während die Aufnahme von B16F1 wiederum als Transportprotein unabhängig erschien, wurde die Aufnahme dieses Radiotracers in HCC827 Zellen durch TC und mTC erhöht und konnte nicht durch Cbi geblockt werden. Zusammengefasst lassen diese Resultate auf einen möglichen alternativen Aufnahmemechanismus von Cbl Derivaten in Tumorzellen schliessen, der durch weitere Untersuchungen eine schlüssige Antwort für die Aufnahme von Cbl Derivaten in Tumorzellen ermöglichen könnte.

Abbreviations

% ID/g	percentage of injected dose per gram of organ
AC_{50}	concentration of ligands to achieve half-maximal protein stabilisation
AdoCbl	5'-deoxy-5'-adenosyl-Cbl
ASGP-R	asialoglycoprotein receptor
BSA	bovine serum albumin
bTC	bovine transcobalamin
Cbi	cobinamide
Cbl	cobalamin, vitamin B12
cDNA	complementary DNA
CHCA	saturated sinapinic acid
CNCbl	cyano-cobalamin
cubam	cubilin and amnionless
DMB	5,6-dimethylbenzimidazole
DNA	deoxyribonucleic acid
DSF	differential scanning fluorimetry
DTPA	diethylenetriaminepentaacetate
Endo F1/H	endoglycosidase F1/H
ESI	electrospray ionisation
FA	formic acid
FCS	fetal calf serum
GdnHCl	guanidine hydrochloride
GlcNAc	N-acetyl glucosamine
GnTI	N-acetylglucsoaminyltransferase I
H_2OCbl	aquo-cobalamin
HC	haptocorrin
HEK293	human embryonic kidney cells
HEPES	4-(2-hydroxyethyl)-1-piperazineethanesulfonic acid

HFIP	hexafluoro-2-propanol
HRP	horseradish peroxidase
IAM	iodoacetamide
IF	intrinsic factor
IFN-β	interferon β
i.v.	intravenous
Man	mannose
MeCbl	methylcobalamin
MRP1	multidrug resistance protein 1
mTC	mouse transcobalamin
NO	nitric oxide
p.i.	post injection
PAMA	(pyridine-2-yl-methyl-amino)-acetic acid
PAS	periodic acid-Schiff
PBS	phosphate buffered saline
PNGase F	N-glycosidase F
Pt	cisplatine
PVDF	polyvinylidene difluoride
rhHC	recombinant human haptocorrin
rhHC*	recombinant human haptocorrin expressed in GnTI- cells
rhTC	recombinant human transcobalamin
rmTC	recombinant mouse transcobalamin
RT	room temperature
s.c.	subcutaneous
SD	standard deviation
SDS/PAGE	sodium dodecyl sulphate polyacrylamide gel electrophoresis
TC	transcobalamin
TCA	trichloroethane
TCbl-R	transcobalamin receptor, CD320

TFA	trifluoroacetic acid
TH	tetrahydro-
T_m	melting temperature
TOF	time-of-flight
UV	ultraviolet
w/o	without

1 Introduction

1.1 Historical outline

Vitamin B12 (cobalamin, Cbl) – nature's most beautiful but also most complex cofactor [1,2] has a rich history in which many of its landmarks were also milestones in the history of biochemistry [3].

The discovery of Cbl and the elucidation of its biological function goes back to the early 1920s when G.R. Minot and W.P. Murphy, two American physicians, successfully treated patients suffering from pernicious anaemia with a liver diet [4]. For the next 20 years liver was the main source of this unknown curing factor, until the isolation of pure crystalline Cbl was achieved [5].

For the elucidation of the X-ray structure of Cbl in 1956 [6], Dorothy Hodgkin was awarded with the Nobel Prize for Chemistry in 1964. Soon after this landmark discovery, total synthesis of Cbl was achieved by R.B. Woodward and A. Eschenmoser in a joint effort of more than 100 co-workers over 25 years after the first isolation of Cbl [7].

Since these early milestones, thousands of articles about the chemistry, biochemistry and enzymology of Cbl have been published [2]. Besides the complete elucidation of the biosynthetic pathway to Cbl in aerobic and anaerobic microorganisms, the crystal structures of several Cbl-dependent enzymes and two of the three Cbl transport proteins in mammals have been solved [8-12].

These recent studies gave rise to the rational design of Cbl-based bioconjugates for tumour imaging; as well as for targeted delivery of anti-tumour agents to malignant cells starting possibly a new era of Cbl research [2].

1.2 Cobalamin structure and function

1.2.1 General structure of cobalamins

Cobalamins are organometallic compounds with a central positively charged cobalt-ion. All Cbls show the same core structure consisting of a chiral corrin, containing four reduced pyrrole rings (A, B, C, D), linked through four nitrogen atoms to a cobalt ion and possessing seven amide side chains (*a*-*g*) three acetamides (*a, c, g*) and four propionamides (*b, d, e, f*)

(Figure 1.1A). The fifth nitrogen atom links the cobalt's lower axial (α-side) ligand, a 5,6-dimethylbenzimidazole (DMB) ribonucleotide moiety. The sixth or upper axial (β-side) ligand is exchangeable. The three major occurring Cbls in living organisms are 5'-deoxy-5'-adenosyl-Cbl (AdoCbl) (≈ 60%), methyl-Cbl (MeCbl) (≈ 20%) and H_2OCbl (≈ 20%) [13].

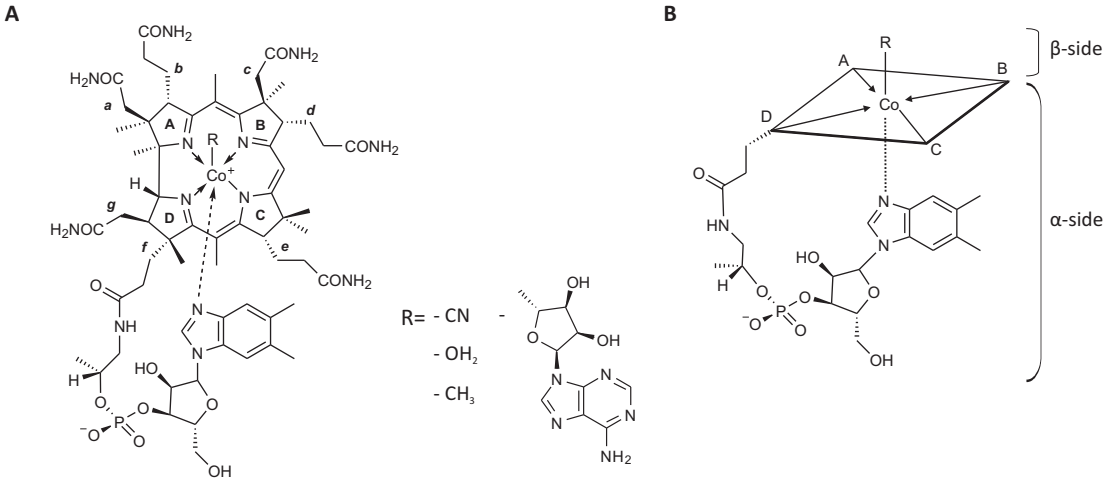

Figure 1.1 Structural formulae of Cbl. **A**. The core or Cbl consists of a central corrin ring that coordinates a central cobalt ion and possesses seven amide side chains (*a-g*) **B**. Perspective view of Cbl indicating the lower α-side and the upper β-side in a base-on coordination with the 5,6-dimethylbenzimidazole ribonucleotide moiety. The corrin ring is indicated as square. A number of different entities may be present in the upper axial position (designated ''R''), including -CN (cyanocobalamin, CNCbl), -H_2O (aquocobalamin, H_2OCbl), -CH_3 (methylcobalamin, MeCbl) and 5'-deoxy-5'-adenosyl (adenosylcobalamin, AdoCbl).

Cyanocobalamin (CNCbl) possesses a cyano group as upper axial ligand and is the most important synthetic form of the cobalamins. Despite its lack of direct physiological function it is used in many pharmaceuticals and food additives due to its stability and lower cost [14-16]. Because only AdoCbl and MeCbl are used as active cofactors, Cbls with different upper axial ligands are readily converted by the trafficking chaperone MMACHC inside the cells [17-19]. Structural differences other than the upper axial ligand are a feature of the so-called Cbl analogues, most typically having either a substituted or an absent nucleotide moiety. In humans these analogues are inactive, in contrast to bacteria where many of them are catalysing Cbl dependent reactions [13,20]. The term corrinoids refers to Cbls as well as Cbl analogues.

1.2.2 Cobalamin cofactors

AdoCbl is not only the most abundant natural Cbl, it is also used as a cofactor for the mitochondrial L-methylmalonyl-CoA mutase, one of the two human enzymes that require Cbl. AdoCbl is involved in catabolism of different organic compounds such as branched amino acids and odd-chain fatty acids, whereby it acts as a cofactor in the conversion of methylmalonyl-CoA to succinyl-CoA [21] (Figure 1.2). Deficiency of AdoCbl leads to high level of methylmalonic acid (MMA) and is a possible indicator of Cbl-deficiency [22].

Methylcobalamin is the cofactor for methionine synthase. It mediates the transfer of the methyl group from the inactive form of folate (methyl tetrahydrofolate, 5-methyl TH) to homocysteine and thereby catalyses the methylation of homocysteine and its conversion to methionine [21]. Cbl deficiency results in high levels of homocysteine, but it accounts for only a minority of all cases of high homocysteine levels [22].

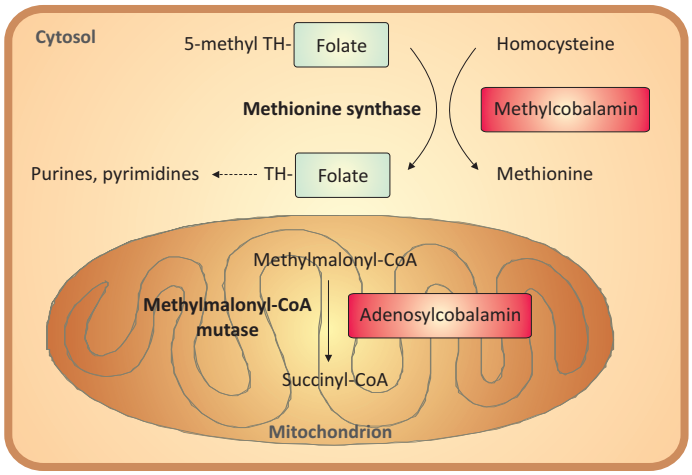

Figure 1.2 Coenzyme function of Cbl. Cbl is involved in two distinct enzymatic processes involving the methionine synthase and the methylmalonyl-CoA mutase. The former converts homocysteine to methionine by linkage to the folate metabolism whereas the methyl group transferred to homocysteine is provided by the conversion of 5-methyl tetrahydrofolate to tetrahydrofolate. Methylmalonyl-CoA mutase converts methylmalonyl-CoA to succinyl-CoA. TH: tetrahydro- (Figure modified from [14]).

1.3 Cobalamin transport and uptake in humans

1.3.1 Transport proteins and their receptors

As Cbl is exclusively produced by bacteria, humans are dependent on the nutritional intake of Cbl from dietary sources such as meat, milk, eggs and fish [13,23,24]. The limited amount of Cbl available from food is compensated by a complex and efficient transport and cellular uptake system involving three transport proteins as well as a number of receptors [14,25-27]. These three proteins are intrinsic factor (IF), transcobalamin (also known as transcobalamin II, TC) and haptocorrin (previously referred to as transcobalamin I or R-binder, HC). Based on the amino acid sequence, the molecular weights of the three proteins are very similar (approximately 45 kDa), however, IF and HC are glycosylated and therefore show apparent molecular weights of approximately 55 kDa (IF) and 65 kDa (HC) [13,28]. The glycosylation of these two proteins hinders partial proteolysis in the intestine and prevents HC from glomerular filtration [13]. However, these oligosaccharides are not involved in protein or receptor binding in the case of IF [13,29,30]. Each protein carries a single Cbl molecule which is tightly bound and only released after degradation of the transport protein (Figure 1.3).

Although IF is synthesised and secreted primarily from the gastric mucosa [31] , binding to Cbl is only possible in the neutralised environment of the intestine and only after enzymatic cleavage of the HC-Cbl complex in the duodenum [32,33]. IF plays a crucial role in Cbl absorption by the intestinal enterocytes via the specific receptor cubilin [34], a process that is facilitated by the transmembrane protein amnionless. The receptor complex of cubilin and amnionless is known as cubam (**cub**ilin and **am**nionless) [35,36] and is specific for the IF-Cbl complex as it binds to neither IF nor free Cbl alone [37,38].

TC is produced by all tissues of the body with the highest expression found in kidneys, lymphatic nodes and liver [39]. The essential role of TC is to transport absorbed Cbl in the blood to all cells of the body. Cellular uptake of Cbl bound to TC is achieved via the transmembrane protein CD320 (TC-receptor; TCbl-R), a 60 kDa heavily glycosylated protein [40]. This protein is present on the cell surface of virtually all tissues [41,42] and is regulated according to the proliferative and differentiation status of the cell [41,43]. Recently, a soluble form of this receptor has been identified [44]. CD320 binds preferentially to the TC-

Cbl complex (with a 30-fold lower affinity for TC alone) and neither IF nor HC bind to CD320 [45]. Upon binding to CD320, TC-Cbl is internalised and Cbl is released from TC within the lysosomes [14].

Another uptake mechanism of the TC-Cbl complex is mediated via megalin, a 600 kDa multi-ligand receptor [46]. Megalin is located mainly on the apical membrane of proximal tubule cells but is also found on other absorptive epithelia such as the visceral yolk sac, lungs and intestine [47,48]. In the kidneys this receptor is responsible for the prevention of urinary loss of Cbl [46,49], consequentially minimising the daily dietary requirement of Cbl.

HC is the third Cbl transport protein and is secreted into many body fluids including saliva, breast milk and plasma from many types of cells (i.e. granulocytes, mammary glands, salivary duct and gastric mucosa) [50-52] including some tumour cells [53,54]. It is responsible for escorting Cbl down the upper part of the gastrointestinal tract, but it also binds to a considerable amount (up to 75%) of Cbl in the plasma. Depending on the source of synthesis, different glycoforms of HC have been described [55]. HC originating from granulocytes lacks terminal sialic acid and is known to be rapidly cleared by the asialoglycoprotein receptor (ASGP-R) found mainly in the liver [56]. This receptor consists of two homologous subunits, H1 and H2 that form a noncovalent hetero-oligomeric complex [57]. However, the physiological relevance of this interaction still remains unclear. No receptor has yet been identified for HC containing high amounts of sialic acids and, as a consequence, the half-life of HC in plasma is much longer ($t_{1/2} \approx 10$ days) than that of TC ($t_{1/2} \approx 15$ h) [58].

HC differs from the other transport proteins because it also binds to corrinoids other than Cbl, showing the lowest ligand specificity of all human Cbl transport proteins [59,60].

1.3.2 Cobalamin transport

As it enters the body, Cbl is released from food mainly in the stomach through peptidic activity combined with a low pH [61]. Free Cbl is then bound rapidly by gastric HC and is escorted through the upper part of the gastrointestinal tract by this transport protein. Although a much higher concentration of IF is available in the stomach [61], Cbl preferentially binds to HC in the low acidic gastric environment. Binding between IF and Cbl only takes place in the neutralised environment of the duodenum, where Cbl is released by the degradation of HC by pancreatic enzymes [32,33]. Cbl is then transferred to IF, a

transport protein that has a high preference for “true” Cbl and omits binding of Cbl analogues, consequently building the first step in a specific filter system to ensure that Cbl binds to transport proteins over Cbl analogues [62]. The IF-Cbl complex travels to the terminal ileum, where Cbl-IF is absorbed by endocytosis via the cubam receptor complex [27].

Inside the endosome cubam is released and recycled to the cell surface [14]. The IF-Cbl complex is transferred to lysosomes where Cbl is released by proteolytic breakdown of IF. For Cbl trafficking within the cell, several proteins involved in the intracellular processing and transport of Cbl have been identified. However, the exact details of the transport mechanism are yet to be solved (reviewed in [63,64]). Eventually, Cbl can either be used as a cofactor or it can be exported to the blood plasma or extracellular fluid [14].

For export of Cbl from the epithelial cells the multidrug resistance protein 1 (MRP1) has been identified as a possible transport candidate [65]. Upon release of Cbl into the bloodstream, Cbl is transported by TC and is readily taken up by cells of the liver and other tissues through the interaction of the transmembrane protein CD320 with the TC-Cbl complex [40]. Like IF-Cbl, TC-Cbl is degraded in the lysosomes and the free Cbl molecule is released and potentially metabolised to the two cofactors AdoCbl and MeCbl [64]. The role of the other Cbl transporting protein in blood, HC, is still obscure.

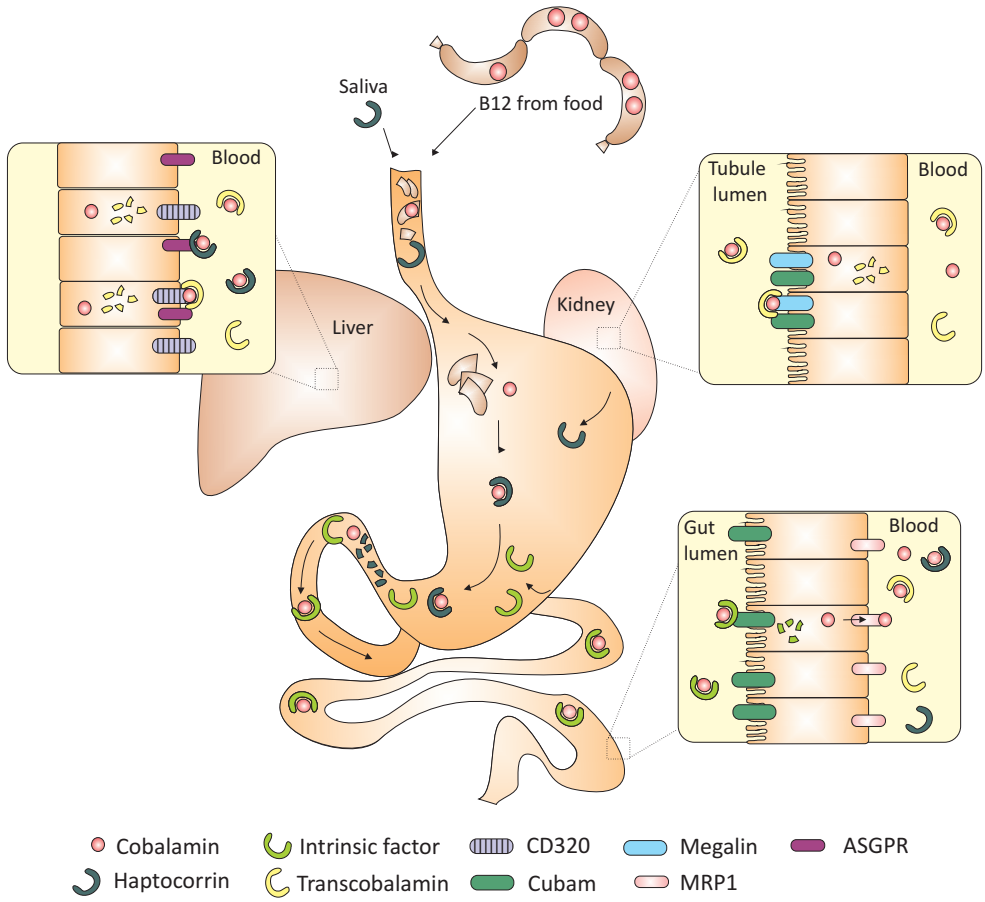

Figure 1.3 Overview of Cbl transport in humans. Cbl released from food is first bound to HC present in the saliva and gastric fluids. In the duodenum HC is degraded by pancreatic enzymes and Cbl is transferred to IF. The Cbl-IF complex is then endocytosed by the receptor complex cubam. In the intestinal cells IF is degraded and Cbl is released into blood plasma from the basolateral side of the cell by MRP1, a multidrug resistance protein. In the blood plasma Cbl is bound either to HC or TC, where only TC is responsible for the Cbl uptake into cells. This uptake is mediated by the TC receptor CD320. In the kidney, megalin instead of CD320 is the receptor responsible for uptake of Cbl. (Figure modified from [14]).

1.4 Modifications of Cobalamins

Despite its structural complexity, it is possible to selectively modify Cbl at various sites, for example alkylation of the cobalt ion; modifications of the lower 5,6-dimethylbenzimidazole nucleotide; modified side chains or replacement of the central cobalt ion [66,67].

Given the complexity of Cbl transport and cellular uptake, a suitable Cbl derivative needs to bind at least to one transport protein in order to be preserved in the human body. Therefore, structural aspects of Cbl binding to the transport proteins become important for the design of new Cbl derivatives.

1.4.1 Protein structures

The first crystal structure of a mammalian Cbl transport protein was solved in 2006 with the structure of human and bovine TC in complex with H_2OCbl [11]. This was followed by the crystal structure of IF in 2007 [12]. Both proteins are composed of two domains, α and β, which are connected by a flexible linker (Figure 1.4A). The N-terminal "α-domain" is composed of twelve α-helices whereas the C-terminal "β-domain" is built of a five and a three stranded β sheet and one α-helix (Figure 1.4C). Cbl is captured in the interface of these two domains via a number of hydrogen bonds in addition to some hydrophobic interactions (Figure 1.4B) [11]. In contrast to the enzymatic Cbl binding proteins methylmalonyl-CoA mutase and methionine synthase, the transport proteins bind to Cbl in its "base-on" state, where the 5,6-dimethylbenzimidazole moiety is coordinated to the cobalt ion [11].

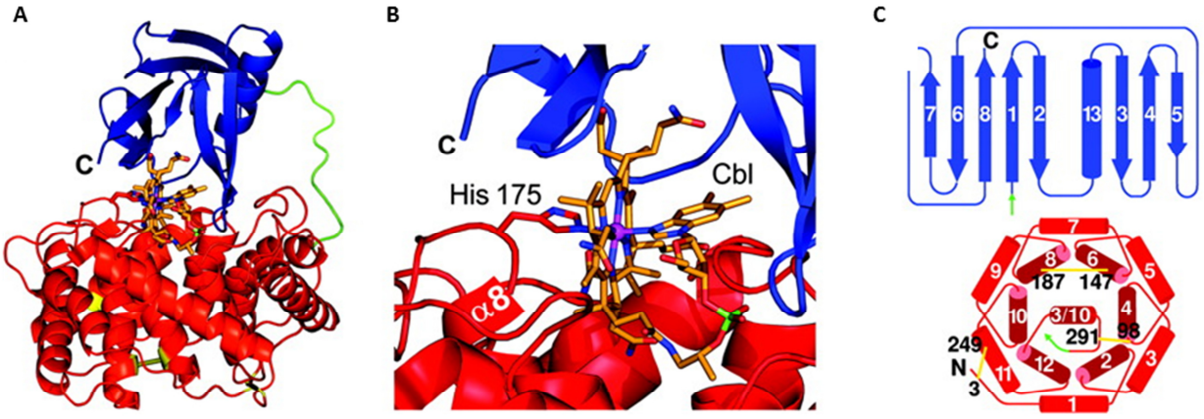

Figure 1.4 Overall structure of TC-H_2OCbl [11]. **A**. Secondary structure cartoon of bovine TC, with the N-terminal α-domain in red and the C-terminal β-domain in blue, the flexible linker in green and Cbl in orange. **B**. Enlarged view to the histidine-coordinated Cbl (in ball-and-stick representation (magenta, Co ion; lime, phosphorus; red, oxygen; blue, nitrogen; orange, carbon). **C**. Topology diagram of the two domains with a separate numbering for helices and strands and the colour scheme of A. In the α-domain's α_6-α_6 barrel, the helix orientations run clockwise in the inner α6 bundle and counterclockwise in the outer. A 3/10 helix at the bottom shields the hydrophobic core of the domain. The three disulfide bridges are shown as yellow sticks and cysteine residues are labelled according to TC numbering.

Crystallisation of TC with its ligand H_2OCbl showed a coordination bond of the cobalt ion to a histidine side chain (His172/173) at the β-side of H_2OCbl. Only the ribose group of the nucleotide moiety maintains its contact to the bulk solvent and therefore becomes a potential site for substitution and derivatisation of Cbl [11]. This His-Co^{III} interaction is

conserved among TC from other origins, but it is not conserved in the other transport proteins IF and HC, where H_2O remains coordinated and the β side of the Cbl becomes accessible for solvent or external ligands, resulting in a solvent accessibility of about 17% [2].

Although only sharing 27% sequence identity with human TC, the crystal structure of IF-CNCbl solved at a resolution of 2.6 Å revealed a similar overall structure [12]. Due to proteolysis during the process of crystallisation the proposed dimer status of IF could not be corroborated [68]. Oligomerisation was found only to happen for uncleaved full-length IF, and only if Cbl was bound [68]. Furthermore, the linker region was cleaved but previous studies in solution showed that independent α- and β-domains of IF can still form a functional IF-Cbl complex that is able to bind to cubam [12,68,69]. Only small structural differences in the N-terminal domain were seen locally for the X-ray structure compared to TC and the homology IF models [12]. Furthermore, two polar side chains (His73 and Asp204) are exclusively found in the Cbl binding site of IF and were hypothesised to affect the stability of the IF-Cbl complex at low pH [12]. Similar to the solvent accessibility of TC-CNCbl, IF-CNCbl shows a solvent accessible surface of approximately 19% with the ribose 5'-hydroxyl group and the β-side of Cbl being exposed to solvent [12].

As the crystal structure of HC was not available, multiple sequence alignments and comparative modelling of HC based on the structure of human and bovine TC are the only tools for structural predictions of the protein so far. HC and TC share approximately 25% sequence identity, and so it is assumed that the overall architecture, in particular the α-domain, of HC is very similar to that of TC. Adopting the same fold as TC permitted the mapping of potential glycosylation sites onto the surface of HC which showed that, in contrast to IF which displays these sites exclusively on its β-domain, HC possesses glycosylation sites on the α- and β-domain as well as on the N-terminal side of its linker region [70].

Nevertheless and as it was seen for IF [12], the homology model for HC derived from the experimental TC model [70] might still miss some outstanding features, therefore the crystal structure of HC is clearly of high value.

1.4.2 Protein binding

Binding of Cbl to the transport proteins in mammals occurs both very quickly and with exceptionally high affinity, whereupon all three transport proteins show a dissociation constant of about 10^{-15} M towards Cbl [69,71,72]. However, these proteins differ in the specificity for Cbl analogues, and can be ranked in the order HC << TC < IF. HC is the least specific transport protein and is able to bind not only to Cbl and slightly modified Cbl derivatives, but also to Cbl analogues that possess major structural differences such as Cbi, a Cbl analogue that lacks the nucleotide moiety [60,70].

The general model for the binding of Cbl to its transport proteins contains the following steps: (i) initial attachment of the ligand to the high-affinity C-domain, (ii) primary assembly of N- and C-domains, and (iii) slow adjustments and fixation of the ligand at the domain-domain interface [72]. While the binding of Cbl to human IF, the most specific binding protein, appears to follow a complex kinetic pattern with mutual re-arrangements of the protein domains, binding to TC occurs by almost simultaneous attachment of Cbl to the two domains with a subsequent gradual adjustment [72]. In contrast, all ligands tested attached almost instantly to HC, thereby characterising the binding kinetics of this transport protein by a minimal number of steps [72]. Therefore the number of conformational steps can be directly correlated to Cbl specificity with HC being the least and IF the most specific human transport protein.

1.4.3 Cobalamin derivatives

There are four described sites for Cbl conjugation resulting in the recognition of all three transport proteins: i) the *e*-propionamide of the peripheral corrin ring, ii/iii) the 2'- and 5'-hydoxyl group of the ribose unit at the α-side of Cbl, iv) the cobalt ion [73].

In an elaborate work of Pathare *et al.* [74] six Cbl-biotin conjugates were synthesised. Four were modified on the *b*-, *c*-, *d*- and *e*-side chain, one was conjugated to the 5'-OH group of the ribose moiety and another was attached to the cobalt ion, replacing the CN-group of CNCbl.

Based on their observations, the preferable sites of conjugation that ensure binding to TC are the ribose 5' hydroxyl group and derivatisation on the cobalt ion itself by exchanging the β-axial ligand. However, conjugation to the various propionamide side chains resulted in a

large variation in their binding ability. *e*-propionamide side chain conjugates had little effect on the binding to TC, the binding of *b*-isomer conjugates to TC was lowered, the binding of *d*-propionamide conjugates was lowered further still and *c*-acetamide conjugates exhibited poor binding. These observations are in good agreement with the conclusions from the crystal structures that demonstrated solvent accessibility of the ribose 5' hydroxyl group and β-axial ligands and also structural explanations for the different side chain modifications [11,12,70].

By introducing appropriate linkers, *b*-propionamide conjugates may regain their ability to bind to TC. This approach requires controlled hydrolysis of the propionamide chains and isolation of the *b*-monocarboxylic acid prior to conjugation. For ^{99m}Tc-PAMA derivatives (see section 6.2.5), a long spacer of >5 CH_2 ensured binding to TC, while derivatives with shorter spacers were still able to bind HC and IF, but not TC [75].

Stupperich and Nexø [60] used so-called base-off corrinoids, whose nucleotides at the lower side of Cbl is not coordinated to the cobalt ion of the corrin ring. While binding of these derivatives to IF and TC was abolished, HC bound efficiently to all of them, thereby emphasising its unique role in binding to Cbl derivatives. These findings were in full agreement with the structural features of the X-ray and homology models of HC which revealed that small modifications at the DMB moiety can be accommodated by the environment of the nucleotide base [70].

In Cbl based targeted delivery, the different binding ability of Cbl derivatives has recently been used to overcome the background uptake by healthy proliferating tissue associated with TC-bound Cbl. By modifying the *b*-propionamide side chain of the peripheral corrin ring, binding to TC was abolished, but tumour uptake was still observed [75].

1.5 Diagnostic and therapeutic uses of cobalamin derivatives

All living cells are dependent on vitamins for survival. Rapidly dividing cells, such as tumour cells, up-regulate their receptors in order to meet their increased demand for vitamins. In this context several vitamins including Cbl have been investigated as potential targeting agents. Most prominently, vitamin B9 (folic acid) derivatives have been successfully used for tumour imaging or drug delivery [76,77]. In contrast to drug delivery with folic acid, Cbl-mediated tumour targeting is much more challenging as it has a very complex transport and

uptake system consisting of three transport proteins and several receptors (see section 1.3.1).

1.5.1 Targeted drug delivery with cobalamin derivatives

Various Cbl derivatives have been developed with the aim of delivering cytotoxic moieties into tumour cells by selective uptake through the TC receptor CD320. Cbl derivatives should fulfil two prerequisites: (i) they should still bind TC with high affinity, and (ii) only become cytotoxic once they are internalised. This can be achieved by the introduction of an acid-labile linker between Cbl and the attached cytotoxic moiety, for example. Furthermore, the toxicity of the drug must be high enough to kill cells even at the low concentrations that can be reached by targeted delivery of Cbl conjugates.

Several examples of successful *in vitro* targeting with Cbl derivatives have been described in literature such as coupling colchicine, a very potent inhibitor of tubulin polymerization to the β-axial site of Cbl via an acid-labile hydrazone linkage [78]. At a neutral pH, this linkage provides a stable bond until the bioconjugate undergoes endocytosis and therefore moves into a low pH environment. There, the linker between Cbl and colchicine is cleaved, releasing the active drug [78] (Figure 1.5D). Other Cbl derived prodrugs modified at the β-axial side made use of the low dissociation energy of the carbon-cobalt bond yielding Cbl-derivatives that could be photocleaved by visible light [66] or indirectly cleaved through $H^{\cdot}$ and $OH^{\cdot}$ radicals obtained through the sonolysis of aqueous solutions [79]. Similarly, the metal Gd^{3+} is highly toxic unless it is chelated, and has been used for Cbl-mediated delivery into leukaemia cells [80] (Figure 1.5B).

Mundwiler *et al*. were the first to described cyanide-bridged-Cbl-cisplatine conjugates in which they built a binuclear complex containing structural {Co-CN-Pt} arrangements [81,82]. These conjugates were still recognised and converted to AdoCbl by the corresponding intracellular enzyme [83] (Figure 1.5C). Furthermore, *in vitro* cytotoxicity studies showed DNA damage by the Pt^{II} complex and a TC-dependent uptake mechanism [84].

For all these approaches, expression of the receptors involved in TC uptake is the limiting factor, and so combination therapy coupled with synergistic mechanism of drug treatment seems to be an interesting option. An increase in the uptake and toxicity was seen when nitric oxide (NO)-Cbl derivatives were administered in combination with interferon β (IFN-β),

an agent that potentially up-regulates CD320 expression [85] (Figure 1.5E). Another study with NO-Cbl showed an enhanced cytotoxic effect of standard chemotherapeutics [86].

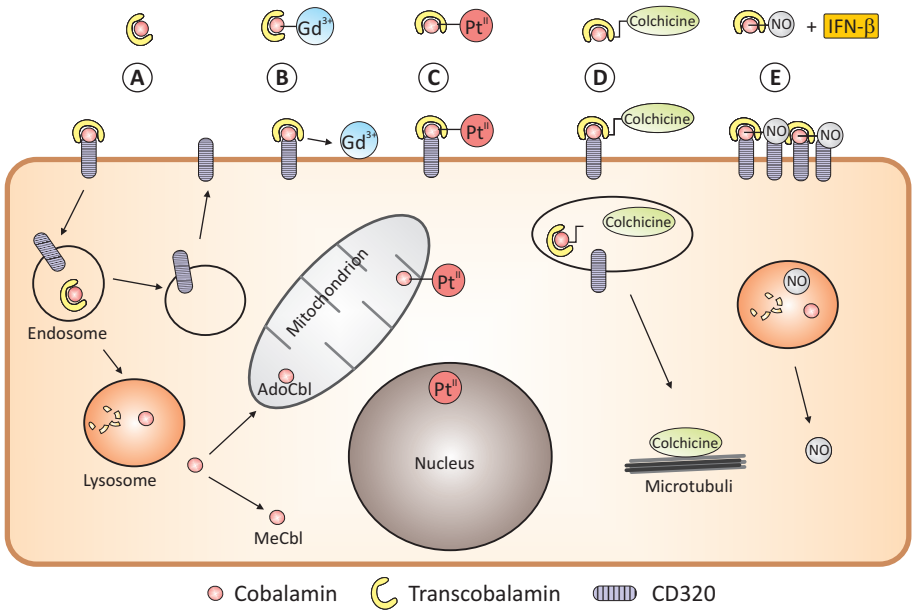

Figure 1.5 Cell uptake and cytotoxicity of different Cbl derivatives. By binding to CD320, TC-Cbl is internalised (**A**). After dissociation in the endosome TC-Cbl is separated from the receptor that recycles back to the cellular membrane, while TC is degraded in the lysosome and frees Cbl is exported to the cytoplasm. There (MeCbl) and in the mitochondria (AdoCbl) act as a cofactors for two enzymes. Cytotoxic metals like Gd^{3+} (**B**) or Pt^{II} (**C**) have been conjugated to Cbl. Gd^{3+} ions are thought to be released near the cytoplasmic membranes, while Pt^{II} is putatively released from Cbl after adenosylation and introduces DNA damage in the nucleus. Colchicine is released in the lysosomes by cleavage of an acid-labile linker (**D**). Similarly, NO is thought to dissociate from NO-Cbl derivatives in the lysosomes (**E**). Expression of CD320 can be upregulated by co-administration of IFN-β.

Cbl derivatives with a high affinity not only to TC but also to IF are especially useful for the oral delivery of bioactive peptides that are only required in small amounts, such as granulocyte-colony stimulating factor G or erythropoietin [87-89]. These peptides showed a higher affinity for IF when conjugated to the 5'-hydroxyl moiety of the ribofuranoside than when conjugated to the *e*-propionamide side chain [90]. In another approach, Petrus *et al.* attached insulin to the 5'OH-ribosyl moiety [91]. However, due to a limited oral uptake capacity (1-2 µg of Cbl per day [13]), the blood glucose level could not be reduced sufficiently to meet the requirements for clinical practice. In respect thereof, the use of Cbl conjugated nanospheres shows a promising potential in order to circumvent this problem [92,93].

By using fluorescent Cbl-Re^{I} conjugates bound to IF, living cells could easily be screened for cubilin receptor. Cubilin expression found in a placental choriocarcinoma [94] and a lung carcinoma cell line [95] showed the potential that such IF-binding Cbl derivatives could have to specifically target cubilin-expressing tumours *in vivo*.

1.5.2 Imaging with cobalamin derivatives

Shortly after the first isolation of the crystalline Cbl and the discovery of the cobalt ion within, replacement of the cobalt ion with radionuclides (^{57}Co, ^{58}Co, ^{60}Co) resulted in the first radioactive Cbl derivatives [96-98]. Early ^{57}Co-Cbl, ^{58}Co-Cbl and ^{60}Co-Cbl biodistribution studies of mice with transplanted tumours showed high uptake of radioactivity in the kidney, the pancreas and the liver [99]. In addition, the long half-lives of ^{57}Co ($t_{1/2}$: 271 days) limited the maximal dose applicable for humans excluding external imaging of biodistribution.

Since then, several pharmacokinetics and biodistribution studies with radiolabelled Cbl derivatives have been described, including ^{125}I-arylstannane Cbl derivatives [100], ^{99m}Tc-labelled Cbl derivatives either linked directly to the cobalt centre [101], or conjugated to the different side chains of Cbl linked via histidine [102] or diethylenetriaminepentaacetate (DTPA) [103,104]. ^{111}In-DTPA Cbl analogues had been developed by Collins and Hogenkamp [103] for the purpose of CD320 imaging in mice, pigs and later in humans [105,106]. Although increased sequestration of the radiolabelled Cbl derivative in primary and metastatic tumours including breast, lung (Figure 1.6E), prostate, colon, thyroid and sarcomatous malignancies have been visualised by single-photon emission computed tomography (SPECT) imaging, background uptake in some healthy organs was high, especially in liver, spleen and lacrimal, nasal and salivary glands (Figure 1.6E). Activity associated with kidneys was found to be variable in the different tumour patients [105].

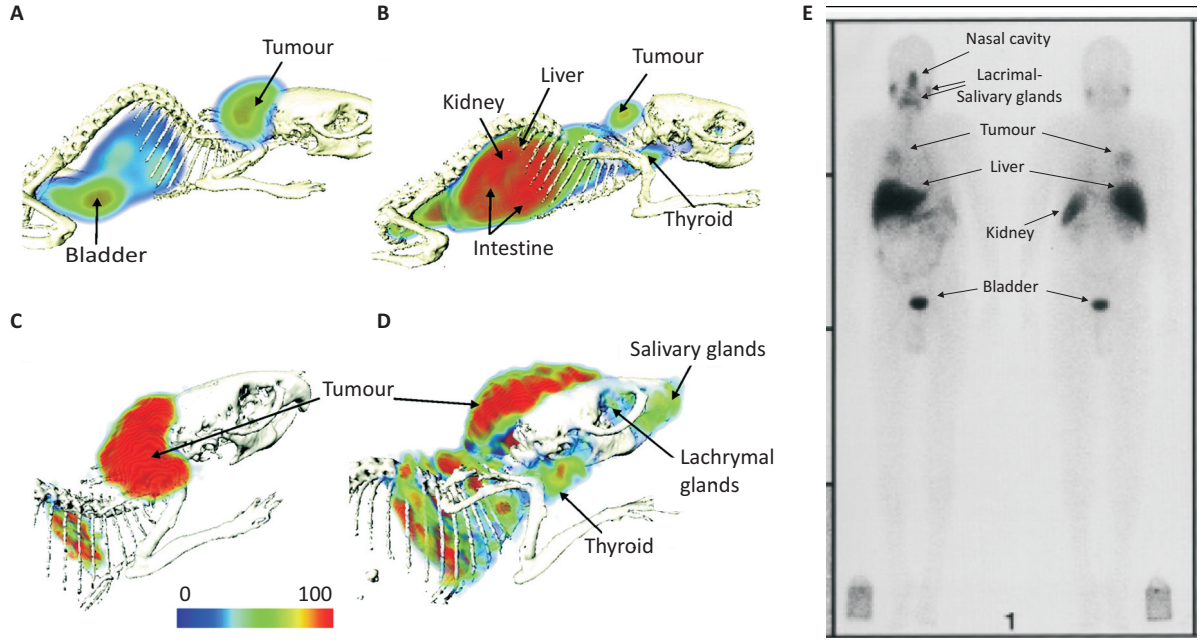

Figure 1.6 *in vivo* tissue distribution of Cbl derivatives in mice and humans. **A-D**. From Waibel *et al*. [75]. Whole body SPECT/CT scans of tumour bearing mice 24 h after i.v. injection. **A**. three-dimensional picture of a mouse with a B16F10 tumour at the neck injected with ^{99m}Tc-PAMA(4)-Cbl (TC nonbinder; low resolution, high sensitivity). **B**. three-dimensional picture of a mouse with a B16F10 tumour injected with ^{99m}Tc-PAMA(6) (TC binder). **C.** SPECT/CT (high resolution, low sensitivity, pinhole collimator) scan of the head 24 h after i.v. injection with ^{99m}Tc-PAMA(4)-Cbl. **D.** SPECT/CT (high resolution, low sensitivity, pinhole collimator) scans of the head 24 h after i.v. injection with ^{99m}Tc-PAMA(6)-Cbl. The colour scale is normalised to the highest activity. **E**. From Collins *et al*. [105]. Lung tumour patient with a 6 cm tumour in the right parahilar region. Anteriour (left) and posterior (right) whole body images at 4 hours after i.v. injection of ^{111}In-DTPA-Cbl demonstrating the tumour within the right hemithorax but furthermore accumulation in the liver, the kidneys, the urinary bladder and the nasal cavity, as well as the lacrimal and salivary glands.

However, in a recent study by Waibel *et al.* [75], a ^{99m}Tc-labelled Cbl derivative, ^{99m}Tc-PAMA(4)-Cbl (Figure 6.6), showed a promising accumulation in tumours with a low background activity in kidneys and other vital organs in mice (Figure 1.6A-D) [75]. Interestingly, this derivative only bound to HC, while binding to TC was prohibited [75]. The mechanism by which these Cbl derivatives accumulate in tumours is still obscure.

Another group of Cbl derivatives showing potential for *in vivo* tumour imaging are fluorescently labelled Cbl conjugates. Smeltzer *et al.* developed the so-called CobalaFluors by conjugation of the fluorophores fluorescein, naphtofluorescein or Oregon Green for use in Cbl receptor imaging using epifluorescence microscopy or flow cytometry [107]. Similarly, the fluorescent dye Cy5 was linked to the 5'OH-group of the ribosyl moiety of Cbl, which subsequently showed successful lymphatic mapping in pigs [108]. Furthermore, rhodamine-

labelled polymers conjugated to folate, biotin and Cbl were used for tumour targeting *in vitro* and *in vivo* [109] revealing increased uptake of the vitamin-conjugated polymers.

According to these findings, fluorescent Cbl derivatives may soon have an implementation in intraoperative imaging similar to the successful use of fluorescent folate conjugates in clinical trials [110].

1.5.3 Therapy with cobalamin derivatives

Although the above described NO-Cbl derivative has been used in several therapy and combination therapy studies in mice [85,111] and in dogs [112], general therapy with cytotoxic or radiotherapeutic Cbl derivatives has not been feasible so far due to the high background activity of kidney and liver (Figure 1.6). This may possibly lead to severe side effects. The binding of a Cbl derivative to TC and its subsequent receptor mediated endocytosis leads to accumulation not only in tumours but also in the liver and kidneys. While CD320 is expressed on virtually all tissues [14], megalin is abundantly expressed in the proximal tubule of the kidney and in several epithelia [113]. As a consequence, accumulation of a Cbl radiotracer in healthy tissue cannot be prevented.

1.6 Outline of the thesis

After many years of intensive research on Cbl and its transport and uptake mechanisms in the human body, HC's role in Cbl homeostasis has remained obscure. Targeted drug delivery to tumour cells using Cbl analogues modified with conjugated cytotoxins or radionuclides is still of major interest, as seen by the large amounts of different Cbl analogues developed. While most of the analogues aim to bind to to TC, newly synthesised Cbl derivatives that specifically bind to HC showed preferential accumulation in tumours and to a much smaller degree in healthy tissues such as liver and kidneys. These findings set the focus again on HC's role in Cbl transport. As a consequence, the main aim of this thesis was to elucidate HC's role in Cbl transport, especially transport to tumour cells with a special regard to HC's structure and binding to the different Cbl analogues.

In the first part of the project, recombinant expression of human HC was established in human embryonic kidney cells (HEK293). The mammalian expression system was used, in order to achieve fully glycosylated protein as this is one of the major characteristics of human HC. Characterisation and comparison to native HC showed that recombinant HC has properties very similar to the native one and only slight different ligand binding kinetics, making it a valuable tool for further biochemical and structural studies (see section 2).

The established expression system was further used in order to recombinantly express human TC, mouse TC (mTC) and a glyco-variant of human HC. Comparison of UV-spectra and glycosylation pattern analysis with literature-reported data implied the suitability of the recombinant proteins for future studies (see section 3).

In a next step, we set out to solve the crystal structure of HC. Crystals of HC in complex with CNCbl or Cbi were obtained and the structures of the complexes were determined to 2.35 and 3.0 Å resolution respectively. While structural analysis of the CNCbl binding to HC only showed marginal differences to the binding of CNCbl to IF and TC, an alternative conformation of Cbi upon binding to HC could be revealed. Further, general aspects of ligand specificity among the transport proteins were discussed (see section 4).

With regard to different newly synthesised Cbl derivatives and their divergent abilities to bind to the transport proteins, we established a method in order to assess in a quick and easy way the binding of different Cbl derivatives to the Cbl transport proteins (see section 5).

Finally, we wanted to elucidate the uptake of specific Cbl derivatives in tumour cells. For this purpose, we radiolabelled Cbl derivatives that would either bind to all three transport proteins or only to IF and HC and performed *in vivo* biodistribution studies in mice, as well as *in vitro* internalisation studies (see section 6).

2 Comparison of Recombinant Human Haptocorrin Expressed in Human Embryonic Kidney Cells and Native Haptocorrin

Evelyne Furger, Sergey N Fedosov, Dorte Launholt Lildballe, Robert Waibel, Roger Schibli, Ebba Nexø, Eliane Fischer

PLoS One 2012; 7(5): e37421

Author contributions:

Evelyne Furger carried out the expression and purification of the recombinant human Haptocorrin, the glycosylation assay, the *in vitro* experiments with the HepG2 cells and wrote the paper.

Sergey N Fedosov carried out the absorbance spectra and the binding and dissociation kinetics.

Dorte Launholt Lildballe performed the corrinoid binding assay.

2.1 Introduction

Cbl is a water soluble vitamin which is involved in biosynthetic processes in every living cell. Its transport within the human body is mediated by an elaborate system involving three soluble binding proteins, haptocorrin (HC) (previously referred to as transcobalamin I or R-binder), intrinsic factor (IF) and transcobalamin (TC) as well as their receptors [13].

IF ensures the uptake of Cbl in the intestinal cell, and once Cbl is transferred to the blood, TC is needed in order to transport Cbl into all cells of the body. The role for HC is only partially known [50]. In the upper digestive tract, salivary HC captures dietary Cbl and mediates its transport through the stomach. Subsequently, HC is degraded by pancreatic enzymes in the duodenum, whereupon the released Cbl binds to IF and is transferred to the blood. In the blood, approximately 75% of all Cbl is bound to HC whereas the remaining fraction is bound to TC [26]. Interestingly, HC binds not only Cbl but also so-called Cbl analogues, which are corrinoids without cofactor activity in mammalian cells. Up to 40% of all corrinoids bound to HC in plasma are Cbl analogues [50,59,114].

While the presence of IF and TC is restricted to a few compartments in the body, HC is present in both the circulation and in most exocrine secretions such as saliva, tears, and human milk [50].

In contrast to TC, HC is heavily glycosylated and has an apparent molecular mass of 60-70 kDa, of which approximately 25% are attributed to glycans. Depending on the source of synthesis, different glycoforms of HC have been described [55]. HC that lacks terminal sialic acid is known to be rapidly cleared by the asialoglycoprotein receptor in the liver [56], while no receptor has been identified for sialylated HC.

Interestingly, some tumour types, including fibrolamellar hepatocellular carcinoma, have been described to express high amounts of HC [115,116]. In recent studies, this protein has been proposed as a diagnostic marker in breast cancer [75,117] and fibrolamellar hepatocellular carcinoma [115]. Expression of HC in cancer cells can reach high levels, and HC has very recently even been proposed as a target molecule for cancer diagnosis or therapy [73,75].

Both IF and TC have been expressed in various hosts such as plants, yeast, and insect cells [39,118-120], and their structures in complex with Cbl have been solved by X-ray crystallography [11,12].

The overall structure of both proteins is similar and consists of an N-terminal α-domain and a C-terminal β-domain connected by a flexible linker. In contrast to IF and TC, neither expression of recombinant HC nor its crystallisation have been reported so far. Thus, the only source of HC for biochemical studies is purified protein from human serum, saliva, or milk, which hinders protein consuming experiments, e.g. crystallographic analysis.

The work presented here reports the expression, purification and characterisation of recombinant human HC (rhHC) in the cell line HEK293. The C-terminal Myc-His-tag was removed using a thrombin-cleavage site, and the protein was further purified to >98% purity. We compare the biochemical properties of rhHC to native human HC isolated from the plasma of a cancer patient [121].

2.2 Results

2.2.1 Purification of rhHC from HEK293 culture supernatant

We developed a mammalian cell expression system for production of rhHC which contained a thrombin-cleavable, C-terminal fusion tag consisting of the Myc epitope followed by six histidine residues (Myc-His-tag) for immunological detection by an anti-Myc-tag antibody and affinity purification respectively (Figure 2.1A). The expressed fusion protein was purified by Ni^{2+} affinity and size exclusion chromatography. Tagged protein was obtained at high yields (10 mg/L culture supernatant) and relatively high purity (Figure 2.1B, lanes 3 and 4). Subsequently, the fusion tag was removed from rhHC by cleavage with thrombin and rhHC was further purified by a Ni^{2+} affinity chromatography step to remove uncleaved rhHC, the cleaved tag peptides and any protein impurities with affinity for Ni^{2+} (Figure 2.1B, lane 5). A final size exclusion chromatography step was performed to remove thrombin (Figure 2.1B, lane 6). Western blotting of the tagged and untagged products indicated complete removal of the fusion tag after thrombin cleavage (Figure 2.1C).

Comparison of the two size exclusion chromatograms showed that the tagged intermediate product was eluted as a main rhHC peak with a shoulder and some impurities (Figure 2.1D), whereas only a single peak was observed in the final untagged rhHC preparation (Figure 2.1E).

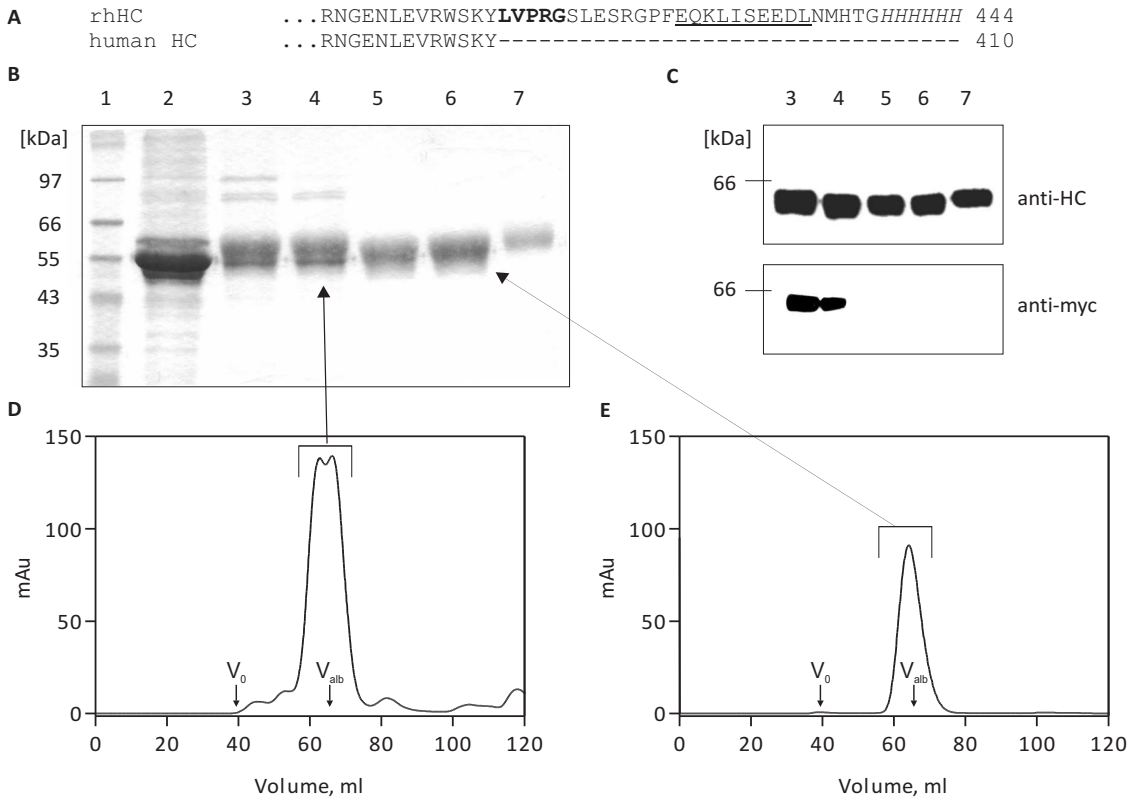

Figure 2.1 Purification of rhHC. rhHC purified from approximately 0.5 L HEK293 cell culture supernatant. **A**. Sequence alignment of native HC and tagged rhHC. Thrombin cleavage site (bold), Myc-tag (underlined) and 6xHis-tag (italic) **B**. Coomassie stained SDS/PAGE and **C**. Western blot analysis of the different purification steps. Lanes: 1, standards, 2, supernatant of HEK293 cells transfected with rhHC, 3, elution of first Ni^{2+} affinity chromatography (tagged rhHC), 4, peak fraction of first size exclusion chromatography (tagged rhHC), 5, flow-through of second Ni^{2+} affinity chromatography after thrombin cleavage, 6, peak fraction of second size exclusion chromatography, 7, human native HC [116]. **D**. and **E**. UV-chromatograms at 280nm of first and second size exclusion chromatography before and after thrombin cleavage on a Superdex 200 column at a flow rate of 48 ml h^{-1}. Elution volumes of Blue Dextran 2000 (V_0) and albumin (V_{alb}, 67 kDa) are marked with arrows.

The purified rhHC appeared as one broad band on SDS/PAGE after Coomassie staining (purity >98%), and the yield of rhHC was estimated to be 6 mg (90 nmol/L) from one litre of cell culture supernatant. N-terminal sequencing (EICEVS…) confirmed the identity and correct maturation of the purified protein. At the C-terminus, four excessive amino acid

residues (…LVPR) remained after cleavage with thrombin. The apparent molecular weight of rhHC on SDS/PAGE was comparable to the weight of native HC purified from plasma of a patient hepatocellular carcinoma [54] (Figure 2.1B and C, lane 7).

2.2.2 Glycosylation pattern of rhHC

The molecular weight of the purified rhHC was approximately 60 kDa as determined by 10% SDS/PAGE gel stained by Coomassie Brilliant Blue (Figure 2.2A lane 2) and Western blotting (Figure 2.2B, lane 1 and 2). This is significantly higher than the theoretical value of the protein backbone of 46 kDa. In agreement with SDS/PAGE, MALDI-MS analysis also revealed a molecular mass of rhHC of approximately 65 kDa (Figure 2.2C). The broad peak of mass distribution is expected due to heterogeneous glycosylation patterns of rhHC.

To further analyse the extent of glycosylation, several deglycosylation procedures were used. Incubation with PNGase F alone did not remove N-glycans completely (Figure 2.2A, lane 5 and 10). Simultaneous treatment of rhHC with Neuraminidase and PNGase F resulted in a lower molecular weight of the protein, indicating a high content of terminal sialic acids (Figure 2.2A, lane 4 and 9). For complete deglycosylation with PNGase F, a denaturation step prior to deglycosylation was needed in order to decrease the protein mass to the expected value of approximately 46 kDa (Figure 2.2A, lane 3). MALDI-MS analysis of the denatured and deglycosylated protein showed two peaks, one of which had the expected mass of the protein backbone of 46058.6 Da, which was close to the theoretical value of 46076.1 Da for rhHC (NCBI Reference Sequence: NP_001053) including the mass of the four excessive residues present (…LVPR), reduced S-S bonds and assuming eight converted Asn to Asp residues by action of PNGase F [122]. The second peak had a noticeably higher mass of 47054.4 Da (Figure 2.2D). This strongly indicates remaining posttranslational modification of rhHC even after removal of N-linked glycans. Periodic acid-Schiff (PAS) staining supports this finding as a residual amount of carbohydrates can still be detected after the deglycosylation procedure (Figure 2.2A, lane 8). Altogether, our results indicate that carbohydrates contribute approximately 20 kDa to the total mass of rhHC.

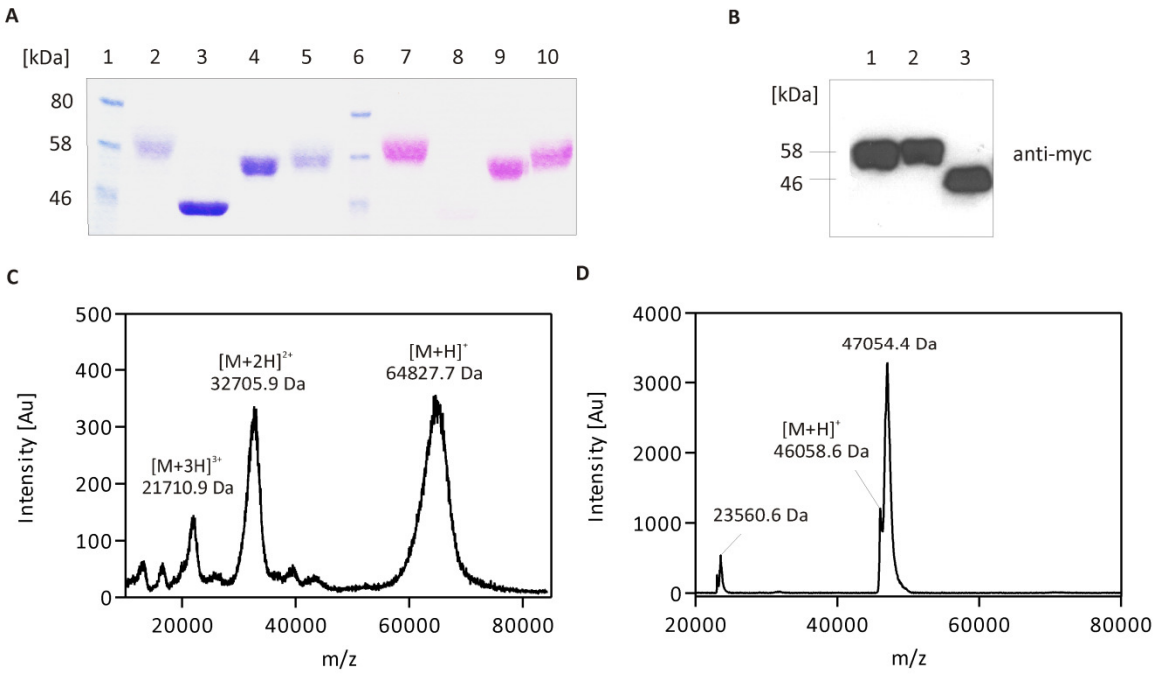

Figure 2.2 Glycosylation Pattern of rhHC PAS staining revealed heavy glycosylation of rhHC. **A**. Coomassie (lane 1-5)/PAS (lanes 6-10) staining of proteins separated on 10% SDS/PAGE. Lanes: 1/6, standards, 2/7, rhHC, 3/8, denatured and deglycosylated (PNGase F) rhHC, 4/9, rhHC overnight incubated with PNGase F and Neuraminidase, 5/10, rhHC overnight incubated with PNGase F. **B**. Western blot analysis of tagged rhHC using anti-Myc-tag antibody. Lane 1: denatured rhHC, lane 2: rhHC, lane 3: denatured and deglycosylated rhHC. **C**. MALDI-MS analysis of rhHC. **D**. MALDI-MS analysis of the denatured and deglycosylated (PNGase F) rhHC.

There are nine sequences for N-linked glycosylation in HC that show the consensus sequence Asn-X-Thr/Ser. Database research and previous published studies [70,123] predict only eight of them to be glycosylated. In contrast to IF, which is glycosylated only at its C-terminus, the predicted glycosylation sites of HC are situated on both the α- and β-subunit as well as the N-terminal part of the linker region [70].

We analysed the sequence for putative O-glycosylation sites using NetOGlyc 3.1 [124]. Two potential sites for mucin-type O-linked glycosylation were identified on Thr301 and Thr303, which are located on the linker region between the α- and β-subunit of HC. Analysis of the sequences of 25 orthologues (ExPasy) revealed putative O-glycosylation sites in the linker region in 21 of 25 HC-like-sequences (Table 2.1). Thus, O-glycosylation of the linker may be a common feature of HC-like proteins in various species.

Table 2.1 Amino acid sequences of the linker region connecting the α- and β-domains of HC aligned from different species.

Species	Sequence
ORNAN14853	ALEGKTYLDVTR--GCCDSDP-DNLTLSSPSPTAPTN-PSTITVTYKVTDGISNTFADSI
ANOCA05883	SLWGRTYLDVNR--FNCSKDKGDHFTYFAFQQIMPFASQRSITVIY------SNRFSEST
MACEU14399	ALEGKTYLDN----VSCQSTP-GHLSITPKPTEPTHQFYESISVTYR---VVDSINKTST
TURTR11138	ALMGKTYLDVNKNSSCACSPDKFNISTDEPVPVTPTISLSNISVNYS---VQINEIFNST
LAMPA04138	ALMGKTYLDVNNHSACARSPVDFNISSDDPVSVTPTVSPSNITVNYY---VQINETQP-I
BOVIN15542	ALMGKTYLDVTN-PSCGLNPVKFNTSTEKPGTVTPTTAPLNILVKYS---VRINKTSH-T
CANFA13900	ALLGKTYLDVNKDSPCVYKSGAFNLSTQEPTSGPPAVSHPQIQVNYS---VVINTTYN-I
FELCA05217	ALMGKTYLNVNKDSPCVYGPGDFNISTVEPITVTPPLSPSQIQVNYSV--VIIEETHS-T
HUMAN26634	ALMGKTFLDINKDSSCVSASGNFNISADEPITVTPPDSQSYISVNYS---VRINETYF-T
PANTR07054	----------NFNISADEPITVTPPDSQSYISVNYS---VRINETYF-T
PONAB07473	ALMGKTFLDINKDSSCVSASGNFNISSDEPVTVTPPDSQSYISVNYS---VRINETYF-A
MACMU16369	ALMGKTFLDVNKDSSCVSAAGNFSNSTHEPVTVTAPGSQSSISVNYS---VTINETYS-A
CALJA02898	ALLGKTYLDVNRDSSCVSGSGNFNISIPEPVTVTPPESQSNISVNYS---VRINETYS-A
SPETR03410	----------
OTOGA09004	AVMGKTYLDVN---SCVSSAGNFNISNPVPITVSPPDSPSNISVNYS---VRINETYF-T
TARSY06067	ALVGKTYLDINNNSACVSGSGIFNVSIHEPITMTPPVSLSYISVNYS---VRISETYS-I
LOXAF05754	ALMGKTYLYVNKDSPCVSGSD-FNVSAPVPGSVTPENSPSAITVRYS---VQINETYS-T
ECHTE10303	----------LNVSIPESGPVSPPPPSSLITVHYS---VKVNKTDS-T
PROCA06728	ALLGKTYLDVNKNSSCVYRKD-IKVVTPVSTSVIPTKSPSLITVHYS---VQINKTYS-T
CHOHO05486	ALMGKTYLDVNKDAPCVYDN--FNISIHEPGPAPPTKLPSVITVHYS---VQINETYS-T
SORAR02966	ALLGKTYLDVNKDSSCVYDSGKFNVSTHQPLSVTPTHAIADISVHYS---VKINETYS-T
PTEVA01690	ALMGKTYLDINKNSFCVNGSGNFSISIHEPVSVASSSSSSYISVHYS---VKINETYP-T
HORSE17505	ALVGKTYLDINKDSPCVSDPD-FNSPTPKPTSERYTNSPSNILVHYS---VKINRTYS-T
RABIT02686	ALMGKTYLDVSKDSSCVSGSGTFNISSHVPKSVTTPNPPSNISVNYS---VVITKTYS-T
CAVPO17819	ALVGKTYLDVSQDSSCASRLGNSHISSHKPTSITPLNSPLDTSVHYS---VKISN-YS-T
DIPOR07926	PLLGKTYLDVTKDSPCTYGLGNSPLSIPVRTTVTPTYSPSLISVHYS---VKINKTYS-I

Putative N-glycosylation sites are indicated in red. Putative O-glycosylation sites (predicted by NetOGlyc 3.1) are indicated in bold letters.

2.2.3 Absorbance spectra of rhHC

The absorbance spectrum of rhHC in complex with H_2O-Cbl is presented in Figure 2.3A and shows characteristics similar to those previously reported for native human HC (Table 2.2). The addition of azide caused a remarkable shift in the absorption maximum of the gamma peak, which is also characteristic of native human HC [125,126]. This change is caused by

attachment of azide-anion to the “upper surface” of Cbl accompanied by rearrangements in the binding site of HC [126].

The spectral features of the rhHC·H_2O-Cbl complex were explored further when rhHC was saturated with H_2OCbl added in steps at concentrations below the total binding capacity of the protein (Figure 2.3B). This allowed calculation of the molar absorbance coefficients of H_2OCbl when bound to rhHC (Table 2.2). These parameters helped to evaluate the active protein fraction (AP) as previously shown for IF [69]. For rhHC, the value of AP was calculated from the ratio of $R = A_{280} / A_{356}$ according to the equation below and the values of absorbance coefficients from Table 2.2.

$$AP = \frac{52200 - R \cdot 100}{R \cdot 26100 - 23100}$$

All examined samples of rhHC showed an AP ≥ 0.95 (i.e. ≥ 95% of the protein bound Cbl more strongly than adsorbent of H_2OCbl, see methods). The best measured values were R = 2.89 and AP = 0.99 indicating an excellent binding activity. In contrast to previously reported purification methods [127-129], rhHC was produced and isolated directly in the unsaturated (apo-) form without exposure to Cbl-containing adsorbents and denaturing agents. The absence of a refolding step in the purification of rhHC was apparently beneficial for the protein quality, resulting in a high AP-value. Nevertheless, the effect of GdnHCl treatment was examined on a preparation with AP = 0.95. rhHC was saturated with Cbl and then subjected to dialysis against GdnHCl [125]. No decrease in the binding activity was found after refolding of apo-rhHC (AP = 0.95).

Table 2.2 Coefficients of molar absorbance of rhHC (free or in complex with H_2OCbl, pH 7.5)

Protein species, ε	280 nm	γ, 356 nm	D, 415 nm	β, 509 nm	α, 529 nm
apo-rhHC, ε0	52 200[a)]	100	20	20	20
apo-rhHC + H_2OCbl, +Δε	+23 100	+26 100	5 480	9 930	10 030
holo-rhHC, ε	75 900	26 200	5 500	9 950	10 050
Native holo-HC, ε	n.d.	28 600 [b)]	5 400 [b)]	10 300 [b)]	10 400[b)]

[a)]Calculated from the composition of the mature protein, $\varepsilon_{280} = 5500 \cdot N_{Trp} + 1490 \cdot N_{Tyr} + 125 \cdot N_{S\text{-}S}$, $M^{-1}cm^{-1}$ [130] [b)]From reference [125]; n.d. not determined.

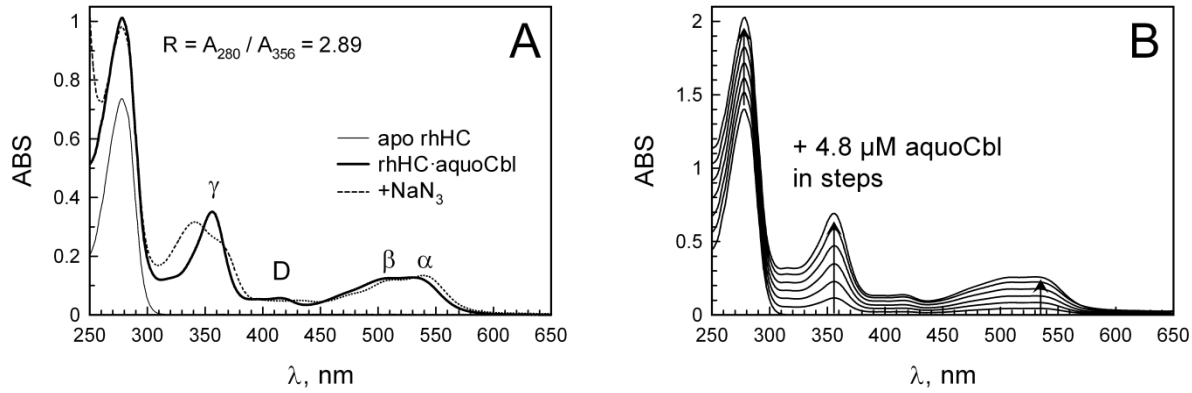

Figure 2.3 Absorbance spectra of rhHC-Cbl complexes. The absorbance spectrum of Cbl bound to rhHC exhibited a normal transition pattern. **A**. Spectrum of rhHC (13.8 µM) in either apo-form or saturated with H_2OCbl (excess removed) with or without sodium azide (2 mM), pH 7.5, 22°C. **B**. Spectra of H_2OCbl (4.48 µM) added stepwise to rhHC (26.3 µM), dilution was corrected, pH 7.5, 22°C. The data were used for calculation of the coefficients of molar absorbance, see main text and Table 2.2.

2.2.4 Binding of Cbl and Cbi to rhHC

The most prominent characteristic of HC is its ability to bind not only Cbl but also Cbl analogues, for example the baseless corrinoid Cbi. We analysed the ability of Cbl and Cbi to compete with labelled ^{57}Co-Cbl for binding to rhHC. Comparable binding curves for rhHC and native HC (Figure 2.4) point to the preservation of this characteristic in rhHC. It should be mentioned that half-inhibition concentrations (IC_{50}) cannot be connected directly to the dissociation constants (see below). For Cbi, this is because equilibration of the mixture of labelled Cbl + Cbi + HC may require several days of incubation.

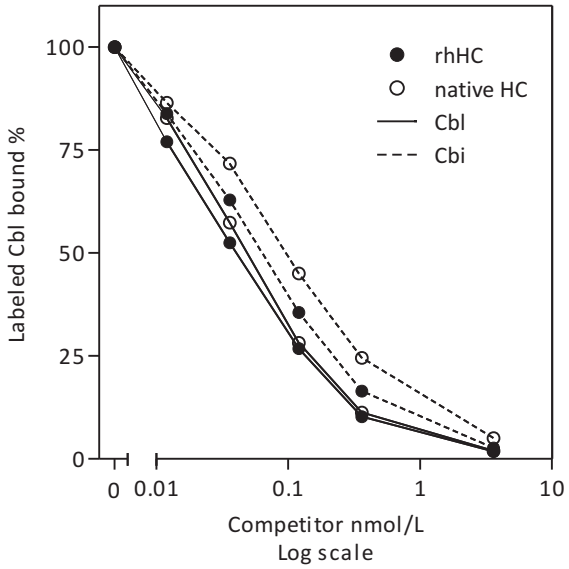

Figure 2.4 Interaction of rhHC with labelled Cbl in competition with Cbl or Cbi. rhHC and native HC showed a very similar binding behaviour towards Cbl and Cbi. rhHC and native HC were incubated with increasing concentrations of unlabelled Cbl or Cbi (competitor) and the amount of labelled Cbl bound to the proteins was recorded in % of the amount of labelled Cbl bound without the presence of competitor.

2.2.5 Binding and dissociation kinetics of the fluorescent Cbl-conjugate CBC, Cbl and Cbi

A more detailed examination of the binding kinetics was performed in a competitive assay in which the fluorescent ligand CBC [71] alone or in the mixture with a test ligand (Cbl or Cbi) reacted with rhHC over time. Attachment of CBC to Cbl-binding proteins causes an increase in the quantum yield of the fluorophore, which facilitates monitoring of the protein-CBC interactions [71,72]. The presence of a non-fluorescent ligand X decreases the signal, because the binding goes along two competing routes HC·CBC ← HC → HC·X (reactions behave as irreversible processes within 0.2 s). The data for the interactions between rhHC and either CBC alone or CBC + Cbl/Cbi mixtures are shown in Figure 2.5A. The binding and dissociation rate constants k_{+s} and k_{-s}, as well as the equilibrium dissociation constant K_d, were calculated for all ligands by computer fitting as explained elsewhere [72] and the results are listed in Table 2.3. The binding rate constants (k_{+s}) obtained in these experiments were 2-3 fold lower than values previously reported for native HC. This difference could not be explained by possible concentration error (±10%, examined by simulations). Deterioration

of ligands was also ruled out because the concurrent tests with two other proteins (TC and IF) revealed the expected values of k_{+S} = 60-70 · 10^6 $M^{-1}s^{-1}$ for both CBC and Cbl [72] (data not shown).

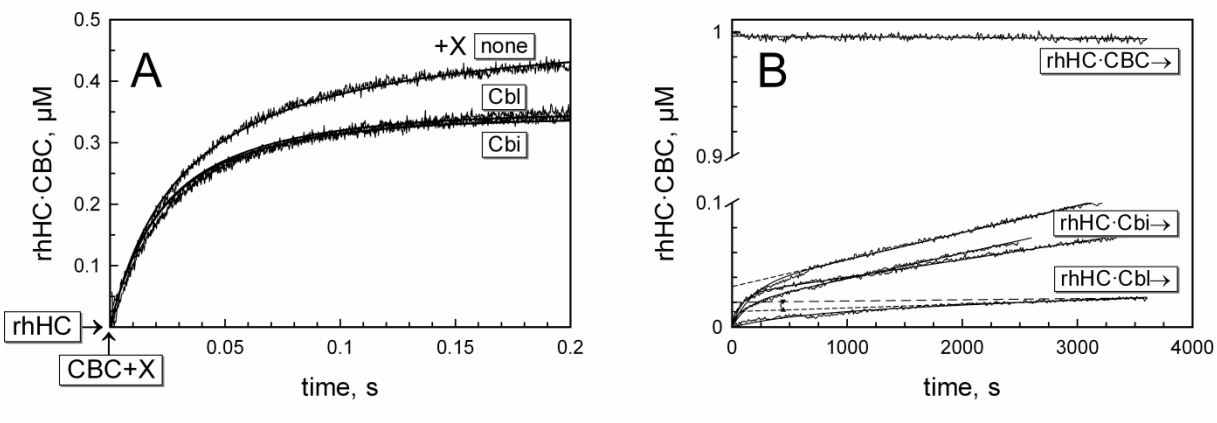

Figure 2.5 Binding and dissociation kinetics of the fluorescent conjugate CBC and Cbi. Kinetic measurements revealed a subtle difference between rhHC and native HC. **A**. Binding kinetics. rhHC was mixed with either CBC or CBC + Cbl/Cbi (all 0.5 μM), pH 7.5, 22°C. Appearance of rhHC·CBC complex was monitored over time according to increasing fluorescence normalised to the maximal amplitude of the signal. The binding rate constants were calculated by computer fitting (solid lines). **B**. Dissociation kinetics. rhHC was mixed with either CBC or the non-fluorescent test ligands Cbl and Cbi (all 1 μM, pH 7.5, 22°C, 2 min incubation), whereupon either Cbl (1 μM) or CBC (1 μM) was added. Change in the concentration of rhHC·CBC complex was monitored over time according to the normalised fluorescent response. Dissociation of Cbi was tested in three different preparations of rhHC (all three curves are presented, see also Table 2). Best fits are shown by solid lines. The dissociation rate constants were calculated from the linear slopes of the produced charts (examples indicated by dashed lines). Alternative linear slopes are shown for rhHC·Cbl dissociation.

The dissociation kinetics were examined in chase experiments which obeyed (within the examined time scale) one of the below schemes: HC·CBC → HC → HC·X or HC·X → HC → HC·CBC (first step was rate limiting). The dissociation kinetics of the ligands CBC, Cbl and Cbi were measured after formation of the corresponding complexes with rhHC, followed by addition of external CBC (or Cbl, in the case of CBC itself) (Figure 2.5B). The dissociation rate constants were then calculated from linear slopes (Table 2.3). In several cases a small "jump" in the dissociation was observed at the beginning of the reaction (e.g. dissociation curves for Cbl and Cbi, 0-1000 s interval). This fast exponential increase (0.5-3% of the total amplitude) was ascribed to the presence of a small fraction of partially denatured protein where the exchange of ligands was facilitated. This part of the curve was ignored and only the following linear component was used to calculate the dissociation velocity of the ligand (v_{-} = k_{-S} ·

[rhHC·S]). It should be understood that evaluation of rate constants below $3 \cdot 10^{-6} s^{-1}$ within the examined time scale cannot be precise, and that the records were used for comparison of different ligands rather than for precise quantification of k_{-S}.

Table 2.3 Binding and dissociation rate constants ($k_{+/-CBC}$, $k_{+/-Cbl}$, $k_{+/-Cbi}$) and equilibrium dissociation constants (K_d) at 20°C and pH 7.5

	k_{+s} ($M^{-1}s^{-1}$)	k_{-s} (s^{-1})	K_d (M)
rhHC			
CBC	62 / 64 / 56 [b] $\cdot 10^6$	≈ 0.5 / 2 / 1 [b] $\cdot 10^{-6}$	≈ $20 \cdot 10^{-15}$
Cbl	X / 19 / X $\cdot 10^6$	X / ≤ 3 / X $\cdot 10^{-6}$	≤ $100 \cdot 10^{-15}$
Cbi	33 / 21 / X [b] $\cdot 10^6$	1.4 / 2.2 / 2.1 [b] $\cdot 10^{-5}$	$1000 \cdot 10^{-15}$
Native HC a)			
CBC	$124 \cdot 10^6$	≈ $5 \cdot 10^{-7}$	(≈ $4 \cdot 10^{-15}$)
Cbl	$90 \cdot 10^6$	≈ $5 \cdot 10^{-7}$	(≈ $6 \cdot 10^{-15}$)
Cbi	$73 \cdot 10^6$	≈ $5 \cdot 10^{-7}$	≈ $7 \cdot 10^{-15}$

[a]From Reference [72]; [b]Measurements on different rhHC preparations with the active protein fractions of 0.99 / 0.95 / 0.95 (the last sample was obtained after GdnHCl refolding of rhHC). If no measurement was conducted, the result is notated as X.

The rates of CBC and Cbl dissociation from rhHC ($k_{-s} \leq 3 \cdot 10^{-6} s^{-1}$) were apparently similar to each other and also to the constants reported for native HC ($k_{-s} = 5 \cdot 10^{-7} s^{-1}$) as they were measured more accurately over a period of 100 h [72]. However, dissociation of the analogue Cbi from rhHC was noticeably faster ($k_{-Cbi} \approx 2 \cdot 10^{-5} s^{-1}$). An earlier study demonstrated nearly equal dissociation velocities for native HC and a group of corrinoids including Cbl and Cbi ($k_{-s} = 5 \cdot 10^{-7} s^{-1}$) [72]. Three preparations of rhHC (one after GdnHCl refolding) were examined and none of them showed dissociation of Cbi comparable to that of Cbl or CBC (Figure 2.5B). Repeated data for the same preparation did not reveal much variation (not shown). Though the overall affinity of rhHC for Cbi was formidable ($K_{d,Cbi} \approx 1$ pM), it was noticeably lower than that of native HC ($K_{d,Cbi} = 7$ fM). It seems that positioning of Cbi in the binding site of rhHC is not identical to that found in native HC. Considering the two other ligands (Cbl and CBC), the difference between rhHC and native HC was less obvious and concerned mostly k_{+s}.

2.2.6 Interaction of rhHC with the asialoglycoprotein receptor

Depending on the source of expression, different isoforms of HC exist in human blood and extracellular fluids [121]. Notably, different half-lives are associated with these isoforms, probably caused by fast clearance of HC-isoforms with low sialic acid content by the asialoglycoprotein receptor (ASGP-R) [56]. We tested whether ^{125}I-labelled rhHC would be readily taken up by HepG2 cells expressing the ASGP-R involved in HC clearance [131]. As with native HC, rhHC was not internalised over the measured time span of 6 h (Figure 2.6B). Only after the removal of terminal sialic acids by neuraminidase were rhHC and native HC internalised. Removal of the terminal sialic acid residues was qualitatively determined by SDS/PAGE (Figure 2.6A). The cellular uptake did not depend on the saturation of the protein with Cbl (data not shown).

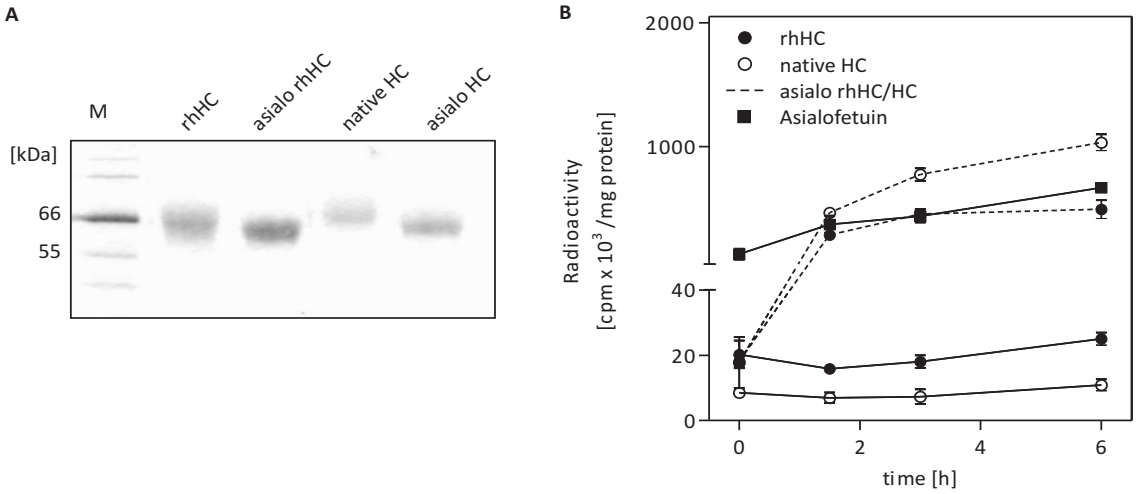

Figure 2.6 Internalisation of ^{125}I-rhHC into HepG2 cells. Comparison of rhHC and human native HC with or without pre-treatment with neuramidase in order to remove terminal sialic acid. **A**. SDS/PAGE analysis after treatment with neuraminidase. **B**. Internalisation of ^{125}I-labelled proteins after 0, 1.5, 3 and 6 h incubation time. Standards are indicated with M.

2.3 Discussion

We here report the first successful expression system for recombinant HC. Unlike the expression systems used for the production of IF and TC, mammalian cells (i.e. human embryonic kidney cells) are able to glycosylate proteins in patterns characteristic of higher

eukaryotes, yielding products that are expected to be highly similar to their natural human counterparts [132].

In comparison to other sources of human HC such as saliva (15-72 nmol/L), plasma (0.25-84 nmol/L) and milk (4.5-180 nmol/L) [50], the obtained yield of recombinant protein (90 nmol/L) is comparable or substantially higher. The recombinant protein demonstrated a high Cbl binding capacity of 95-99%, and its glycosylation pattern indicated the presence of N- and O-glycosylations. Unlike HC present in saliva and granulocytes, rhHC was highly sialylated. Interaction with ASGP-R only took place after removal of terminal sialic acids. We therefore concluded that rhHC represents an isoform that is comparable to HC present in human serum.

We demonstrated the recombinant protein's ability to bind Cbl as well as its baseless analogue Cbi. Furthermore, the absorbance spectrum of rhHC showed close similarity to the spectrum of native HC. The spectral transition in rhHC and native HC verifies the hypothesis that the organisation of the Cbl binding site in rhHC is comparable to that of native HC.

At the same time, the binding rate constants of all ligands were lower than those of native HC while the dissociation velocity of the examined analogue Cbi was also higher than expected. These subtle differences of rhHC compared to native HC were explained by presence of a peptide elongation attached to Tyr410 involved in the interaction with Cbl.

The purified form of rhHC had four excess residues (...LVPR) remaining at its C-terminal end discriminating it structurally from native HC. We hypothesise that the attachment of these non-native residues (...LVPR) to the C-terminal residue might affect the binding of ligands to rhHC resulting in lower affinity. This peptide is directly conjugated C-terminal to Tyr410 (located in the β-domain of HC), a residue which is potentially involved in the binding of Cbl according to the 3D model of HC-Cbl complex deduced from the crystallographic studies of TC and IF [70]. Such a disturbance might negatively affect the overall affinity (K_d) and the binding rate constant (k_{+s}), because the C-terminal β-domain is suggested to be the primary binding site of all corrinoids [69,72]. Reduction in affinity was particularly visible for the analogue Cbi, whose binding probably requires more structural accuracy of the protein.

In conclusion, we report that rhHC has comparable biochemical and kinetic properties to native HC and that the expression system provides us with the possibility to produce the protein in a sufficient amount for further biochemical and structural studies.

2.4 Materials and Methods

2.4.1 Materials

Most reagents including salts and buffer components were analytical grade and obtained from Sigma (Sigma-Aldrich Logistics GmbH, Buchs, Switzerland), unless stated otherwise. Ni-NTA Agarose was purchased from Qiagen (Hombrechtikon, Switzerland). Restriction endonucleases, DNA ligase and *Pfu* DNA Polymerase were obtained from Fermentas (Thermo Fischer, Lausanne Switzerland). For comparative binding studies, native human HC present in saliva [60] or purified to homogeneity from human plasma as previously described [129] was used. Saliva was collected as part of a previously published research project on HC in saliva [133] and as stated in the paper all of the individuals gave informed consent. Plasma was obtained from a patient with hepatocellular carcinoma left over from routine testing [116].

2.4.2 Cell Culture

HEK293 cells (DSMZ-Deutsche Sammlung von Mikroorganismen und Zellkulturen GmBH, Braunschweig, Germany) were grown in Dulbecco's modified Eagle's medium containing 4.5 g/L glucose, supplemented with 10% fetal calf serum, 100 U/mL penicillin, 100 µg/mL streptomycin, 0.25 µg/mL fungizone, and 2 mM glutamine in a 5% CO_2 incubator at 37°C. HepG2 cells (Institut für angewandte Zellkultur, Dr. Toni Lindl GmbH, Munich, Germany) were grown in minimum essential medium with Earl's basal salts supplemented with 10% fetal calf serum, 100 U/mL penicillin, 100 µg/mL streptomycin, 0.25 µg/mL fungizone, 2 mM glutamine, 1% non-essential amino acids, and 1 mM sodium pyruvate. All tissue culture reagents were purchased from BioConcept (Basel, Switzerland).

2.4.3 Plasmid Construction

The cDNA for human HC (pCMV6-TCNI RC222285, Myc-DDK-tagged ORF clone of Homo sapiens transcobalamin I (TCN1) NCBI Reference Sequence: NM_001062.2, as transfection-ready DNA) purchased by Origene (Lab Force, Nunningen, Switzerland) was cloned into the EcoRI/XhoI site of pcDNA4/*myc*-His A vector (Invitrogen AG, Basel) by standard molecular

biological techniques. A thrombin cleavage recognition site (LeuValProArg↓GlySer) was positioned at the fusion junction to release the HC protein from its tag. The primers (Microsynth AG, Balgach, Switzerland) used were 5'-TAATACGACTCACTATAGGG-3' and 5'-CCGCTCGAG AGATCCACGCGGAACCAGGTATTTGCTCCAGCG AACC-3'. All selected clones were verified by DNA sequencing (Microsynth AG, Balgach, Switzerland).

2.4.4 Expression of rhHC

Cells were transfected using Lipofectamine 2000 (Invitrogen AG, Basel) following the manufacturer's instructions. After 72 h, the cells were detached with phosphate-buffered saline (PBS)/1 mM EDTA and replated onto 10 new 10 mm cell culture dishes in complete medium supplemented with 400 µg/mL Zeocin™ selection reagent (Invitrogen AG, Basel, Switzerland) and 20 mM HEPES, which was changed every 4-5 days. After about 3 weeks, resistant colonies were isolated and grown as described elsewhere [134].

2.4.5 Purification of rhHC and thrombin treatment

High producer transfectomas were stimulated with 6 mM sodium butyrate in growth medium (without Zeocin and HEPES) for 8 days. The cell culture medium was centrifuged for 30 min at 7000 g, 4°C, clarified by filtration through a 0.2 µM Express plus filter (Millipore AG, Zug, Switzerland) and concentrated using an Amicon Filter device (MWCO 10000, Millipore AG). After adding 300 mM NaCl and 5 mM imidazol to the obtained solution (0.2 L) it was applied to a Ni^{2+} affinity column. Absorption of rhHC was carried out at room temperature with gravity flow. The resin was washed with 6 volumes of PBS, 6 volumes of PBS/1 M NaCl and 6 volumes of PBS/0.5 M NaCl/20 mM imidazole. Bound proteins were eluted in 1 mL fractions with PBS/300 mM imidazole. Fractions were analysed by SDS/PAGE, and the peak fractions were polished using HILoad™ 16/60 Superdex 200 gel filtration column and Äkta™*prime* system (Amersham Biosciences). Gel filtration was conducted at room temperature at a flow rate of 48 mL h^{-1} using PBS.

The peak fractions were subsequently dialysed against thrombin cleavage buffer (20 mM Tris-HCl pH 8, 150 mM NaCl, 2.5 mM $CaCl_2$) and incubated for 72 h at room temperature with thrombin (from human plasma, Sigma) (5 U/mg protein) on an orbital shaker. The Myc/His-tag was then removed by using a Ni^{2+} affinity column (2.5 mL) with gravity flow and

the flow-through was collected in 1 mL fractions using PBS. The rhHC-containing fractions were then subjected again to gel filtration as described above. The fractions with pure and untagged rhHC were pooled and concentrated to 1-2 mL by ultrafiltration on an Amicon filter (MWCO 30000, Millipore AG). The protein was stored frozen at -20°C.

2.4.6 Edman degradation

The Edman degradation was performed at the Functional Genomics Center Zürich, Switzerland. 5 µl of the sample was diluted with 100 µl 0.1% trifluoroacetic acid (TFA) and loaded on a PVDF membrane (ProSorb, Applied Biosystems). The membrane was washed with 100 µl 0.1% TFA and dried. Edman degradation was performed on a Procise 492 cLC (Applied Biosystems) according to the manufacturer's instructions.

2.4.7 Deglycosylation of rhHC

rhHC was denatured for 5 min at 95° C in denaturation buffer (100mM, pH 8 Na-phosphate, 25mM EDTA, 0.5% (w/v) Triton X-100, 0.2% (w/v) SDS, 1% (v/v) β-mercaptoethanol), cooled down and deglycosylated using the enzymes PNGase F (Roche diagnostics GmbH, Rotkreuz, Switzerland) and Neuraminidase (Sigma-Aldrich, Switzerland) according to Morkbak *et al*. [135].

2.4.8 SDS/PAGE and Western blot analysis

Proteins were separated by SDS/PAGE under reducing conditions and were transferred to PVDF (polyvinylidene difluoride) membranes (Millipore AG, Switzerland) using a semi-dry blotting device (Bio-Rad Laboratories AG, Reinach, Switzerland). PVDF membranes were probed with the following primary antibodies according to the manufacturer's protocol: anti-myc-tag mouse mAb (9B11; Cell signalling Technology, Bioconcept, Basel, Switzerland) or Transcobalamin I (M-16; Santa Cruz Biotechnology, Lab Force, Nunningen, Switzerland). The PVDF membranes were incubated overnight at 4°C in TBST (20mM Tris HCl pH 7.5, 500mM NaCl, 0.05% Tween 20) containing 2% BSA. Proteins were visualised by incubating the PVDF membrane with a horseradish peroxidase (HRP)-conjugated secondary antibody (Cell Signalling Technology; Santa Cruz Biotechnology). Chemoluminescence was detected

using an enhanced chemoluminescence (ECL) Western blotting substrate (Pierce, Perbio Science Switzerland).

2.4.9 Mass spectrometric analysis

The MALDI-MS analyses were performed at the Functional Genomics Center Zürich, Switzerland. The denatured and deglycosylated sample was first precipitated by Trichloroethane (TCA). The dried pellet or 1 µl of the untreated sample was dissolved in 5 µl hexafluoro-2-propanol (HFIP) diluted 1:10 in matrix (saturated sinapinic acid (CHCA) in 0.1% trifluoroacetic acid (TFA) and 50% acetonitrile) and then spotted onto the target. In order to remove salts, buffer and inorganic impurities, the dry crystals were washed with 0.1% TFA solution and air dried. The samples were then analysed by MALDI-MS on a Bruker Autoflex II mass spectrometer equipped by a 337 nm Nitrogen laser.

2.4.10 Spectral studies

Absorbance spectra were recorded on a Varian Cary 50 spectrophotometer (Varian, Australia) at 5-15 µM concentrations of Cbl and rhHC dissolved in 0.2 M Na-phosphate buffer, pH 7.5, 22°C.

Prior to AP measurements, rhHC was saturated with an excess of H_2OCbl, free H_2OCbl was bound to the specific tetrazole adsorbent [136], whereupon the spectrum of rhHC·Cbl was recorded and compared to the control sample (buffer + H_2OCbl + adsorbent). After subtraction of the control spectrum, the absorbance ratio and AP were calculated.

2.4.11 Binding of Cbl and Cbi to rhHC

The ability of rhHC to bind Cbl (Sigma-Aldrich, Denmark) and Cbi (Sigma-Aldrich, Denmark) was explored using a competitive assay previously described [60]. In brief, rhHC or partly purified native apo-HC was incubated with ^{57}Co-Cbl (Kem-En-Tec, Taastrup, Denmark) together with increasing amounts of Cbl or Cbi overnight. Unbound ^{57}Co-Cbl was removed by charcoal precipitation and bound ^{57}Co-Cbl was measured employing a Wizard Automatic Gamma Counter (Perkin Elmer).

2.4.12 Refolding of rhHC

rhHC (10 µM) was saturated with an excess of CNCbl (20 µM) and subjected to dialysis against a 50-fold volume excess of 5 M GdnHCl (30°C, 180 rpm). The solution was changed at days 2 and 3. Incubation was stopped after day 4, whereupon rhHC was renatured by dialysis against 0.2 M Na-phosphate buffer pH 7.5, see also ref. [125].

2.4.13 Binding studies with fluorescent Cbl-conjugate CBC

All reactions were performed in 0.2 M Na-phosphate buffer, pH 7.5, 22°C. The binding kinetics were monitored by means of stopped flow method (DX.17 MV stopped-flow spectro-fluorometer, Applied Biophysics, UK) using the fluorescent response from a Cbl-conjugate CBC [71,72], excitation 525 nm, emission > 550 nm, slit 1.5 mm, voltage 390, bandpass of 18.6 nm, light path of 1 cm. The binding reaction was started after mixing rhHC with CBC alone or CBC + corrinoid. The final concentration of all reacting species was 0.5 µM. The maximal amplitude of the fluorescent response in the mixture rhHC + CBC corresponded to 0.5 µM of rhHC·CBC complex. Competition between CBC and a non-fluorescent ligand for the binding to rhHC decreases the amplitude. The relevant rate constants of association were calculated by computer fitting, as described elsewhere [71,72].

The dissociation reactions were monitored on fluorometer Varian Eclipse (Varian, Australia) using the fluorescent response of CBC, excitation 525 nm (slit 5 nm), emission 550 nm (slit 5 nm), photomultiplier 600 V. In one setup the pre-formed rhHC·CBC complex (1 µM, 2 min) was mixed with free Cbl (1 µM), and decrease in fluorescence was registered due to rhHC·CBC ↔ Cbl exchange. Dissociation of the non-fluorescent ligands (Cbl or Cbi) was measured in similar chase experiments. The test ligand was mixed with rhHC (1 + 1 µM, 2 min), whereupon 1 µM of exogenous CBC was added. The endogenous ligand dissociated from the protein (rate limiting step), whereupon CBC immediately bound to rhHC and increased fluorescence.

2.4.14 Internalisation studies

The proteins were labelled with ^{125}I using the Iodogen method (Pierce). Labelled protein was purified on a PD10 column (GE healthcare, Glattbrugg, Switzerland). HepG2 cells were incubated in twelve-well plates in triplicates with approximately 1 µg of labelled protein for

1 h at 4°C. The plates were then incubated for 0, 1.5, 3, 6 h at 37°C for internalisation. After these times, the cells were washed twice with PBS/0.1% bovine serum albumin and then incubated for 5 min with ice-cold acid wash buffer (50mM Glycine-HCl, 100 mM NaCl, pH 2.8) to remove the cell-surface bound radioligand. Subsequently, cells were solubilised by incubation with 1 N NaOH for 5 min. at 37°C. At each time point the radioactivity in the cell medium (released), the acid wash (cell-surface bound) and the solubilised cells (internalised) were determined with a NaI-γ-counter (Cobra II Packard, Canberra Packard GmbH, Frankfurt, Germany).

3 Expression, Purification and Characterisation of Recombinant Transcobalamin and a Haptocorrin Glyco-variant

Evelyne Furger, Marie-Sophie Rotter

Author contributions:

Marie-Sophie Rotter carried out the expression, purification and characterisation of recombinant mouse transcobalamin.

Evelyne Furger carried out the expression, purification and characterisation of recombinant human haptocorrin in GnTI- cells, and of recombinant human transcobalamin, measurements of the absorbance spectra and *in silico* studies of a homology model of mouse transcobalamin.

3.1 Introduction

The successful expression of large amounts of pure rhHC prompted us to attempt to solve its crystal structure. Several initial attempts to crystallise our rhHC failed, possibly due to its high level of glycosylation. One way to overcome this problem is to use a stable mammalian expression system, wherein folding and initial glycosylation proceed normally, but processing of the N-glycans is restricted in a way that allows their subsequent enzymatic removal with either endoglycosidase H (Endo H) or endoglycosidase F1 (Endo F1). Both enzymes hydrolyse the glycosidic bond of the di-N-acetylchitobiose core structure, leaving a single N-acetylglucosamine (GlcNAc) residue at the glycosylation site [137,138]. This section describes expression and purification of HC in such an expression system.

In the human body two circulating transport proteins of Cbl are found: Haptocorrin (HC) and transcobalamin (TC). Due to a very low plasma concentration of TC (0.5-1.5 nM) [139], isolation and purification of this protein was only achieved by using affinity chromatography in 1972 by R. H. Allen and P. W. Majerus [140]. Their purification resulted in two distinctive peptides with a molecular weight of 38 kDa and 25 kDa respectively. By including an additional washing step, Van Kapel and co-workers [141] were able to purify a protein with a molecular weight of 42 kDa, possibly by removing residual proteases in the sample. Nevertheless, degradation of the protein was a major problem and several modifications of purification procedures have been described [142]. Although it is possible to purify native TC [140,142] for some experiments that do not require large amounts of protein (i.e. analytical experiments), investigations requiring high amounts of pure TC, such as crystallisation, required recombinant expression of TC. Having an abundant, well characterised and standardised protein source facilitates the exploration of molecular mechanisms *in vitro* as well as *in vivo.* Indeed, shortly after isolation of the full length cDNA of human TC [143], the successful recombinant expression of TC in different expression systems was described [39,120,144] resulting in the elucidation of the crystal structure of TC in 2006 [11].

Mouse transcobalamin (mTC) is much less well characterised than human TC. Early studies identifying the sole Cbl transporter in mice serum always underlined its similarity to human TC [145,146] including its molecular weight [147], cellular uptake of Cbl [146], and absence of glycans [148,149]. A recent publication [149] confirmed its resemblance to TC but also showed features of mTC similar to HC including the ability to bind to Cbi. Studies conducted

with mTC mostly used mouse serum itself or mouse fibroblast cells producing mTC [145,146,150] and so far no recombinant expression of mTC has been described.

Because mice are a commonly used model to investigate biochemical pathways or drug delivery *in vivo*, a better characterisation of the murine Cbl transport protein would help us to understand the mechanism of Cbl or Cbl derivative transport in rodent models.

3.2 Results

The recombinant proteins were stably expressed in HEK293 or HEK293 GnTI- cells and obtained at yields between 2-10 mg/L cell supernatant with relatively high purity. The purity of the recombinant proteins was verified by SDS/PAGE with subsequent Coomassie staining and Western blotting. LC/MS analysis and N-terminal sequencing confirmed the identity and correct maturation of the purified protein.

3.2.1 Expression and purification of rhHC in GnTI- cells (rhHC*)

The high degree of glycosylation of HC has so far posed a severe obstacle for the determination of its native structure. We therefore expressed human recombinant HC in HEK293 GnTI- cells according to the expression of rhHC in normal HEK293 cells [28] with a similar yield of approximately 10 mg/L cell culture supernatant. Tag removal and the several purification steps resulted in a final yield of approximately 6 mg (approximately 100 nmol) of pure and untagged protein. Like rhHC, the rhHC* was purified directly in its unsaturated (apo-) form (Figure 3.1B) and shows no signs of degradation for at least two weeks stored at 4°C.

Due to the lack of N-acetylglucosaminyltransferase I (GnTI) activity no complex N-glycans are synthesised in the expression system. Instead, N-glycans are uniform and consist of two N-acetylglcusomanines (GlcNAc) and five mannose (Man) residues (Figure 3.1A). Because of this homogeneous glycosylation pattern, a much more distinct band at lower molecular weight was visible in Coomassie-stained gels when compared to rhHC expressed in HEK293 cells (Figure 3.1B). The identity of the protein bands was confirmed by Western blotting (Figure 3.1B).

The expected weight of the protein backbone is 46062.1 Da, whereas mass spectrometry analysis revealed an apparent weight of about 56-57 kDa (Figure 3.1C). Knowing the exact glycosylation pattern of the protein, we could calculate the amount of potential sugar residues by dividing the difference between the measured and the expected value by the weight of one sugar tree (2 GlcNAc, 5 Man residues: 1216 Da). In this way, we were able to identify eight glycosylation sites that could be confirmed by NetNGlyc database and peptide mapping [123]. Deglycosylation with Endo H followed by ESI-MS analysis confirmed this finding by showing the expected value of 47686.7 Da (protein backbone plus eight GlcNAc: 1624.6 Da) (Figure 3.1D). For a detailed peptide mapping analysis see section 3.2.4.

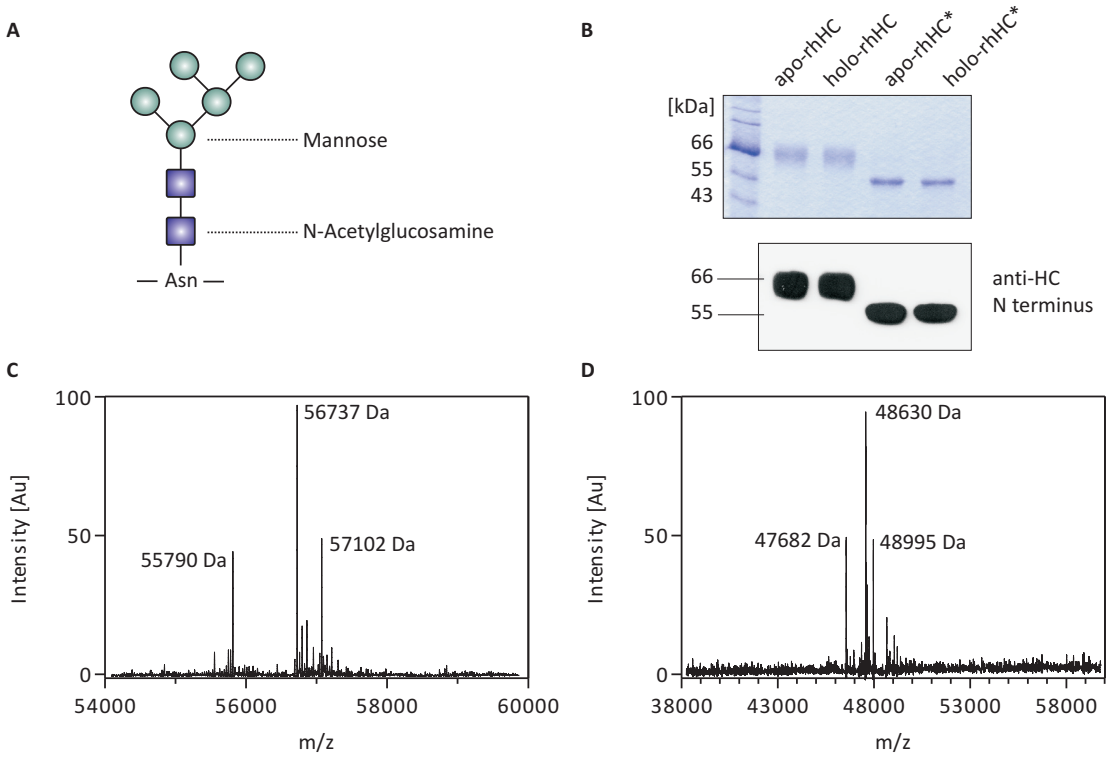

Figure 3.1 Characterisation of rhHC expressed in GnTI- cells. **A**. Homogeneous glycosylation pattern of GnTI- cells. **B**. Coomassie stained SDS/PAGE and Western blot analysis of apo- and holo-rhHC* expressed in GnTI- cells compared to apo- and holo-rhHC expressed in normal HEK293 cells. **C**. ESI-MS analysis of rhHC expressed in GnTI-cells. **D**. ESI-MS analysis of the deglycosylated (EndoF1) rhHC from GnTI- cells.

3.2.2 Expression and purification of rhTC

Based on the successful expression of rhHC in the mammalian cell line HEK293, this expression system was selected for the expression of rhTC. Due to alternative splicing, two known isoforms of the TCN2 gene exist. In our studies we used the full-length cDNA (transcript variant 1, NCBI reference sequence: NM_000355) according to the cDNA of TC sequenced in 1991 [151]. We were able to obtain rhTC protein containing a His- and Myc-tag in addition to a thrombin cleavage site with a molecular weight of approximately 50 kDa (Figure 3.2B). N-terminal sequencing and LC/MS analysis confirmed the presence of two isopeptides, one having the predicted amino acid sequence of EMCEI…(expected mass 49541 Da) and the other missing the first two residues, starting at CEIPE…(expected mass 49281 Da) (Figure 3.2C). This is a known feature of native as well as recombinant TC [120,142] and is probably due to alternative cleavage of the signal peptide, or cleavage of the first two N-terminal amino acids by alternative amino peptidases [152-154].

The obtained protein was much more unstable than rhHC after the first gel filtration purification, resulting in low molecular weight fragments when analysed by Western blotting (not shown). An overall yield of approximately 5 mg of tagged protein per litre cell supernatant was lower compared to the yields obtained with rhHC and further cleavage with thrombin resulted in a substantial loss of protein. However, spectral studies (see section 3.2.5) verified that when fused to a tag, the recombinant TC showed similar properties to the native TC. Based on this finding, it was therefore decided to use the protein without cleavage of the tag.

3.2.3 Expression and purification of rmTC

Of the three splice variants of mouse TC we used again the full-length variant 1 (NCB1 reference sequence: NM_015749). The same expression system was used for rmTC as was used for rhTC and rhHC, resulting in a His- and Myc tagged protein containing a thrombin cleavage site showing the expected mass of 49690 Da (Figure 3.2B and D). Like rhTC, rmTC was very prone to degradation. However, changing the buffer from PBS to a high salt PBS resulted in a reduction of degradation when the protein was stored at -20°C. The yield of tagged protein of approximately 11 mg per L cell supernatant was comparable to the yield obtained with rhHC.

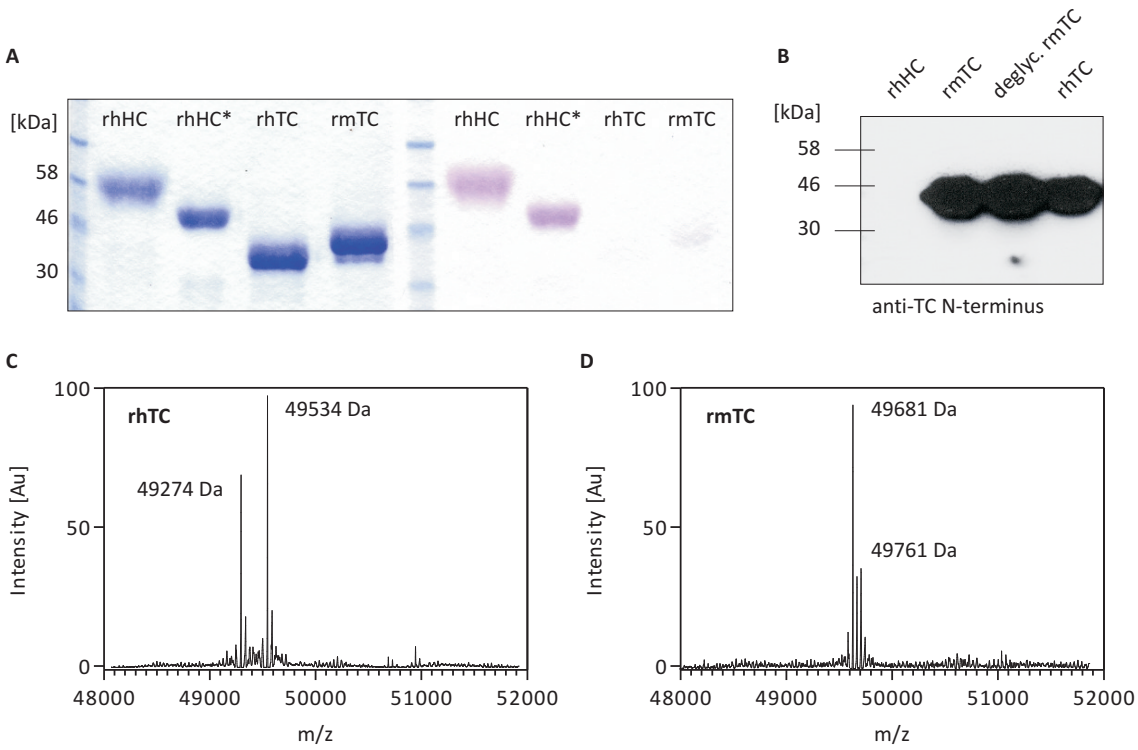

Figure 3.2 Characterisation of rhTC and rmTC. **A**. Coomassie stained SDS/PAGE and PAS staining of the different recombinant proteins. **B**. Western blot analysis of rhHC, rmTC, denatured and deglycosylated (PNGase F) rmTC and rhTC. **C**. ESI-MS analysis of rhTC showing the two isopeptide forms. **D**. ESI-MS analysis of rmTC.

3.2.4 Glycosylation of the recombinant proteins

The sequence of HC shows nine possible sites for N-linked glycosylation (three in the α-domain, one at the N-terminal part of the linker and five in the β-domain). However, although presence of the consensus sequence Asn-X-Thr/Ser is mandatory for N-linked glycosylation, not every potential site is actually glycosylated.

To determine site-specific glycosylation in HC we used a combination of specific enzymatic fragmentation with trypsin and formic acid and deglycosylation with EndoF1. The generated peptides were then analysed with LC/MS. With this method the potential glycosylation sites were separated in order to investigate site occupancy and site-specific heterogeneity. Of the nine sites showing the consensus sequence Asn-X-Thr/Ser eight of them could be identified to be glycosylated (Table 3.1).

One major structural difference between the Cbl transport proteins is their level of glycosylation. While IF and HC are known to be glycosylated, human TC is not. Database

analysis of the recombinant proteins using NetOGlyc 3.1 and NetNGlyc 1.0 [123,124] predicted no O-glycosylation sites for either rhTC or rmTC; one N-glycosylation site for rhTC; and two N-glycosylation sites for rmTC. The predicted glycosylation site for both proteins rhTC and rmTC at Asn33 is most probably not glycosylated as it is adjacent to a proline residue. This is known to inhibit glycosylation by rendering the Asn residue inaccessible for glycosylation. The second predicted position for rmTC at Asn75 was only low (0.63) above the threshold value of 0.5. Analysis of these glycosylation sites was performed with a homology model of mTC (see section 3.2.6). With PAS staining analysis (Figure 3.2A) carbohydrates could be detected on rhHC*, but not on rmTC and rHTC. These findings were in accordance with the presence (HC) or absence (TC) of glycans described for the native transport proteins [140,144,149,155].

Table 3.1 Site specific glycosylation analysis of rhHC expressed in HEK293 GnTI-

Cleavage sites	Modification	Sequence and modification site	Theoretical MW	Retention time [156]	Glycopeptide		Calculated MW	Found			
					m/z	Charge		Native	Mass error (ppm)	Deglyc	Mass error (ppm)
102-127	No	FQAEIENMEAHNGTPLTNYYQLSLD	2897.3	41.8	966.8	+3	2897.3	X	3.9	X	1
127-152	No	VLALCLFNGNYSTAEVVNHFTPENK	2779.4	45.1	927.5	+3	2779.4	X	0.7	X	-1.6
127-152	$[GlcNAc]_2[Man]_5$	VLALCLFNG**N**YSTAEVVNHFTPENK	3995.8	43.6	999.9	+4	3995.8	X	-5.1	-	-
127-152	GlcNAc	VLALCLFNG**N**YSTAEVVNHFTPENK	2982.4	44.2	995.2	+3	2982.5	-	-	X	2.3
192-199	No	NISIYTK	837.5	20.8	419.7	+2	837.5	X	-9.4	X	-8.5
192-199	$[GlcNAc]_2[Man]_5$	**N**ISIYTK	2053.9	18.8	1027.9	+2	2053.9	X	-3.2	-	-
192-199	GlcNAc	**N**ISIYTK	1040.5	18.8	521.3	+2	1040.5	X	-9	X	-7.1
282-297	$[GlcNAc]_2[Man]_5$	SSCVSASGNF**N**ISAD	2674.0	25.9	892.4	+3	2674.0	X	1.9	-	-
282-297	GlcNAc	SSCVSASGNF**N**ISAD	1660.7	27.0	831.3	+2	1660.7	X	-9	X	-5.5
306-318	No	SQSYISVNYSVR	1401.7	46.8	701.9	+2	1401.7	X	2.7	X	1.9
306-318	$[GlcNAc]_2[Man]_5$	SQSYISV**N**YSVR	2618.1	23.0	873.7	+3	2618.1	X	4.7	-	-
306-318	GlcNAc	SQSYISV**N**YSVR	1604.8	18.9	803.4	+2	1604.8	-	-	X	-6.9
318-341	$[[GlcNAc]_2[Man]_5]_3$	I**N**ETYFT**N**VTVL**N**GSVFLSVMEK	6253.6	45.0	1564.4	+4	6253.5	X	-8.39	-	-
318-341	$[[GlcNAc]_2[Man]_5]_2$	I**N**ETYFT**N**VTVL**N**GSVFLSVMEK	5037.2	48.3	1260.3	+4	5037.1	X	-6.9	-	-
318-341	$[[GlcNAc]_2[Man]_5]_2$ GlcNAc	I**N**ETYFT**N**VTVL**N**GSVFLSVMEK	5240.2	45.4	1311.1	+4	5240.2	X	-6.9	-	-
318-341	$[GlcNAc]_3$	I**N**ETYFT**N**VTVL**N**GSVFLSVMEK	3213.6	54.5	1072.2	+3	3213.5	-	-	X	-6.3
347-357	$[GlcNAc]_2[Man]_5$	M**N**DTIFGFTMEER	2806.1	37.8	1404.0	+2	2806.1	X	-15.6	-	
347-357	GlcNAc	M**N**DTIFGFTMEER	1792.8	40.1	897.4	+2	1792.7	X		X	-20.3

3.2.5 Absorbance spectra of the recombinant proteins

The absorbance spectrum for rhHC*, rhTC and rmTC in complex with H_2OCbl and azidoCbl were measured and compared to those described in the literature [125,126,157] (Figure 3.3). The spectra of rhHC* expressed in GnTI- cells showed the same characteristics as the spectra of rhHC expressed in HEK293 cells. It also showed a remarkable shift at the γ peak when 20 mM NaN_3 was added, pointing to an immediate rearrangement of the binding site, when the azide ion replaces the upper axial ligand of Cbl [126]. This shift could be explained by a movement of the electron density from the cobalt ion and the planar corrin ring. Upon binding of a strong electron donating upper ligand (e.g. azide) the lower ligand (DMB base) is weakened and pulled slightly away from the ring. The gamma peak subsequently shifts then to a shorter wavelength, because the electrons on the cobalt ion interact more weakly with the conjugation of the ring [20,26].

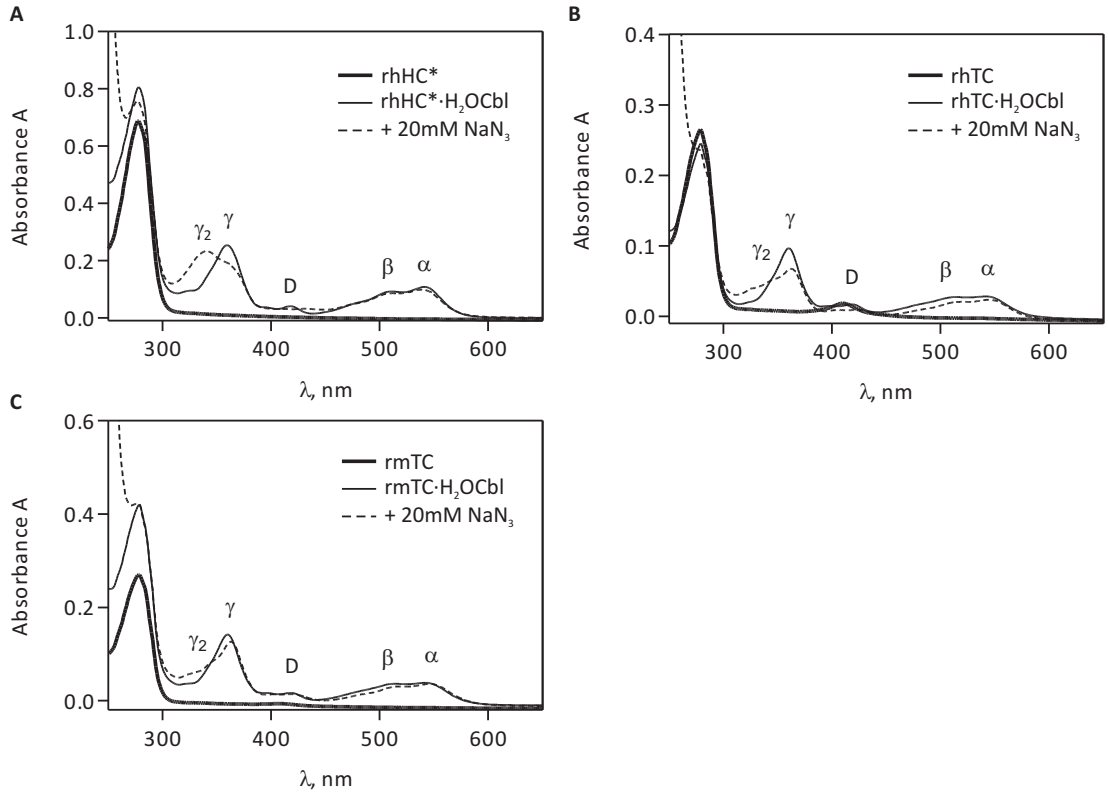

Figure 3.3 UV spectra of recombinant proteins expressed in HEK293 and HEK293 GnTI- cells respectively. The data were recorded at RT pH 7.4, with 1 nm steps in PBS. The depicted spectra correspond to 5-10 µM of the protein-ligand complexes. The spectra of the free proteins 5-10 µM are given for a comparison. **A**. Absorbance spectra of rhHC expressed in GnTI- cells (rhHC*), **B**. of rhTC and **C**. of rmTC in either apo-form or saturated with H_2OCbl (excess removed) with or without sodium azide (20 mM). Spectra with azide were recorded after 5 min. Strong absorbance below 280 originates from azide.

The absorbance spectra of rmTC in complex with H_2OCbl displayed a γ-peak at 362 nm and an α-peak at 544 nm showing a higher resemblance to the spectrum of TC (γ = 362 nm, α = 546 nm) than of HC (γ = 356 nm, α = 528 nm). No remarkable shift was seen after addition of sodium azide to mTC as was seen in the spectra of human TC [39]. Furthermore the calculated molar absorbance coefficients for rmTC are comparable to the coefficients of human TC (Table 3.2).

Table 3.2 Molar absorption coefficients of rhHC, rhTC and rmTC

	HC-H_2OCbl[1)]	**rhHC*-H_2OCbl**	**TC-H_2OCbl**[1)]	**rhTC-H_2OCbl**	**rmTC-H_2OCbl**
α-peak	10 400 (528)	10 384 (536)	9 300 (546)	13 638 (542)	12 267 (544)
γ-peak	28 600 (356)	27 611 (356)	30 000 (362)	33 778 (362)	31 033 (362)
γ_2-peak	26 300 (342)	26 833 (340)	-	-	-

The wavelength in nm is given in brackets below the absorption coefficients (M^{-1} cm^{-1}).
[1)] From reference [125].

No large shift was seen in the γ peak upon addition of 20 mM NaN_3 to the rmHC or to rhTC, resulting in spectra that are comparable to the spectra reported in the literature [157]. This indicates that the sixth ligand of Cbl is already coordinated to an endogenous histidine residue and that a change of H_2OCbl to azido-Cbl does not affect the spectrum. Structural studies of TC and H_2OCbl defined a coordination of His172/173 of human TC to the cobalt ion [11]. According to the sequence alignment (Figure 3.4), the residue in mouse TC that corresponds to His172/173 in human TC is expected to be His175 as it is in bovine TC (Figure 3.4) [11]. This strongly indicates that also in mTC a His-based coordination to the cobalt ion of H_2OCbl takes place (see also section 3.2.6).

```
Human TC   EMCEIPEMDSHLVEKLGQHLLPWMDRLSLEHLNPSIYVGLRLSSLQAGTKEDLYLHSLKL 60
Mouse TC   EFCVIPRIDSQLVEKLGQRLLPWMDRLSSEQLNPSVFVGLRLSSMQAGTKEDLYLHSLKI 60
Bovine TC  NICEITEVDSTLVERLGQRLLPWMDRLSQEQLNPSIYVGLRLSSLQAGAKEAHYLHSLKL 60
           ::* *..:** ***:***:********* *:****::*******:***:**  ******:

Human TC   GYQQCLLGSAFSEDDGDCQGKPSMGQLALYLLALRANCEFVRGHKGDRLVSQLKWFLEDE 120
Mouse TC   HYQQCLLRSTSSDDNSSCQPKLSGGSLALYLLALRANCEFFGSRKGDRLISQLKWFLEDE 120
Bovine TC  SYQQSLLRPASNKDDNDSEAKPSMGQLALYLLALRANCEFIGGRKGDRLVSQLKRFLEDE 120
            ***.** .: ..*:...: * * *.**************. .:*****:**** *****

Human TC   KRAIGHDHKGHPHTSYYQYGLGILALCLHQKRVHDSVVDKLLYAVEP---FHQGHHSVDT 177
Mouse TC   KKAIGHNHEGHPNTNYYQYGLSILALCVHQKRLHDSVVGKLLYAVEHDYFTYQGHVSVDT 180
Bovine TC  KRAIGHNHQGHPRTSYYQYSLGILALCVHQKRVHDSVVGKLLYAVEHKPHLLQDHVSVDT 180
           *:****:*:***.*.****.*.*****:****:*****.*******      *.* ****

Human TC   AAMAGLAFTCLKRSNFNPGRRQRITMAIRTVREEILKAQTPEGHFGNVYSTPLALQFLMT 237
Mouse TC   EAMAGLALTCLERFNFNSDLRPRITMAIETVREKILKSQAPEGYFGNIYSTPLALQMLMT 240
Bovine TC  MAMAGMAFSCLELSNLNPKQRNRINLALKRVQEKILKAQTPEGYFGNVYSTPLALQLLMG 240
            ****:*::**:  *:*.  * **.:*:. *:*:***:*:***:***:*********:**

Human TC   SPMRGAELGTACLKARVALLASLQDGAFQNALMISQLLPVLNHKTYIDLIFPDCLAPRVM 297
Mouse TC   SPASGVGLGTACIKAGTSLLLSLQDGAFQNPLMISQLLPILNHKTYLDLIFPDCQASRVM 300
Bovine TC  SLRPSVELGTACLKAKAALQASLQHKTFQNPLMISQLLPVLNQKSYVDLISPDCQAPRAL 300
           *   .. *****:** .:*  ***. :***.********:**:*:*:*** *** *.*.:

Human TC   LEPAAETIPQ--TQEIISVTLQVLSLLPPYRQSISVLAGSTVEDVLKKAHELGGFTYETQ 355
Mouse TC   LVPAVEDPVH--ISEVISVTLKVASALSPYEQTFFVFAGSSLEDVLKLAQDGGGFTYGTQ 358
Bovine TC  LEPALETPPQAKVPKFIDVLLKVSGISPSYRHSVSVPAGSSLEDILKNAQEHGRFRFRTQ 360
           * ** *   :    :.*.* *:* .  ..*.::. * ***::**:** *:: * * : **

Human TC   ASLSGPYLTSVMGKAAGEREFWQLLRDPNTPLLQGIADYRPKDGETIELRLVSW 409
Mouse TC   ASLSGPYLTSVLGKDAGDREYWQLLRAPDTPLLQGIADYKPQDGETIELRLVRW 412
Bovine TC  ASLSGPFLTSVLGRKAGEREFWQVLRDPDTPLQQGIADYRPKDGETIELRLVGW 414
           ******:****:*: **:**:**:** *:*** ******:*:********** *
```

Figure 3.4 Sequence alignment of human and bovine TC with mouse TC. The sequence identity of mouse TC/human TC is approximately 74%; and mouse TC/bovine TC approximately 67%. The Co-coordinating histidine residue is highlighted in blue. Residues that form disulfide bridges are shown in yellow; residues involved in H-bonds to Cbl are shown in green (accordingly to [11]). * (asterisk) indicates positions which have a single, fully conserved residue. : (colon) indicates conservation between groups of strongly similar properties – scoring > 0.5 in the Gonnet PAM 250 matrix. . (period) indicates conservation between groups of weakly similar properties – scoring ≤ 0.5 in the Gonnet PAM 250 matrix.

3.2.6 Homology model of mouse transcobalamin

The sequences of mTC against human TC (hTC) and bovine TC (bTC) were aligned using ClustalW to produce a target sequence (mTC) and a template sequence (hTC or bTC). Sequence alignment of mTC with human TC resulted in 74% identity, whereas alignment of mTC with bovine TC only showed 67% identity (Figure 3.4). We therefore decided to generate two models: one based on the crystal structure of human TC (Protein data bank: 2BB5) and the other based on the structure of bovine TC (PDB: 2BB6). Using the sequence alignments and the PDB code of the corresponding template protein, Swiss Model was able to generate 3D models of mTC based on the homology between mTC and the template protein [158].

Based on the findings of the UV-spectra of mTC (see section 3.2.5) we used our models to predict a possible His175 coordination of mTC. The crystal structures of both hTC (PDB 2BB5) and bTC (PDB 2BB6) show that His175 is coordinated to the cobalt ion of Cbl (Figure 3.5A and B). Based on the findings from the UV-spectra of mTC we used our models to explore if His175 in mTC is involved in the coordination of the cobalt atom in H_2OCbl. The model generated of mTC based on hTC mapped His175 onto residue His172 of hTC (Figure 3.5C) where it is not in a position to coordinate the Co ion. This is because mTC His175 has been aligned with His172 instead of His173 in the sequence of hTC. However, the model based on bTC places His175 in a position where it is available to coordinate the cobalt ion (Figure 3.5D). Used in conjunction with the UV-Spectra data, we can conclude that His175 in mTC is most probably coordinated to the cobalt-atom of H_2OCbl.

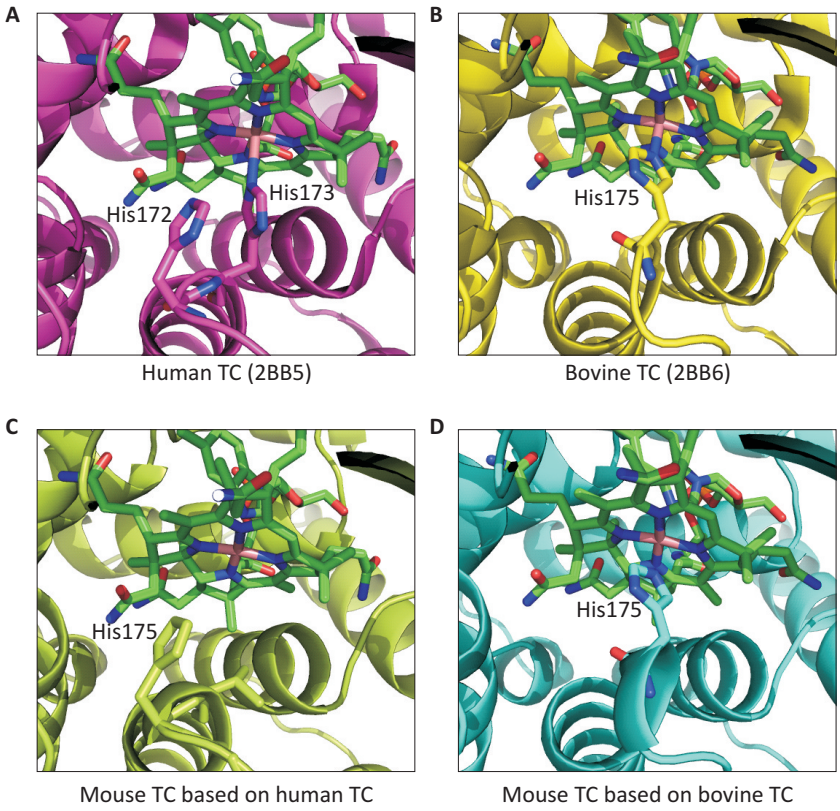

Figure 3.5 Coordination of His175 in mTC. **A**. Coordination of His173 in the human TC crystal structure (2BB5). **B**. Coordination of His175 in the bovine TC crystal structure (2BB6). **C**. No coordination of His175 was found in the human based mTC model. **D**. Coordination of His175 in the bovine based mTC model.

The amino acid sequence of mTC shows two glycosylation consensus sequences Asn-X-Thr/Ser, indicating possible glycosylation sites at Asn33 and Asn75 as predicted by NetNGlyc 1.0 [124] (see section 3.2.4). However, although LC-MS measurements and PAS staining revealed no presence of sugar residues, we were able to explain this finding with a structural analysis of the mouse model (Figure 3.6). In hTC, bTC and mTC, Asn33 is adjacent a proline residue (Pro34) which is known to inhibit glycosylation. The crystal structures of hTC and bTC reveal Asn33 to be orientated towards the protein core, while the relative rigidity of the adjacent proline residues ensures it remains in this position. This means that Asn33 is inaccessible for glycosylation in hTC and bTC. The models generated for mTC based on these structures reveal the same orientation of Asn33 (Figure 3.6A), which would explain why no glycosylation of mTC was shown by LC-MS or PAS staining. The second predicted site of glycosylation is Asn75, which is located in a loop region of mTC. It is likely that Asn75 is forming a salt-bridge to Asp73 across this loop region, thereby rendering the side chain unavailable for glycosylation (Figure 3.6B). This hypothesis is strengthened by the

observation that the equivalent residues in hTC and bTC are aspartic acid residues, which could also form salt bridges in the same manner as Asn75 across the loop region.

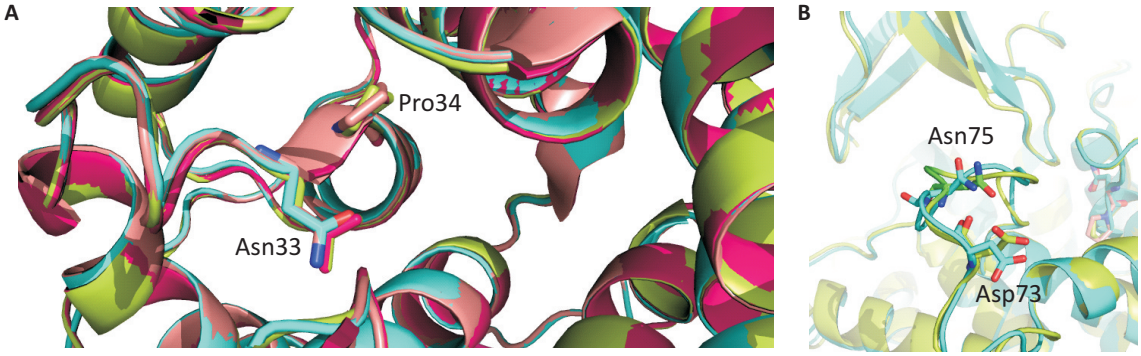

Figure 3.6 Glycosylation sites analysis of mTC. **A**. Overlay of human TC (PDB 2BB5; hot pink); bovine TC (PDB 2BB6; light pink). mTC model based on 2BB5 (green) and mTC model based on bovine TC 2BB6 (cyan). The predicted glycosylation site Asn33 is orientated towards the interior of the protein, making it inaccessible for glycosylation. **B**. Overlay of mouse TC modelled on 2BB5 (green) and 2BB6 (cyan). The predicted glycosylation site Asn75 may form a stabilising salt-bridge with Asp73 across the loop region, making it unavailable for glycosylation.

3.3 Discussion

The expression of rhHC in GnTI- cells resulted in a high yield of uniformly glycosylated protein with the expected molecular weight of approximately 57 kDa when analysed by LC-MS. PAS staining and deglycosylation studies with subsequent peptide mapping of potential glycosylation sites confirmed the glycosylation pattern and UV measurement in addition to competition binding studies with ^{57}Co-Cbl to CN-Cbl and Cbi (Lildballe; Nexø not shown) showed its resemblance to native HC. For further crystallization studies, deglycosylation of the protein was conducted using Endo F1 or Endo H leaving a single GlcNAc residue at each glycosylation site [138]. Cleavage with endoglycosidase rather than PNGase F was done, because previous studies had shown that completely deglycosylated glycoproteins tend to aggregate, whereas Endo H treated proteins behave in a manner very similar to the native protein [159]. The successful crystallization of rhHC is reported in section 04.

Two isopeptides of hTC were obtained when the protein was expressed recombinantly in HEK293 cells. Characterisation of the protein by LC-MS analysis for molecular weight determination; glycosylation analysis and UV spectra measurements corroborated our

hypothesis that our recombinant TC resembles native TC as it has been described previously [142].

We further expressed rmTC using the same well established system as for the other human proteins. The UV spectrum of rmTC, the calculated absorption coefficients and the absence of glycans testified that the protein is very similar to human TC and very likely shows the same His175 coordination with the cobalt ion of H_2OCbl. This could further be confirmed by analysis of the mTC His175 residue in an mTC homology model.

Similar to the earlier attempts to purify TC from human plasma [140,142], rhTC was prone to degradation and only in a high salt buffer the protein could be stored and used for prolonged time. Spectral analysis and binding studies pointed to an indistinguishable physiological behaviour of the tagged and untagged proteins. To preserve a high amount of protein we decided against cleavage of the purification tag. A similar behaviour was seen with rmTC that we also used in the tagged form for further studies.

Overall it was shown that the established expression system using the pcDNA4/*myc*-His A vector and HEK 293 cells can be used very efficiently for the production of glycosylated and unglycosylated Cbl transport proteins.

3.4 Materials and methods

3.4.1 Materials

Most reagents including salts and buffer components were analytical grade and obtained from Sigma (Sigma-Aldrich, Buchs, Switzerland), unless stated otherwise. Ni-NTA Agarose was purchased from Qiagen (Hombrechtikon, Switzerland). Restriction endonucleases, DNA ligase and *Pfu* DNA Polymerase were obtained from Fermentas (Thermo Fischer, Lausanne Switzerland).

3.4.2 Cell Culture

HEK293 cells (DSMZ-Deutsche Sammlung von Mikroorganismen und Zellkulturen GmbH, Braunschweig, Germany) and HEK293 GnTI- (a kind gift of Dr. Andrea Prota, Paul Scherrer Institute Villigen, Switzerland) cells were grown in Dulbecco's modified Eagle's medium containing 4.5 g/L glucose, supplemented with 10% fetal calf serum, 100 U/mL penicillin, 100 µg/mL streptomycin, 0.25 µg/mL fungizone, and 2 mM glutamine in a 5% CO_2 incubator at 37°C. All tissue culture reagents were purchased from BioConcept (Basel, Switzerland).

3.4.3 Plasmid Construction

The cDNA for human HC (pCMV6-TCNI RC222285, Myc-DDK-tagged ORF clone of Homo sapiens transcobalamin I (TCN1) NCBI Reference Sequence: NM_001062.2, as transfection-ready DNA), the cDNA for human TC (pcMV6-TCNII RC200682, Myc-DDK-tagged ORF clone of Homo sapiens transcobalamin II (TCN2), NCBI Reference Sequence: NM_000355, transcript variant 1 as transfection-ready DNA) as well as the cDNA for mouse TC (pCMV6-TCN2 MR206851, OriGene, Myc-DDK-tagged ORF clone of Mus musculus transcobalamin 2 (Tcn2), transcript variant 1 as transfection-ready DNA, NCBI Reference Sequence: NM_015749.2) were purchased by Origene (Lab Force, Nunningen, Switzerland).

rhHC and rhTC were cloned into the pcDNA4/*myc*-His A vector as described previously (Furger) whereas for the rmTC the cloning sites BamHI/XhoI were used. The primers (Microsynth AG, Balgach, Switzerland) used, were:

rhHC	5‘-TAA TAC GAC TCA CTA TAG GG-3‘	5‘-CCG CTC GAG AGA TCC ACG CGG AAC CAG GTA TTT GCT CCA GCG AAC C-3‘
rhTC	5‘-TAA TAC GAC TCA CTA TAG GG-3‘	5‘-CCG CTC GAG AGA TCC ACG CGG AAC CAG CCA GCT AAC CAG CCT CAG CTC GGT CGA TTG GTC GGA GTC GAG-3‘
rmTC	5‘-TAA TAC GAC TCA CTA TAG GG-3‘	5’-CCG CTC GAG AGA TCC ACG CGG AAC CAG CCA TCT AAC TAG CCG CAG CTC-3’

All selected clones were verified by DNA sequencing (Microsynth AG, Balgach, Switzerland).

3.4.4 Expression of rhHC*, rhTC and rmTC

For rhTC and rmTC HEK293 cells were used whereas for the rhHC HEK293 GnTI- cells were used. The transfection procedure was conducted as described before (see section 2.4.4).

3.4.5 Purification of rhHC*

The purification was performed as described elsewhere [28] and section 4.4.1.

3.4.6 Purification of rhTC and rmTC

Cell supernatant was harvested and concentrated as described before (see section 2.4.5). After adding a protease inhibitor cocktail tablet (complete^{TM}, Roche); 300 mM NaCl and 5 mM imidazol to the obtained solution (0.2 L) it was applied to a Ni^{2+} affinity column. Absorption of recombinant protein to the affinity matrix was carried out at room temperature with gravity flow. The resin was washed with 6 volumes of PBS, 6 volumes of PBS/1 M NaCl and 6 volumes of PBS/0.5 M NaCl/20 mM imidazole. Bound proteins were eluted in 1 mL fractions with PBS/300 mM imidazole. Fractions were analysed by SDS/PAGE, and the peak fractions were polished using Superdex 200 10/300GL gel filtration column and Äkta^{TM}*prime* system (Amersham Biosciences). Gel filtration was conducted at room temperature at a flow rate of 24 mL h^{-1} using PBS or high salt PBS (PBS containing 500 mM NaCl). The peak fractions with tagged rhTC and rmTC were stored frozen at -20°C.

3.4.7 SDS/PAGE and Western Blot analysis

Proteins were separated by SDS/PAGE and analysed with Western blotting according to section 2.4.8. For detection of rhTC and rmTC, anti-Transcobalamin II (E-13) (Santa Cruz Biotechnology, Switzerland) was used according to the manufacturer’s protocol. Donkey

anti-goat IgG HRP: sc-2020 (Santa Cruz Biotechnology, Switzerland) was used as secondary antibody.

3.4.8 Edman degradation

Edman degradation was performed at the Functional Genomics Center Zürich, Switzerland (see section 2.4.6).

3.4.9 Deglycosylation of rhHC* and rmTC

rhHC* was deglycosylated using recombinant Endo F1 expressed in E. coli (a kind gift of Thomas Schleier, BMR Paul Scherrer Institute, Villigen) in a 1:100 ratio protein to endoglycosidase and incubation overnight at room temperature.

rmTC was denatured for 5 min. at 95°C in denaturation buffer (100 mM, pH 8 Na-phosphate, 25 mM EDTA, 0.5% (w/v) Triton X-100, 0.2% (w/v) SDS, 1% (v/v) β-mercaptoethanol), cooled down and deglycosylated over night at 37°C using the enzyme PNGase F (Roche, Switzerland).

3.4.10 Mass spectroscopic analysis

LC/MS analysis was performed on a Waters LCT Premier mass spectrometer. Chromatography of the samples was conducted using a Uptisphere BP1 column (50 µm, 150 mm x 2 mm; Interchim, Montluçon, France) heated to 40°C using at a flow rate of 0.5 mL/min using a linear gradient from 20 to 80% A in 20 min plus 5% solvent C (solvent A, 0.1% formic acid in acetonitrile, solvent B, 0.1% formic acid in water, solvent C, isopropanol). The eluent was ionized using an electrospray source. Data were collected using MassLynx^{TM} 4.1 and deconvolution was performed using MaxEnt 1.

3.4.11 Generation of tryptic peptides and mass spectrometry

100 µg of either the native and the deglycosylated rhHC were incubated with 50mM ammonium bicarbonate buffer pH 8.0 containing 0.1% RapiGest SF Surfactant (Waters) and 0.96 µl 1M DTT. The mixture was then incubated at 55°C for 30 min. After cooling down to RT, 1.92 µl 1M iodoacetamide (IAM) were added and incubated in the dark for 40 min at RT.

Trypsin digestion was performed using 5 µg (1:20 w/w ratio) sequencing grade modified trypsin (Promega) overnight at 37°C. Prior to LC/MS measurement the samples were diluted 1:1 (v:v) with 1% formic acid in 10% acetonitrile. An auxiliary pump was used to spray a solution of 50 pmol/ml leucine enkephalin in 50/50 ACN/water containing 0.1% FA for mass accuracy (lockmass channel). The system was calibrated using sodium formate infusion (0.05M NaOH + 0.5% formic acid).

3.4.12 Spectral measurements

The spectra of the recombinant proteins with H_2O- and azido-Cbls (5-10 uM) were recorded in PBS, pH 7.4, on a Lambda™ 35 Double Beam UV Visible Spectrophotometer (Perkin Elmer). Unbound H_2OCbl was removed by charcoal precipitation prior to UV measurements.

3.4.13 Protein alignment

Alignment of human TC (SwissProt entry P20062) and cow TC (Q9XSC9) against mouse TC (O88968) were used. The alignment was performed with Clustal Omega 1.1.0 [160] using default settings.

3.4.14 Modelling

The comparative modelling of mTC is based on the structures of human and bovine TC determined by X-ray crystallography (PDB accession codes 2BB5 and 2BB6 respectively) [11] and on the multiple sequence alignment of mTC with these two forms of TC shown in Figure 3.4. The alignment was performed with CLUSTAL Omega 1.1.0 [160] using default settings. Using Swiss Model models were calculated for mTC using default settings [158]. The model geometry was analysed with MOLPROBITY [156] regarding Ramachandran plot, and with PROCHECK [161] regarding amino acid stereochemistry and protein structures were visualized using PYMOL (DeLano Scientific).

4 Structural Basis for the Ligand Specificity of the Cobalamin Transport Protein Haptocorrin

Evelyne Furger, Dominik Frei, Andrea Prota

Author contributions:

Evelyne Furger and Dominik Frei crystallised recombinant human haptocorrin.

Dominik Frei and Andrea Prota solved the crystal structure of haptocorrin.

Evelyne Furger and Andrea Prota wrote the manuscript.

4.1 Introduction

Cbl is an essential cofactor for central metabolic reactions in the human body such as the biosynthetic pathways of nucleotides; branched chain amino acids; and odd-chain fatty acids [21,22]. Chemically, Cbl consists of a corrin ring coordinating a central cobalt ion through four nitrogen atoms. The fifth coordination site on the lower axial part (α-side) of the molecule is provided by a 5,6-dimethylbenzimidazole ribonucleotide moiety (DMB) while the sixth coordination site (β-side) can be occupied by various ligands such as a cyano (CN), a hydroxyl (OH), a methyl (Me) or a 5'deoxy-adenosyl (Ado) group (Figure 4.1A).

The transport and cellular uptake of Cbl involves three transport proteins: haptocorrin (HC); gastric intrinsic factor (IF); and transcobalamin (TC); as well as a number of receptors [13,14,25-27]. Since humans rely solely on the dietary uptake of Cbl, this complex transport and uptake system guarantees efficient assimilation of Cbl.

IF is the transport protein responsible for the absorption of dietary Cbl via receptor-mediated endocytosis, whereas TC controls the cellular uptake of Cbl. HC is present in secretions, including saliva; milk; and tears but also in blood plasma [50]. It binds Cbl in the upper part of the gastrointestinal tract and is responsible for the stomach passage of Cbl [13]. Depending on the source of synthesis (gastric mucosa, glands, granulocytes etc.) [31] different glycoforms of HC have been described [55]. HC is heavily glycosylated, with 28% of its apparent molecular weight attributed to glycans. The physiological function of HC in plasma still remains unclear. Its low specificity for Cbl analogues - it even binds those Cbl analogues that lack the DMB moiety such as cobinamide (Cbi) [60] - suggests that it might play a role as a scavenger protein in the plasma, preventing the uptake of corrin-like compounds into cells via the TC-receptor pathway. Neither TC nor IF are able to bind such analogues under physiological conditions and show a much higher selectivity for Cbl.

Besides the individual selectivity for natural Cbl analogues, the three transport proteins also discriminate binding of synthetic Cbl derivatives. These substances have been used for targeting tumours with a high demand for Cbl [66,78,80], or as vehicles for oral drug delivery [87,89] or possible antibacterial or antiproliferative compounds [162].

Most prominently, radioactively labelled Cbl-derivatives have been applied both in animal models [100,102-104] and in cancer patients [105,106] for tumour imaging. Interestingly,

derivatives which selectively bind to HC but not to TC have been found to accumulate in tumours without the high accumulation in kidneys and other vital organs, which is usually observed with TC-binding Cbl derivatives in mice [75].

In the last six years the crystal structures of TC [11], IF [12], and cubilin(5-8)-IF-Cbl [163] have been reported. However, high-resolution structural information on the third transport protein HC, in order to reveal the molecular determinants of its unique binding ability for Cbl analogues is still missing to date. Based on homology models it was predicted that the overall architecture of HC is very similar to the structures of TC and IF and it was assumed that HC's low ligand specificity can be explained by three large residues: Arg357, Trp359 and Tyr362 [70]. It is thought that these residues coordinate the binding of Cbi to HC, by compensating for the absence of nucleotide in the Cbl binding site upon nucleotide-free Cbi binding. These residues may also provide hydrophobic contacts with the apolar lower side of Cbi in the same way that the DMP nucleotide forms contacts with the apolar lower side of Cbl. In contrast to HC, TC and IF only possess one of these three bulky amino acids (Tyr and Trp respectively), and thus cannot form hydrophobic contacts with the apolar lower side of Cbi in the same manner as HC [70].

In the present study, we set out to determine the crystal structure of HC in order to understand the molecular details of its unique ligand binding behaviour compared to other reported Cbl transport proteins. To facilitate crystallisation of the heavily glycosylated protein, we expressed recombinant human HC (rhHC) in HEK293 GnTI- cells, thereby producing proteins with a uniform glycosylation pattern. To better understand the interaction of HC with Cbl analogues, we further crystallised HC in complex with Cbi.

4.2 Results

4.2.1 Overall structure of HC

Crystals of HC in complex with the two ligands CNCbl and Cbi (Figure 4.1A and Figure 4.3A) were obtained and the structures of the complexes were determined to 2.35 and 3.0 Å resolution, respectively. Despite the low sequence identity to TC (23%) and IF (30%) [70], HC features a very similar domain architecture. It comprises two globular domains, the α-

domain (residue 1-287) and the β-domain (residues 309-410), which are connected by a flexible linker (Figure 4.1B).

The N-terminal domain, termed the α-domain, consists of a helical barrel formed by an inner and an outer bundle of six parallel α-helices each. The inner α-helices are evenly numbered, while the outer helices have odd numbers and run in the opposite direction. Conformational differences are observed at the loops α1-α2, α3-α4 and α5-α6 which are distant to the ligand interaction site. The α3-α4 loop is much shorter than in TC and is more similar to the corresponding loop in IF. Moreover, the α4-α5 loop of HC adopts a helical conformation. The outer shell helix α7 is shortened by a helix break at Pro149, which is followed by a long α7-α8 loop containing a short β-hairpin (β-1'-β-1"). At the tip of this β-hairpin the side chain of Phe156 is located adjacent to the position of the coordinating His175 in bovine TC (bTC) [11] at the upper axial side and could shift to adopt the coordinating function by a cation-pi interaction (Figure 4.1C). The resulting flexibility of the α7-α8 loop likely has implications on the binding of HC for the Cbl derivatives modified at the *b*-side chain (Figure 4.5). The 3/10 helix capping the bottom of the barrel is one turn shorter than observed in TC and IF. The three disulfide bridges (Cys3-Cys242, Cys82-Cys285 and Cys132-Cys174) that cross-link the α-domain are also conserved.

The C-terminal β-domain consists of an antiparallel β-sheet formed by the strands β1, β2, β6, β7 and β8, a β-hairpin, formed by strands β3, β4, and β5, almost perpendicular to the sheet, and an α-helix (α13) stacked in between [11]. The tight hydrophobic packing is further stabilised by an additional fourth disulfide bridge, which is unique to human HC and not present in either TC or IF. This disulfide bridge (Cys365-Cys370) confers additional stability to the β5 and β6 loop, which is similar to IF and contains a two residue insertion (Asn373, Asn374) compared to TC.

Clear electron density for seven *N*-linked *N*-acetylglucosamine moieties was present in the HC-CNCbl structure (Suppl. Figure 4.6B) at residues Asn193, Asn293, Asn314, Asn320, Asn326, Asn331 and Asn346. Poor density for the eighth N-linked glycosylation was observed at Asn137, therefore it was not modelled.

In contrast to the crystal structure of human TC, the HC linker does not participate in crystal contacts over its full length and is largely disordered (residues 296-307). Linker residues 289-294 form a parallel β-strand interaction to strand β2 of a symmetry related molecule

(residues 321-325). Moreover, the N-glycan at Asn293 is in contact with the symmetry related N-glycans at Asn326 and Asn346.

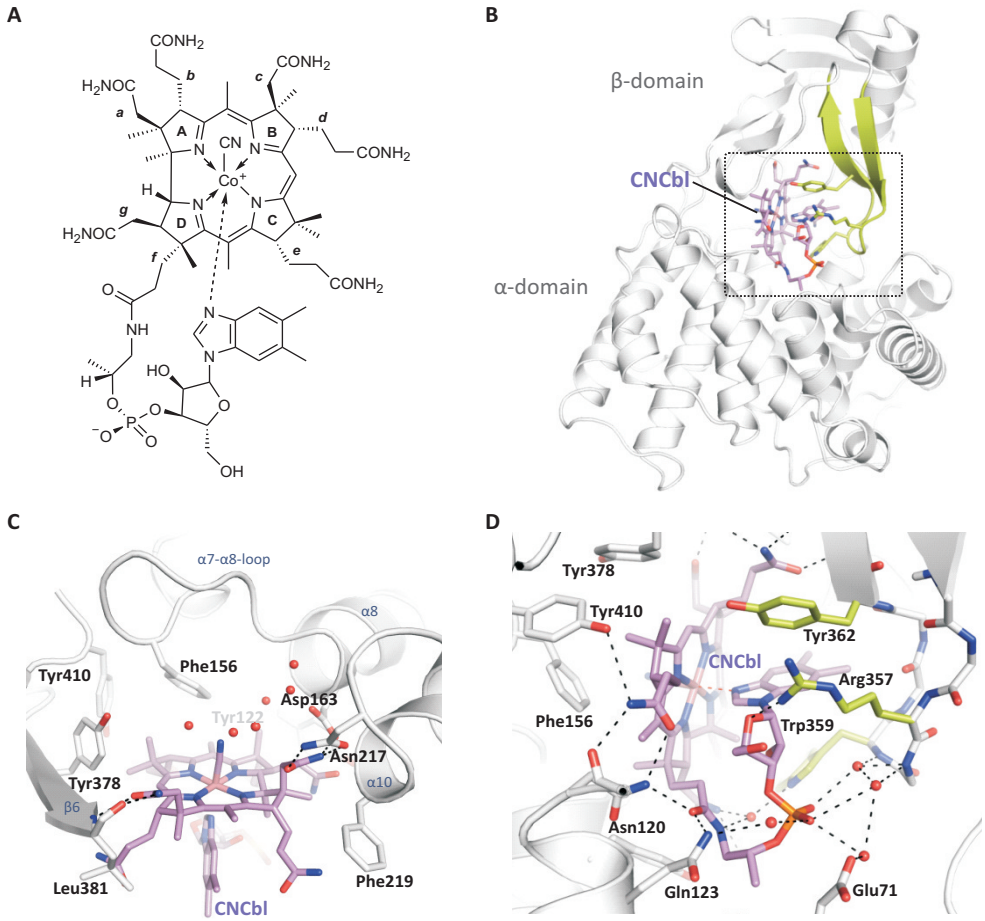

Figure 4.1 Structure of Cbl and comparison of ligand binding properties of the different Cbl binding proteins. **A**. Structural formula of CNCbl with the labels A-D for the corrin ring and *a-g* for the side chains. **B**. Cartoon representation of HC (white) in complex with CNCbl. The CNCbl molecule is displayed in pink stick representation. The β3-β4 hairpin is highlighted in green. The critical residues for interaction with the lower side of Cbl are shown in stick representation. The dashed box depicts the area shown in more detail in panel D. **C**. Close up view of the interaction observed at the upper axial side of CNCbl with HC. The critical binding residues are in stick representation and labelled in the corresponding colours. Water molecules are depicted as red spheres. **D.** Close up view of interactions at the lower axial side of CNCbl observed in HC. For clarity reasons only the three interacting hairpin residues are highlighted in green. Water molecules are shown as red spheres, hydrogen bonds as dashed black lines.

In both complexes (HC-CNCbl, HC-Cbi), the ligands are buried at the interdomain-interface. No major structural domain rearrangements are observed between the two structures. The relative orientation between the α-and β-domains in HC varies compared to TC and IF: the

central axis of the α-domain of HC relative to the β-domain is tilted by 16 degrees compared to TC, and is both tilted and twisted by 12 degrees compared to IF. These differences result in a tighter packing of the HC-ligand complex. Accordingly, the overall structure superimposes to hTC, bTC and IF with rmsds of 2.32 (281 C_α-atoms), 2.31 (302 C_α-atoms) and 1.77 (246 C_α-atoms) Å, respectively. The individual domains align to a higher extent: the α-domains superimpose with rmsds of 1.80 (hTC, 183 C_α-atoms), 2.02 (bTC, 200 C_α-atoms) and 1.21 (IF, 159 C_α-atoms), the β-domains with rmsds of 0.72 Å (71 C_α, hTC), 0.98 Å (86 C_α, bTC), and 0.75 Å (82 C_α, IF).

4.2.2 Binding of HC to CNCbl

The CNCbl molecule is bound at the α-β-domain interface with the corrin ring plane oriented almost parallel to the central axis of the helical barrel. The cobalt ion is coordinated by the four nitrogen atoms of the corrin ring, the N3B atom of the DMB ring and by a CN molecule at the sixth coordination site.

As in TC and IF, the side chains of the CNCbl corrin ring are stabilised by conserved interactions that involve main chain amide and carbonyl of Thr119, the side chains of Tyr122, Gln123, Asp163, Asn217, Phe219, Gln266, Tyr378, Tyr410 and the main chain amide and carbonyl of Leu381 (Figure 4.1C and D). Furthermore, the *e*- and the *f*-propionamides of the corrin-ring are stabilized by three additional hydrogen bonds formed by the side chains of Asn120 and Asn373 which are neither present in TC nor in IF (Figure 4.2A, B and Suppl. Figure 4.7).

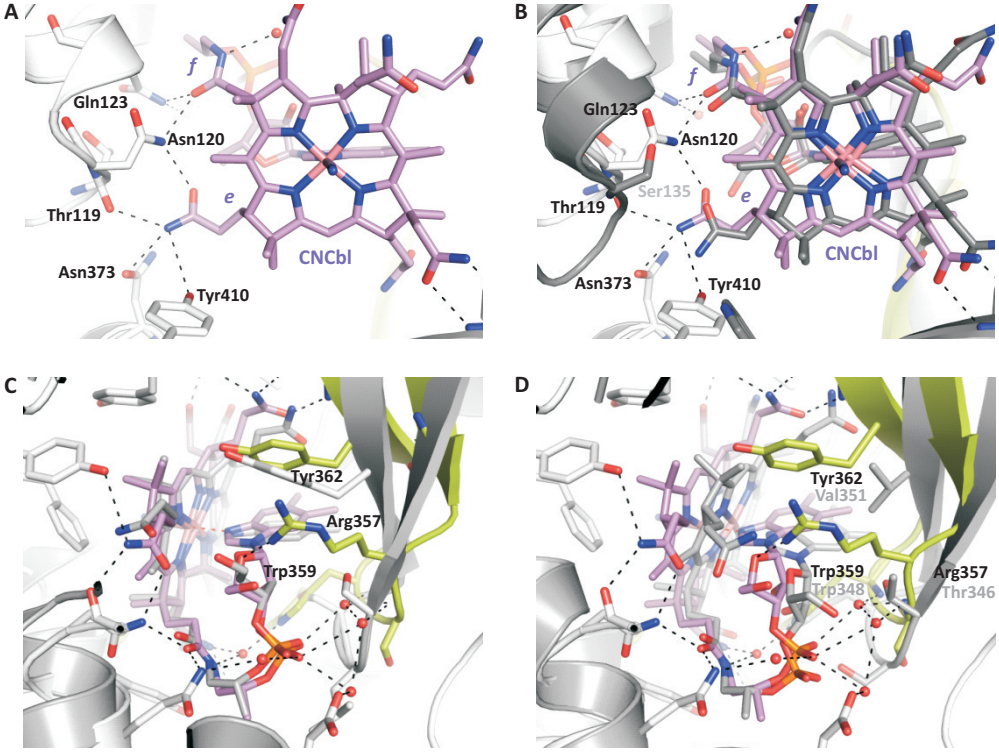

Figure 4.2 Critical residues for ligand specificity of human HC. **A**. Critical interactions at the *e*- and *f*-side chains of CNCbl viewed from the upper-axial side. The same colour code is used as in Fig. 4.1C and D. Hydrogen bonds are depicted as dashed black lines. **B**. Superposition of hTC (grey, PDB-code 2BB5) onto HC. In the absence of the Asn side-chains, three hydrogen-bonds cannot be formed to the ligand. **C.** Comparison of the interactions with the lower axial side of CNCbl between HC (white) and hTC (grey). The HC hairpin residues are highlighted in green and are labelled as in Fig. 4.1D. **D**. Comparison of the interactions with the lower side of Cbl between HC (white) and IF (grey, PDB-code 2PMV). The HC hairpin residues are highlighted in green as in C.

At the lower side of Cbl that hosts the nucleotide moiety, the β-hairpin residue Arg357, which is not conserved in TC and IF (Figure 4.2C, D and Suppl. Figure 4.7), forms a unique hydrogen bond to the ring oxygen of the ribose moiety of CNCbl. Together with the side chains of Trp359 and Tyr362 it further stabilises the DMB moiety by hydrophobic contacts. The stabilisation of this site is complemented by a series of water-mediated hydrogen bonds to the phosphoryl-moiety formed by the main-chain amides of the β-hairpin and by Glu71 and Gln123 of the α-domain (Figure 4.1D).

4.2.3 Binding of HC to Cbi

To understand the molecular details that confer low substrate specificity to HC we determined the crystal structure of HC in complex with Cbi (Figure 4.3A).

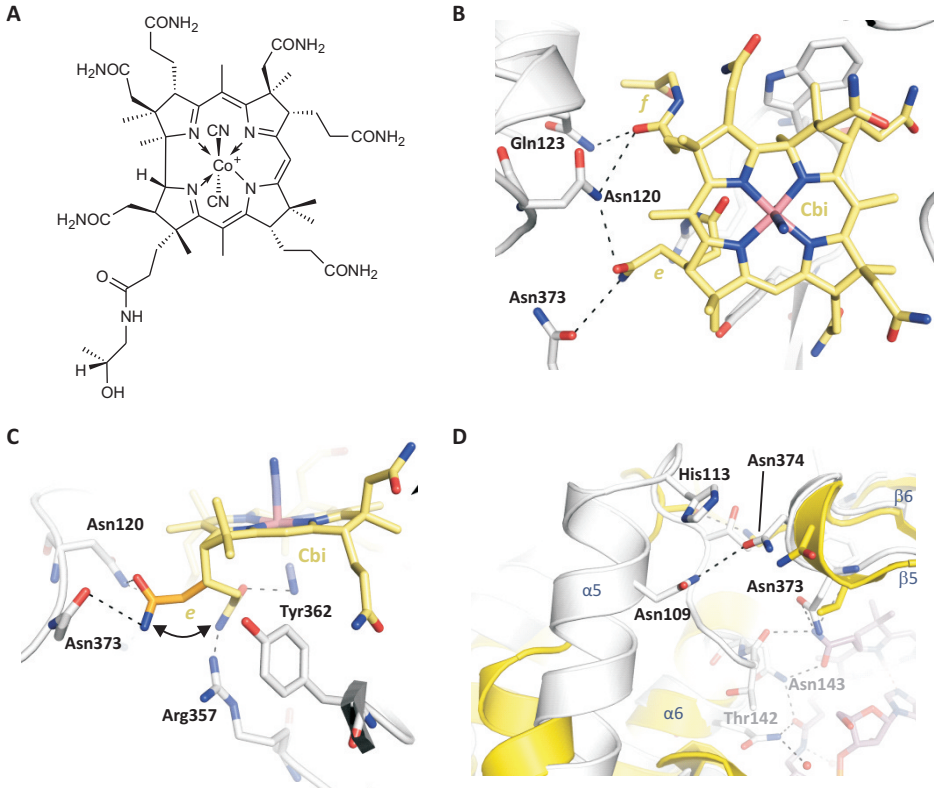

Figure 4.3 Specificity determinants for Cbi binding. **A**. Chemical structure of Cbi. **B**. Stabilisation of the *e*- and *f*-side chains of Cbi. Structure cartoon of HC in white, Cbi in yellow stick representation. Critical hydrogen-bond interactions are highlighted in dashed lines. **C**. *e*-side chain flip at the lower axial side of Cbi. The *e*-propionamide can adopt two different conformations. The "flip-in" conformation is further stabilised by two hydrogen-bonds to Arg357 and the CN-molecule. **D**. Interactions at the α5-β5-β6-site. The structures of HC (white) and IF (yellow) are in cartoon representation and are superimposed on their β-domains. Critical residues and interactions are represented in stick and dashed lines, respectively. Secondary structure elements are labelled in blue.

No differences are observed at the upper axial side. The corrin ring of Cbi is stabilised by the same interactions as described for CNCbl (Figure 4.3B and Figure 4.1C and D). Of particular importance are the interactions observed at the *e*-side chain of Cbi. In addition to a different density observed for the CN-moiety at the 5th coordination site of Cbi, a secondary density blob is visible in the proximity of the CN-moiety, which accounts for an alternative conformation of the *e*-propionamide side chain (Figure 4.3C), filling up the space otherwise

occupied by the DMB-group. In this alternative conformation the *e*-propionamide is in ideal hydrogen-bonding distance to the guanidine group of Arg357. Both conformations are equally occupied, so both were modelled with half occupancy each.

An additional prominent interaction, which confers additional stability to the complex (Figure 4.3D), is observed at the interdomain contact between α5 and the β5-β6-turn of HC involving the three residues Asn109, His113 and Asn374. This interaction can neither occur in TC nor in IF due to a shorter β5-β6-loop (TC, Suppl. Figure 4.7) and a shorter α5 (IF two turns, TC one turn shorter) which is tilted away from the β-domain.

4.2.4 Protein surface properties

The relative domain orientation varies among HC, hTC, bTC and IF and leads to variable tight packing of the domains. To analyse the surface properties at the interdomain interfaces, we calculated the electrostatic surface potential and the total buried surface areas for the individual transport proteins (Figure 4.4).

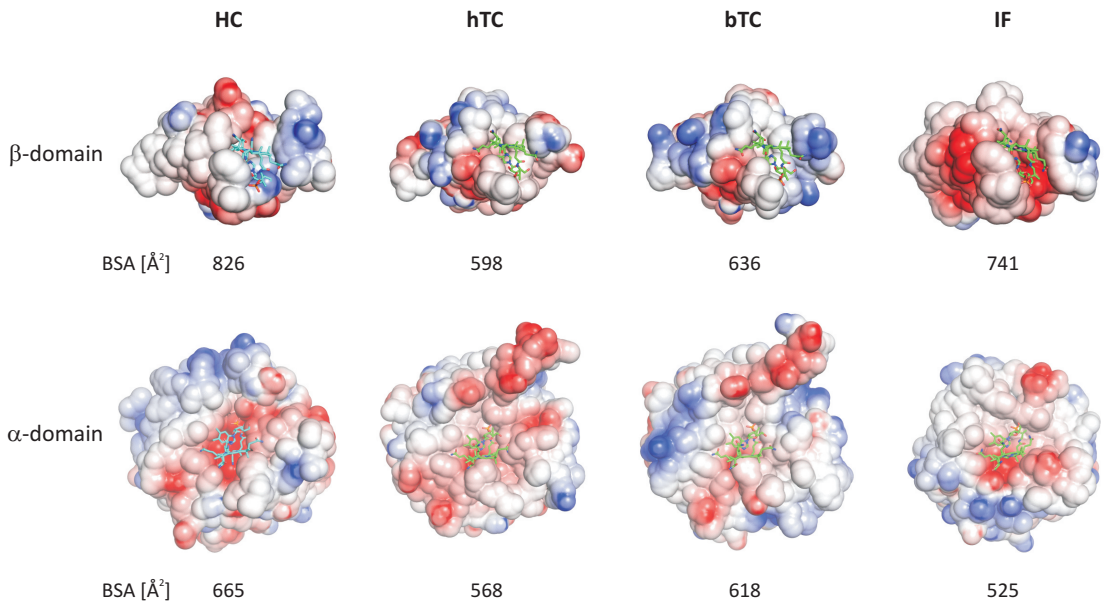

Figure 4.4 Electrostatic surface potential and total buried surface area of different Cbl-transport proteins. The electrostatic surface potential was calculated for the individual α- and β-domains and contoured at +/- 3.5 kT. The buried surface contributions of the individual domains are listed. The total buried surface area are for HC 1491, hTC 1166, bTC 1254 and IF 1266 Å^2.

No clear trend in electrostatic contribution is visible. However, the total buried surface area at the HC interface is larger compared to the other transporters. This would account for more interactions and even more shape complementarity between the two domains.

4.2.5 Binding of HC to *b*-side chain modified derivatives

After the elucidation of the crystal structure of TC and IF [11,12] the crystal structure of HC completes the puzzle of the three transport proteins. Having all three crystal structures at hand allows a deeper understanding of how Cbl, and especially Cbl derivatives, interact with their transport proteins consequentially leading to a much more rational design of Cbl derivatives.

Cbl is, despite its structural complexity, very amenable to selective modifications at various sites [66] and different modifications for the different sites had been described extensively [74,82]. With the crystal structure of TC, it was shown that the 5'hydroxyl group on the ribose was the only site where attachment of a larger ligand would not lead to disturbing interactions with the protein [11]. Modifications on the *b*-, *c*-, *d*- and *e*-side chain were found to result in large variation in their binding ability. While *d*- and *c*-acetamide conjugates prohibited binding to TC, *e*-propionamide side chain conjugates had only little effect on binding [70,74].

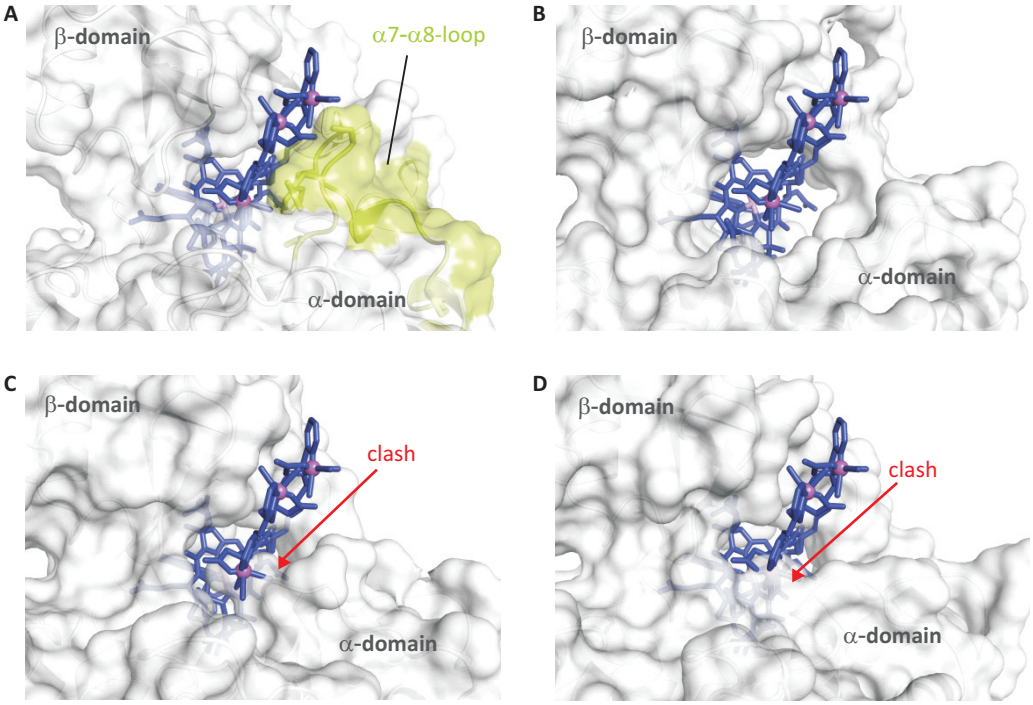

Figure 4.5 Specificity determinants of PAMA(4)-Cbl binding. **A**. Surface representation of the PAMA(4)-Cbl derivative bound to HC modelled in three different orientations. HC is in white, the PAMA(4)-Cbl in blue, the short helix α7 including the 3/10 helix and the α7-α8 loop are highlighted in green. The loop residues in close contact with the ligand are in stick representation. **B**. Surface representation of IF with modelled PAMA(4)-ligand. The binding site is wide and shows no steric hindrance for the binding of PAMA(4)-Cbl. **C**. and **D**. same superposition with hTC and bTC. In both cases the binding site is occupied by one or two histidines, which likely could clash with the PAMA(4)-ligand.

A recent study by Waibel *et al.* used *b*-side chain conjugated ^{99m}Tc-labelled Cbl derivatives for tumour targeting studies in mice [75]. Interestingly, by introducing different linker chain lengths between the radiolabel and the Cbl, the *b*-propionamide conjugate was modified towards its ability to bind TC. A linker chain length consisting of six methyl residues (PAMA(6)-Cbl) bound to all three transport proteins, whereas a linker with a chain length consisting of only four methyl residues (PAMA(4)-Cbl) abolished binding to TC.

We modelled the PAMA(4) ligand with different linker conformations into the binding site of HC and compared it to the binding sites of hTC, bTC and IF (Figure 4.5).

While HC and IF offer a wide groove to accommodate the ligand, the active site of TC is narrowed by the presence of the His residues. Moreover, HC can allow structural adaptation with the flexible H7-H8 loop.

4.3 Discussion

The data presented in this study significantly advance our understanding towards the ligand specificity among human Cbl transport proteins by unravelling the molecular details of substrate recognition by HC. It is well known that HC is the least specific Cbl transport protein, binding to a diversity of Cbl derivatives and analogues [31,60]. However, the molecular details that confer this broad ligand tolerability to HC are poorly understood. Our data provide a rational explanation how the structure of HC permits binding of Cbl derivatives with high affinity.

First and most important, the hydrogen bonds formed by the non-conserved residues Asn120, Asn373 and Arg357 to both the *e*- and *f*-side chains of the corrin ring stabilise ligands with missing or modified DMB moiety. While in TC the *f*-side chain is only stabilised by one hydrogen bond (Gln138), no hydrogen bond formation to the *f*-side chain is found in IF. Interestingly, and according to the sequence alignment (Suppl. Figure 4.7), Asn135 is in a position to form the analogous hydrogen bond of mouse TC (mTC) that is known to bind Cbi. These structural findings correspond to the Cbi binding abilities found in literature of the following order HC >> mTC > TC > IF [72,149]. Furthermore, Arg357 stabilises the “flip-in” conformation of Cbi in HC with a hydrogen bond, what cannot occur in the other transport proteins.

Secondly, at the lower side of Cbl, the three bulky side chains of Arg357, Trp359 and Tyr362 provide hydrophobic and polar contacts to the benzimidazole moiety. Moreover, the guanidine moiety of Arg357 contacts the oxygen of the ribose.

Although the three large hydrophobic residues Arg357, Trp359 and Tyr362 have already been identified as a possible feature for binding to the nucleotide-lacking Cbi [70], the role of Arg357 in stabilising the “flip-in” conformation of Cbi was not predicted, neither was the stabilising hydrogen bond of Asn120 to the *f*-side chain.

Furthermore, the lack of a cobalt-coordinating histidine residue at the upper axial side is compensated by the presence of Phe156 at the tip of the β-hairpin on the flexible H7-H8-loop. This loop is much longer compared to TC and IF as a consequence of helix break by Pro149 in H7. The resulting flexibility at the upper axial side allows for structural rearrangements to accommodate a larger variety of ligands, comparable to a cantilever function.

Finally, the relative α-β-domain orientation in HC results in a more compact structure compared to TC and IF (total buried surface areas: HC > IF $\approx$ bTC > hTC). Based on our analysis, it is unlikely that the stabilisation occurs through electrostatic interactions, but rather by higher shape complementarity in HC.

Altogether, these findings extended the insight into the complexity of Cbl binding to the transport proteins, with special regards to the low ligand specificity of HC and may therefore be useful to a more rational design of new Cbl derivatives in the future.

4.4 Materials and methods

4.4.1 Protein expression and purification

Recombinant human HC (rhHC) was prepared as described previously [28] (see section 3.2.1). Briefly, rhHC was expressed in HEK293 GnTI- cells purified over a Ni-NTA affinity column and gel filtration chromatography using a Superdex 200 column equilibrated in 100mM HEPES pH 7.5, 20mM NaCl. Purification tags were removed with thrombin (Sigma). For the crystallisation and peptide mapping the protein was subjected to deglycosylation using either Endoglycosidase H or Endoglycosidase F1 (New England Biolabs).

4.4.2 Crystallization and structure determination

For crystallization, proteins were supplied with a 1.5 molar excess of cyanocobalamin (Sigma) or dicyanocobinamide (Sigma), respectively, and concentrated to 0.8 mM (36 mg ml^{-1}). Proteins were mixed in a 1:1 ratio with the precipitant and crystallised by the sitting drop vapour diffusion technique at a temperature of 4°C. Hexagonal pink crystals appeared in 50% PEG 400, 0.2 M $MgCl_2$ and 0.1 M sodium cacodylate pH 6.5 after 5-7 days and had grown to full size after 15 days. Crystals were flash frozen in liquid nitrogen without additional cryoprotecting agents.

Diffraction data were collected at beam line X06SA of the Swiss Light Source (Villigen, Switzerland) at cryogenic temperature (100 K). Data were processed with XDS [164]. Molecular replacement search was conducted with PHASER [165] using search models based on database entries 2PMV (human intrinsic factor) and 2BB5 (human transcobalamin). Automated model rebuilding was performed with PHENIX [166] and manual model rebuilding was carried out with COOT [167]. Rigid body refinement was followed by restrained refinement together with TLS refinement in PHENIX [166]. Ligands were manually placed in the difference maps and included in refinement. Suppl. Table 4.1 compiles processing and refinement statistics. Model geometry was analysed with MOLPROBITY [168] and protein structures were visualized using PYMOL (DeLano Scientific).

Supplementary Data

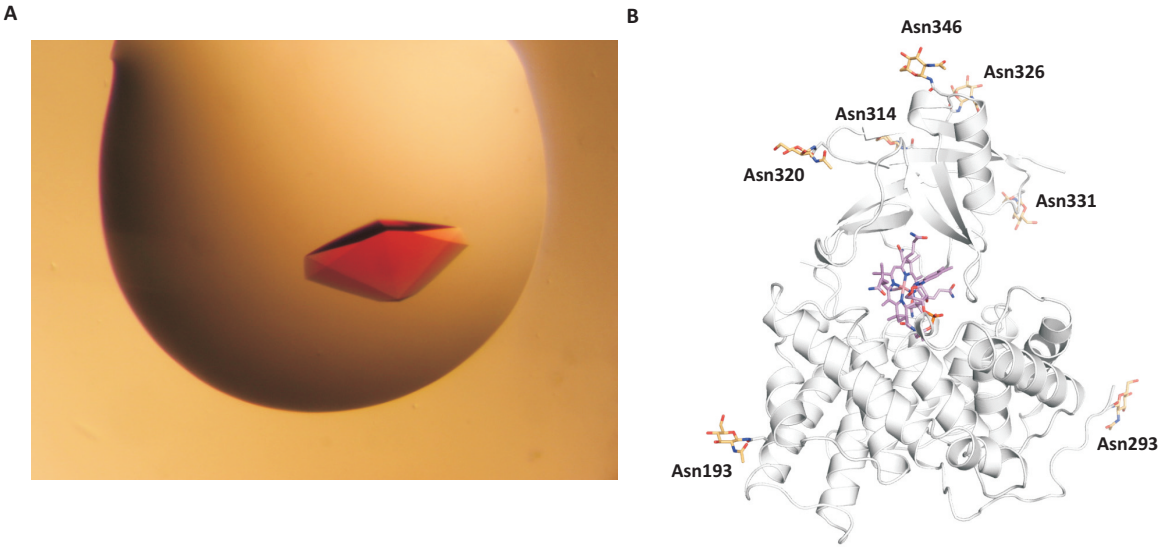

Suppl. Figure 4.6 Crystal and overall structure of glycosylated HC. **A.** Crystal of rhHC **B**. Cartoon representation of HC. The Asn residues carrying a N-acetylglucosamine molecule are shown in stick representation. The modelled sugar moieties are in orange. The bound CNCbl ligand is in violet.

Suppl. Table 4.1 Data collection and refinement statistics.

	Data collection[a]	
	HC-CNCbl	**HC-Cbi**
Space group	$P6_4$	$P6_4$
Cell dimensions		
a, b, c (Å)	149.9, 149.9, 57.5	150.4, 150.4, 60.3
Resolution (Å)	49.0 – 2.35 (2.4 -2.35)	49.2 – 3.0 (3.1 – 3.0)
R_{meas} (%)	10.1 (156.1)	5.8 (176.2)
R_{pim} (%)	3.5 (49.4)	2.0 (66.4)
CC_{half}[c]	99.8 (68.9)	100 (62.6)
<I>/<σI>	13.6 (1.9)	28.5 (1.4)
Completeness (%)	100 (100)	100 (100)
Redundancy	10.2 (10.6)	10.3 (10.8)

	Refinement	
	HC-CNCbl	**HC-Cbi**
Resolution (Å)	49.0 – 2.35	49.2 – 3.0
No. unique reflections	31012 (1565 in test set)	15820 (795 in test set)
R_{work}/R_{free} (%)	19.9 / 24.0	22.0 / 26.4
Average B-factors (Å^2)		
complex	63.5	106.0
solvent	65.1	89.1
ligand	46.9	94.8
Wilson B-factor	55.1	105.7
Root mean square deviation from ideality		
Bond length (Å)	0.009	0.003
Bond angles (°)	1.209	0.773
Ramachandran statistics[b]		
Favored regions (%)	96.7	94.7
Allowed regions (%)	2.5	4.5
Outliers (%)	0.8	0.8

[a]Highest shell statistics are in parentheses. [b]As defined by MOLPROBITY [168]. [c]As defined by Karplus & Diederichs [169].

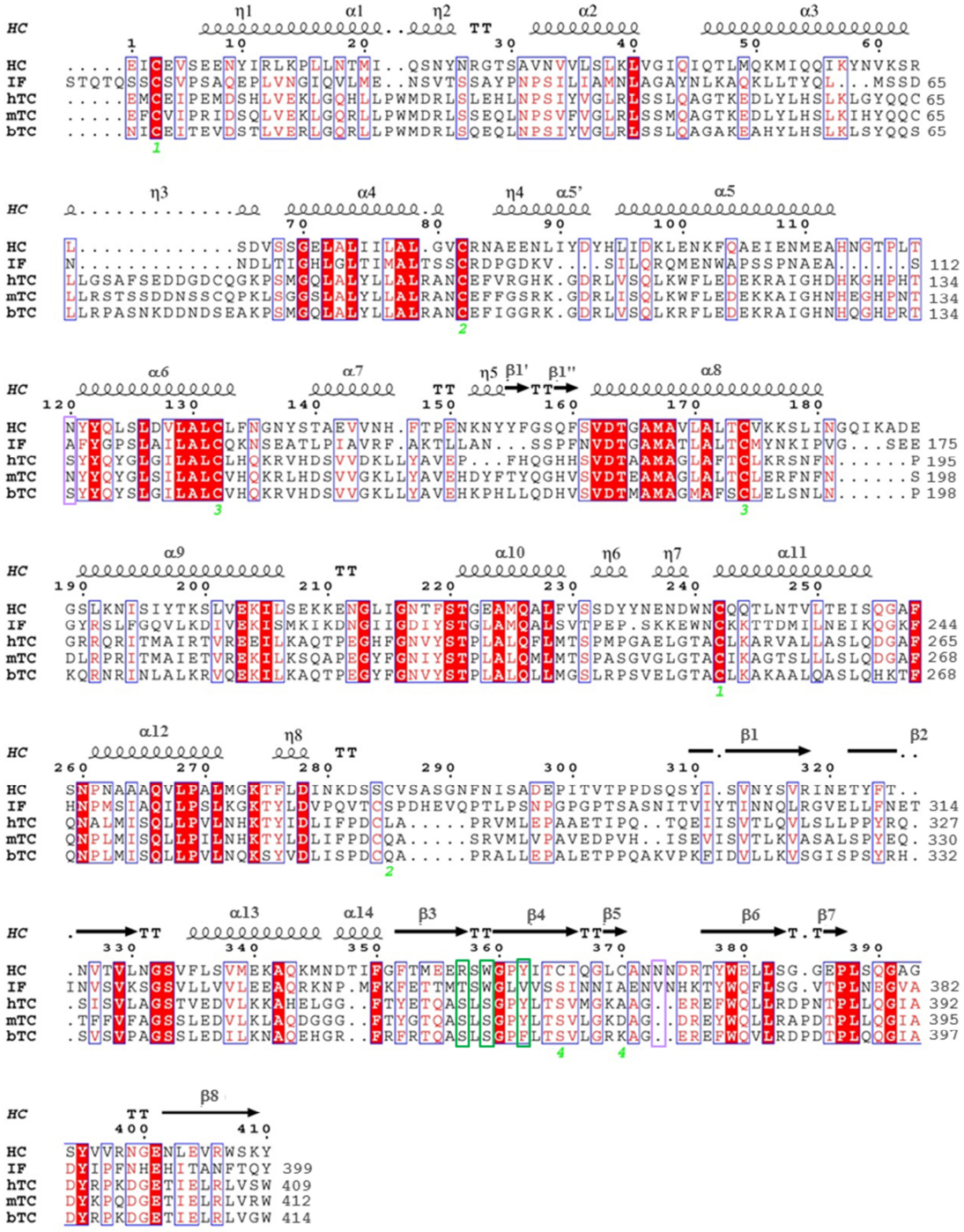

Suppl. Figure 4.7 Multiple sequence alignment of HC, hTC, bTC and IF. The secondary structure elements corresponding to HC are on top of the sequences. Boxed residues represent critical residues for ligand binding, which are discussed in the text. The alignment was prepared using Espript [170].

5 Ranking Cobalamin Derivatives using Differential Scanning Fluorimetry

Evelyne Furger, Kai Zhou

Author contributions:

Evelyne Furger carried out the DSF measrements.

Kai Zhou synthesised the peptidic Cbl derivatives.

5.1 Introduction

In the human body, Cbl is transported by three transport proteins: haptocorrin (HC), transcobalamin (TC) and intrinsic factor (IF) [14]. These proteins are responsible for the absorption, transport and cellular uptake of Cbl and are therefore vital for Cbl homeostasis.

Although the three transport proteins share a similar tertiary structure [70] they display different abilities to bind to the natural Cbl analogues and also discriminate binding of synthetic Cbl derivatives [26,60,171]. HC is the least specific transport protein and is able to bind not only to slightly modified Cbl derivatives, but also to Cbl analogues that are structurally very different to Cbl, such as those that lack the nucleotide moiety like Cbi [60,70]. Cbl binds exceptionally quickly and with femtomolar (10^{-15} M) affinity to all three transport proteins [69,71,72]. Accurate determination of such high affinity constants is difficult due to technical limitations of the different methods [172]. This includes methods such as isothermal titration calorimetry, which is the primary tool for characterising interactions based on thermodynamic parameters. The largest dissociation constant that could reliably be measured is approximately 10^{-9} M, because with increasing affinity, the protein concentration has to be reduced, leading to difficulties in signal detection [173].

As a consequence, reported affinity constants for the binding of Cbl to its transport proteins are controversial with an extraordinary dispersion ranging from K_d 10^{-9} to 10^{-15} M [25,26,72,125,174,175].

In order to develop new Cbl derivatives for targeted delivery, it is of major importance to have sufficient knowledge about the interaction with the specific protein carriers because they account for the final distribution within the body. An easy and commonly used method of estimating the ability of a Cbl derivative to bind to a transport protein is a competitive binding assay. Here, a corrinoid or radioligand competes with Cbl for binding to a transport protein over a range of Cbl concentrations, allowing the realtive affinity of the analogue ($K_{analogue}/K_{Cbl}$) to be calculated [60,176]. However, the obtained K_d values should be handled with care and deviate from the K_d values obtained with the spectrophotometric method used by Fedosov [71,72].

Differential scanning fluorimetry (DSF) was initially developed for drug discovery as it allows rapid screening of compound libraries for identification of ligands of target proteins [177]. It is a fluorescence-based method that has been used to measure changes in the stability of

proteins, for example as a result of ligand binding [178]. By binding to a protein, a ligand can stabilise the protein's native state, which results in a higher melting temperature (T_m). When a protein unfolds, hydrophobic sites become exposed. DSF monitors the binding of the fluorescent dye Sypro® Orange to hydrophobic sites that become available upon thermal unfolding of the protein, resulting in a large increase in fluorescence [179].

In the present study, we describe the ability of new Cbl derivatives to bind to Cbl transport proteins using DSF. In order to validate the method, we analysed the ligand-induced changes in the thermal unfolding of the protein using human HC, human TC, human IF and mouse TC (mTC) and the ligands cyano-Cbl (CNCbl) and cobinamide (Cbi) representing a biologically active form of Cbl and a Cbl analogue, respectively. We compare the obtained thermal shift values with affinity constants that were calculated in an elaborate study by Fedosov *et al*. [72]. Here, a stopped-flow spectro-photometer was used in order to measure the increase or decrease in the quantum yield of a fluorescent Cbl derivative (CBC) upon binding and dissociation to the Cbl transport proteins. With these measurements the binding and dissociation kinetics of Cbl and Cbl analogues could be determined.

Furthermore, a set of newly synthesised Cbl derivatives with artificial peptidic linkers at the "lower" face of the corrin ring were screened for their binding to the different transport proteins.

5.2 Results

5.2.1 Determination of T_m of HC, TC, IF and mTC

Incubation of the recombinant proteins HC, IF, TC and mTC with the fluorescent dye Sypro® Orange over a temperature gradient (25°C-95°C) resulted in sharp sigmoidal curves for all four proteins, indicating a two state transition from the native to the unfolded state (Figure 5.1, insets). T_m values were calculated by determination of the first derivative of the measured fluorescence curve, where the inflection point becomes the maximum (Figure 5.1). Thermal unfolding of IF, TC and mTC showed a second, less populated transition at approximately 50°C (Figure 5.1). This was due to degradation of the protein and could be abolished by using freshly prepared protein (not shown).

The different thermal stabilities of the native transport proteins are shown in Table 5.1. HC shows the highest T_m value (65°C) indicating it to be the most stable protein; in contrast mTC was already thermally unfolded at 55°C. IF and TC show very similar melting temperatures (approximately 58°C). These findings were consistent with the observations at the purification level (see section 3.2.2 and 3.2.3) with HC being the most robust protein in contrast to the faster degrading TC, mTC and IF [180] (see section 3.2.2 and 3.2.3). The widths of the peaks in Figure 5.1 are directly related to the enthalpy of unfolding (ΔH_u) of the protein [181]. The broader peak for IF reflects a significantly lower enthalpy of unfolding compared to the other three proteins.

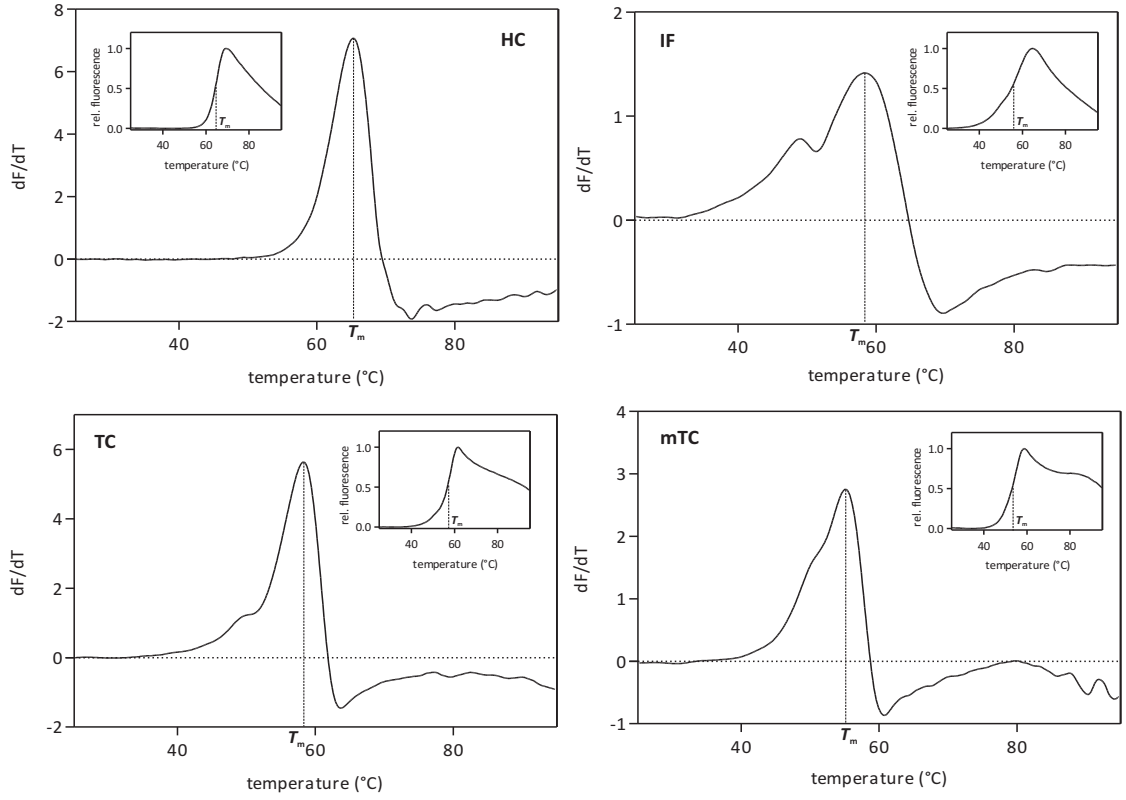

Figure 5.1 Thermal unfolding of apo-HC, TC, IF and mTC. Analysis of the melting curves of the different Cbl transport proteins. The graphs show the first derivative of the raw data (raw data plots in the insets) for the different proteins. The inflection point of the transition corresponds to T_m.

Table 5.1 Melting temperature (T_m) of the apo proteins

Proteins	T_m (°C)
HC	65.27 ± 0.04
IF	58.57 ± 0.32
TC	58.43 ± 0.24
mTC	55.28 ± 0.16

1 µM of protein was incubated in the presence of 5x Sypro® Orange with an increase of temperature from 25-95°C. n = 2 measured in triplicates.

5.2.2 Ligand-induced stabilising effect on Cbl transport proteins

The change in the T_m of a protein upon ligand binding is dependent on both the ligand concentration and its binding affinity [182,183]. In order to determine the concentration-dependent stabilising effect of CNCbl and Cbi on the transport proteins, we measured the T_m of the four proteins in the presence of different concentrations of the ligands (Figure 5.2 and Figure 5.3). In the case of large ligand-induced shifts of T_m (HC-CNCbl, TC-CNCbl, mTC-CNCbl), adding ligand at concentrations lower than the protein concentration resulted in the appearance of two peaks, indicating the presence of both native and ligand-bound protein. In smaller ligand-induced shifts of T_m (IF-CNCbl) it appears as just one shifting peak. In all four series of experiments, T_m was constant for ligand concentrations > 5 µM.

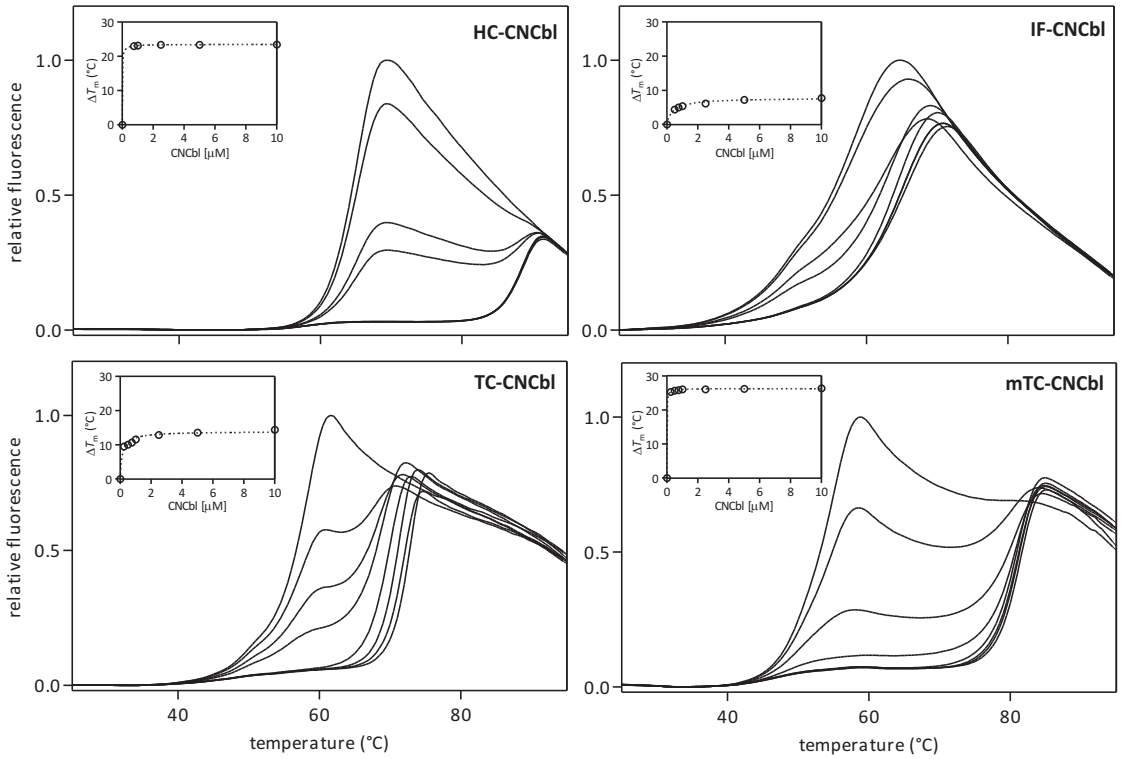

Figure 5.2 Thermal stabilisation of Cbl transport proteins by CNCbl binding. The proteins (1 µM) were incubated in the absence or presence of different concentrations of CNCbl (0.25-10 µM). Each unfolding curve was measured in triplicates. The plots in the insets show ΔT_m versus [CNCbl] and fitting (dashed lines) to a hyperbolic saturation equation.

The presence of CNCbl resulted in a recognisable shift of T_m to higher temperature for all recombinant proteins, indicating a stabilising effect of CNCbl on the proteins (Figure 5.2). This is in contrast to Cbi, where only small shifts were obtained for TC and even smaller for IF (Figure 5.3). From earlier equilibrium studies it is known that CNCbl binds to all Cbl transport proteins in humans as well as in mice. This is in contrast to Cbi, which binds poorly to TC and IF [72,149].

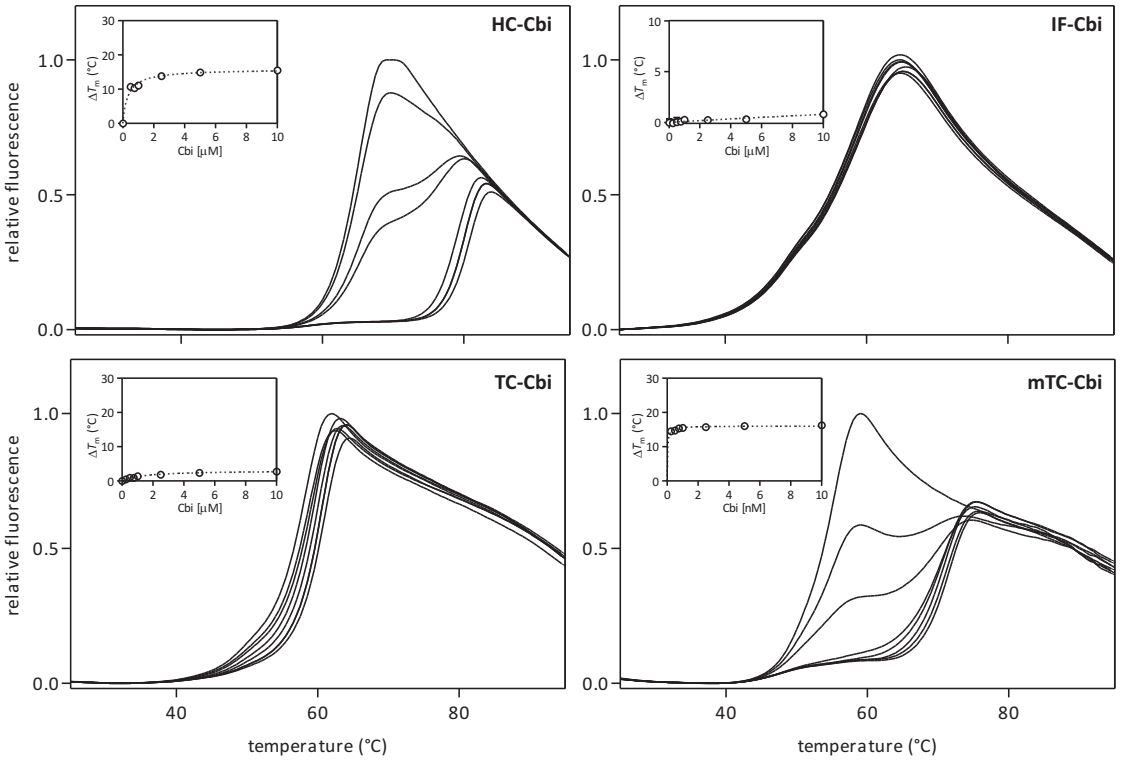

Figure 5.3 Thermal stabilisation of Cbl transport proteins by Cbi binding. The proteins (1 µM) were incubated in the absence or presence of different concentrations of CNCbl (0.25-10 µM). Each unfolding curve was measured in triplicate. The plots in the insets show ΔT_m versus [CNCbl] and fitting (dashed lines) to a hyperbolic saturation equation.

The concentration of ligands to achieve half-maximal protein stabilisation (AC_{50}) and the maximal change in T_m at saturation ($\Delta T_{m\ max}$) values were estimated for CNCbl and Cbi with each transport protein from the plot ΔT_m versus ligand concentration (Figure 5.2 and Figure 5.3 insets) and summarised in Table 5.2. For IF-Cbi, no reasonable AC_{50} value was obtained due to very low ΔT_m values. Thermal stabilisation of HC-CNCbl and mTC-CNCbl seemed to be similarily high ($\Delta T_{m\ max}$ 23.50 ± 0.04°C and 26.28 ± 0.03°C respectively) in contrast to the much smaller effect seen for TC and IF ($\Delta T_{m\ max}$ 13.94 ± 0.23°C and 7.75 ± 0.14°C respectively) (Table 5.2). Interestingly, a small AC_{50} value corresponds to a high $\Delta T_{m\ max}$ value, indicating that the affinity of the ligand to the protein is reflected in its ΔT_m value. While reported K_d values for CNCbl are very similar among the four transport proteins, the ΔT_m obtained for IF differs significantly from the other proteins. In DSF the ΔT_m is dependent on both the enthalpy and entropy of the binding and therefore different ΔT_m values can result when binding to different proteins, even if K_d values are similar. Despite a very similar overall structure, IF is less stabilised by CNCbl binding due to the thermodynamic

properties of the binding reaction. In an early study by Hippe [184], it was shown that binding of CNCbl to IF is exothermically driven (ΔH = -22.7 kcal/mole and ΔS = -31 cal/degree per mole), whereas binding to HC and TC is entropically driven (HC: ΔH = + 4.2 kcal/mole and ΔS = 66.86 cal/degree per mole; TC: ΔH = -1.01 kcal/mole; ΔS = 49.36 cal/degree per mole), indicating that hydrophobic interaction is less important for binding to IF in contrast to binding to HC and TC. Entropically driven binding results in larger T_m [185], therefore binding of CNCbl to TC and HC resulted in much larger shifts of T_m compared to CNCbl binding to IF.

As a consequence, the ΔT_m values of Cbl ligands obtained with two different transport proteins cannot be directly compared to estimate binding affinity. However, ligands with similar physicochemical properties (such as the corrinoids) might still be ranked according to the measured ΔT_m values for a given Cbl transport protein.

Table 5.2 Parameters for thermal stabilisation of HC, TC, IF and mTC by ligand binding

	Ligands			
	CNCbl		Cbi	
Proteins	**AC_{50} (µM)**	**$\Delta T_{m\ max}$ (°C)**	**AC_{50} (µM)**	**$\Delta T_{m\ max}$ (°C)**
HC	0.02 ± 0.00	23.50 ± 0.04	0.35 ± 0.03	15.86 ± 0.29
TC	0.16 ± 0.02	13.89 ± 0.23	1.40 ± 0.16	3.01 ± 0.12
IF	0.42 ± 0.04	7.75 ± 0.14	n.d.	n.d.
mTC	0.01 ± 0.00	26.26 ± 0.03	0.03 ± 0.00	16.07 ± 0.10

Each value was estimated by analysing DSF data; n.d. not determined

Table 5.3 Equilibrium dissociation constants (K_d) at 20°C and pH 7.5 [72]

	K_d [M]	
Proteins	**CNCbl**	**Cbi**
HC	$6 \cdot 10^{-15}$	$6 \cdot 10^{-15}$
TC	$4 \cdot 10^{-15}$	$5 \cdot 10^{-9}$
IF	$5 \cdot 10^{-15}$	$4 \cdot 10^{-8}$

5.2.3 Screening of peptidic Cbl derivatives for transport protein binding

A series of novel Cbl derivatives were screened for their ability to bind to the human transport proteins. In these compounds, the connection between the corrin ring and the DMB base is replaced by a peptidic linker (Suppl. Figure 5.5). The compounds are currently

evaluated as potential inhibitors of Cbl-dependent enzymes. The peptidic linker allows modulation of a “base on/base off” state which is important for the binding to the different proteins [162].

For analysis of ligand binding, the protein should be saturated with ligand. From the above measured values for CNCbl and Cbi we hypothesised that ligand concentrations ≥ 2.5 times above the concentration of protein should fulfil this condition.

In order to rank naturally occurring Cbl derivatives (Figure 5.4A), we determined the ΔT_m for all four transport proteins. In addition to the measurements above we included H_2OCbl.

All ligands bound to the different transport proteins, with Cbi showing the smallest ΔT_m on IF and TC. Interestingly, mTC showed a very similar ranking of the ligands to TC (H_2OCbl > CNCbl > Cbi) but with a much larger ΔT_m comparable to those obtained for HC. The binding of ligands to mTC is therefore suggested to be entropically driven. Interestingly, H_2OCbl induced a larger ΔT_m than CNCbl with TC and mTC, which could be explained by the cobalt-ion coordination of H_2OCbl by a histidine residue elucidated with the TC crystal structure [11]. The same cobalt coordination was proposed for mTC based on a homology model (see section 3.2.6). As already seen in Figure 5.3, Cbi shows only a small stabilising effect on TC and IF, which is in agreement with previous studies conducted on Cbi. The stabilising effect of Cbi on mTC confirms the binding study conducted by Hygum *et al.* [149] where the apparent dissociation constants of native mTC were determined using an isotope dilution method [60], generating a binding affinity for Cbi that was approximately 10-fold less than its affinity for CNCbl. In contrast, TC displays a binding affinity for Cbi that is approximately 1000-fold less than its affinity towards CNCbl.

In Figure 5.4B, C and D, 13 different Cbl derivatives were tested for their ability to bind to the three human transport proteins. These derivatives are Cbl mimics with a peptide backbone that show tuneable coordination and electrochemical properties [67,186] (Suppl. Figure 5.5).

All peptidic Cbl derivatives with the exception of compound 9 bound strongly to HC, resulting in a ΔT_m of >10°C. Compound 9 was the only compound that did not show a stabilising effect on any of the proteins and thus does not bind to a transport protein under the conditions used here. This is probably due to its structural rigidity, as it contains a proline-pyridine moiety that could result in steric hindrance in the binding pocket of the

protein. By ranking the peptidic derivatives according to the induced ΔT_m, the binding pattern of IF and HC to these compounds are very similar. Only compound 3 deviated from the pattern, while being the derivative whose binding induced the highest ΔT_m in HC, it showed a much smaller effect upon binding to IF. A completely different case is found with TC where almost none of the derivatives (with the exception of compound 11) showed a binding ability comparable to CNCbl or H_2OCbl. These compounds are more likely to bind to TC with a similar affinity to Cbi. Notably, compound 3 and compound 13 induced even lower ΔT_m than Cbi.

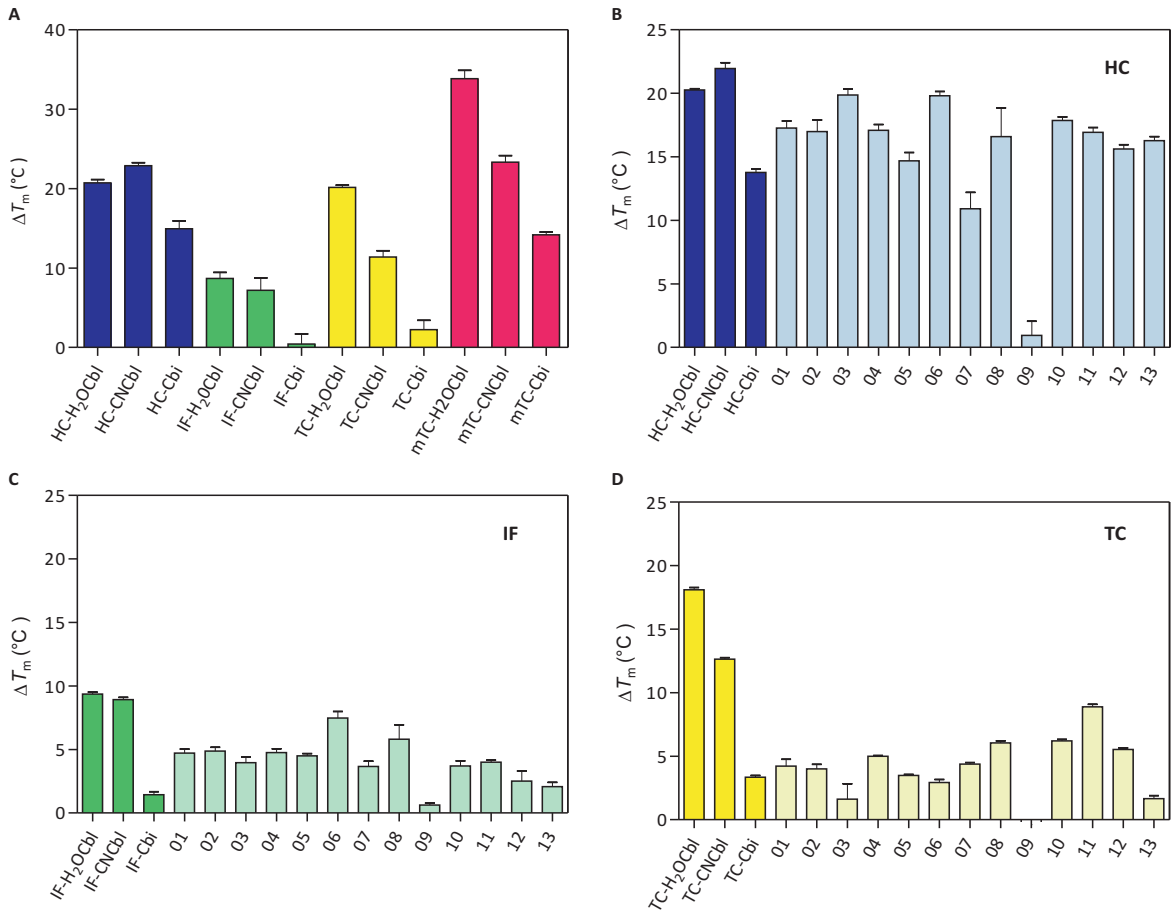

Figure 5.4 Comparison of ΔT_m of human and mouse Cbl transport proteins with different ligands. **A**. The T_m values of HC, TC, IF and mTC were determined either alone (300 nM) or in the presence of an excess (≥ 1 µM) of H_2OCbl, CNCbl and Cbi. The increase in T_m values of the ligand-protein complexes relative to the unbound proteins (ΔT_m) is presented. **B-D.** New synthesised Cbl derivatives (9.5 µM) were tested for their binding to the three human transport proteins (HC, IF and TC) (1.5 µM). H_2OCbl, CNCbl and Cbi (9.5 µM) were measured for comparison.

5.3 Discussion

The femtomolar affinities of Cbl transport proteins for their ligands hinders the measurement of reproducible, accurate binding constants. A simple, inexpensive and robust method to determine the ability of different Cbl derivatives to bind to Cbl transport proteins would facilitate the development of specific binding Cbl derivatives, allowing small libraries of structurally related Cbl derivatives to be screened for their binding strength and their selectivity towards the different transport proteins. Such studies can give valuable insight into structure-binding relationships and may be used to identify lead compounds for development of Cbl-derived inhibitors or tumour targeting agents.

The goal for the series of Cbl derivatives was to screen those containing peptidic linkers that would allow their “base on/base off” state to be modulated. This could potentially lead to the ability to fine-tune the reactivity of these derivatives in cofactor-catalysed reactions [162,186].

The rather low binding ability of the tested peptide Cbl derivatives to TC implies that for sufficient delivery to cells via the TC receptor CD320, compound 11 should be selected as a lead compound as it had the highest binding affinity. This probably needs to be further optimised for efficient binding to TC.

DSF not only requires small amounts of proteins and ligands, it is independent of the availability of ^{57}Co-Cbl, which is hardly produced anymore since the routinely performed clinical Schilling test has been replaced. This is in contrast to the commonly used competitive binding assay [60]. Furthermore, radioactive waste management can be avoided by use of DSF over a radioisotope dilution assay. Another advantage of DSF is that during the measurement the protein and the ligand are in solution and no difference in entropic properties, such as with surface plasmon resonance measurements are assumed [187].

Although affinity constants can potentially be calculated by measuring the T_m values at various ligand concentrations in order to generate a concentration response curve [182], knowledge of the thermodynamics of protein stability is still required. Furthermore, DSF is an indirect method; therefore the binding constants must be estimated and cannot be measured directly [188].

Nevertheless, ranking the different Cbl derivatives based on their measured ΔT_m values can be used in order to determine the ability of a new Cbl derivative to bind to a given transport protein, and the values can be compared to ligands with a known binding behaviour (e.g. CNCbl or Cbi).

Finally, the four transport proteins have very similar overall folds, but clearly different modes of ligand binding. Here, we showed that due to different thermodynamic properties of both unfolding and ligand binding, IF differs from the other transport proteins. As a consequence, thermal stabilisation by Cbl ligands is much smaller for IF. While the ΔT_m values are generally lower than for the other transport proteins, they were still high enough to allow ranking of the peptidic Cbl derivatives. Overall, the simplicity and general applicability of thermal shift assays make this technique attractive for identification and ranking of non-selective and selective Cbl derivatives [189].

5.4 Materials and Methods

5.4.1 Recombinant proteins

The recombinant proteins HC, TC and mTC were expressed and purified as described in sections 2 and 3. Recombinant IF (Cobento, Aarhus, Denmark) was kindly provided by Prof. Ebba Nexø (University hospital Aarhus, Denmark). Protein concentration was measured with a NanoDrop ND1000 spectrophotometer (ThermoScientific).

5.4.2 Cbl derivatives

The peptidic Cbl derivatives were kindly provided by Dr. Kai Zhou and Dr. Felix Zelder, University of Zürich, Switzerland [67]. Cobinamide dicyanide and cyanocobalamin were purchased by Sigma Aldrich (Switzerland).

5.4.3 Differential scanning fluorimetry

A Rotor-Gene cycler (Rotor-Gene 5plex HRM, Qiagen) was used for protein stability measurement by differential scanning fluorimetry (DSF). Stability measurements were performed in phosphate buffered saline (PBS). SYPRO® Orange (Invitrogen) was used at 5x end-concentration. Protein concentration of about 0.3-1.5 µM and excess ligand concentration of approximately 1.5-9.5 µM were used. We programmed HRM to increase the temperature from 25°C to 95°C, collecting the data every 0.5°C, with an equilibration time of 2 seconds. T_m values were determined using the RotorGene Q Software Version 2.0.2.4 (Qiagen).

The concentration of ligands to achieve half-maximal protein stabilisation (AC_{50}) was determined by fitting the plot of changes in T_m (ΔT_m) versus ligand concentrations ([L]) to the equation of $\Delta T_m = \Delta T_{m\ max} \cdot [L]/(AC_{50} + [L])$, where $\Delta T_{m\ max}$ is the maximal change in T_m at saturation [178].

5.4.4 Data analyses

GraphPad Prism 5 software (GraphPad Software Inc., California, USA) was used for the calculations of ΔT_m , AC_{50} and $\Delta T_{m\ max}$ values.

Supplementary Data

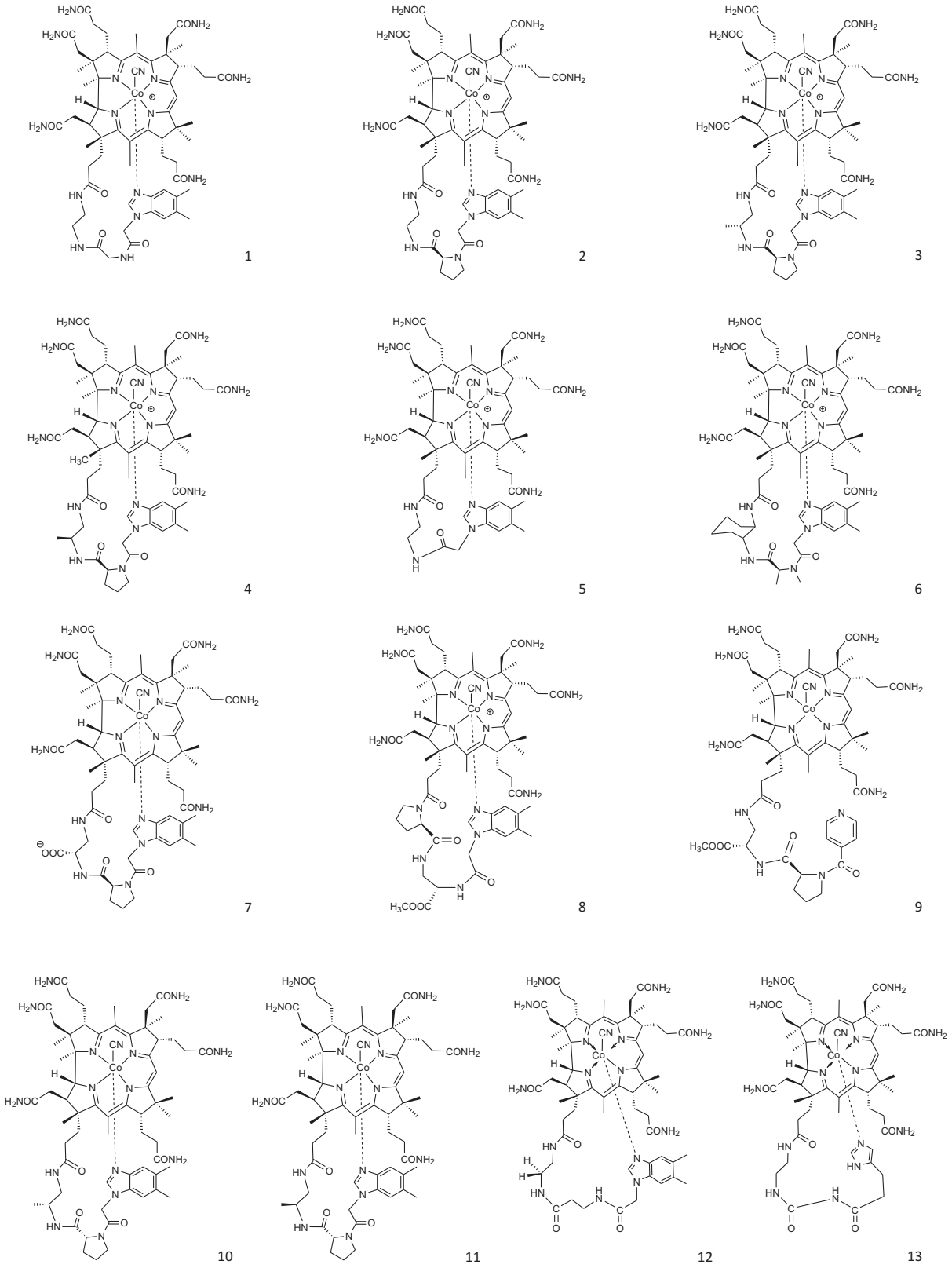

Suppl. Figure 5.5 Peptide Cbl derivatives. Structural formulae for the used peptide Cbl derivatives with the different peptide linkers tethering the corrin macrocycle to the DMB base [67].

6 The Role of Cobalamin Transport Proteins in the Uptake of Cobalamin Derivatives in Tumours

Evelyne Furger, Mai Thanh Quynh Tran, Christine De Pasquale

Mai Thanh Quynh Tran synthesised the R-PAMA(4)-Cbl derivative.

Christine De Pasquale performed the animal experiments.

Evelyne Furger planned and performed the animal experiments and conducted the *in vivo* and *in vitro* assays.

6.1 Introduction

Cbl is an essential cofactor for various steps in human metabolism. Because the body's supply of Cbl is thoroughly dependent on its dietary intake, nature bestowed us with an efficient transport and uptake system involving three transport proteins: intrinsic factor (IF); transcobalamin (TC) and haptocorrin (HC) and several receptors [14]. Dietary Cbl is associated with HC in the acid environment of the stomach. In the intestine HC is digested by pancreatic proteases and Cbl is transferred to IF [32,33]. The IF-Cbl complex is then absorbed in the distal ileum via cubam, a receptor complex of the two proteins cubilin and amnionless [36]. Upon release into the bloodstream via the the multiple drug resistance protein (MRP1) [65] Cbl associates with TC or HC, the two transport proteins found in blood [25-27]. The majority of Cbl in the circulation is bound to HC and can be taken up by the asialoglycoprotein receptor (ASGP-R) expressed mainly on liver cells [31,56] but is unavailable for other cells. Only a minor fraction of Cbl is bound to TC and available for uptake by most cells of the body.

The main receptor which is responsible for cellular uptake of Cbl has been identified as CD320 (TCbl-R), a 60 kDa heavily glycosylated protein [40]. A recent publication also identified a soluble form of this receptor [44]. CD320 binds preferentially to the TC-Cbl complex (with a 30-fold lower affinity for TC alone) and neither IF nor HC bind to CD320. Upon binding, TC-Cbl is internalised and Cbl is released from TC within the lysosomes. CD320 expression is cell cycle dependent and upregulated in actively dividing cells [41,43]. Several studies also identified receptors recognising TC-Cbl on the surface of murine cell lines [190-192].

Another uptake mechanism of Cbl is mediated by megalin, a 600 kDa multi-ligand receptor located on the apical membrane of kidney proximal tubule cells [46]. Studies in animals, particularly in rodents, showed accumulation of Cbl in the lysosomes of the kidneys which function as a Cbl storage organ in rodents [193,194].

Receptors involved in vitamin uptake are over-expressed on tumour cells. This well-known fact has been exploited for the development of vitamin-based tumour targeting approaches [195]. In this context Cbl has been investigated as a potential targeting agent for the delivery of cytotoxic moieties to tumour cells. For example, Cbl conjugates delivering the cytotoxic metals Gd^{3+}, Pt^{II}, or cholchicine [78,80,83,84] have been developed and studied *in vitro*.

Furthermore, radiolabelled Cbl derivatives have been investigated for the *in vivo* imaging of tumours [100,102-104,106]. However, biodistribution studies in mice showed high background uptake in healthy tissue due to high hepatic and renal expression of CD320 and megalin. A primary clinical trial at the Mayo Clinic with an ^{111}In-DTPA derivatized Cbl resulted in the visualisation of several tumours but nevertheless, high background uptake in some healthy organs, such as liver, spleen and several glands could not be prevented [105].

Interestingly, a ^{99m}Tc-labelled Cbl derivative that would not bind to TC, ^{99m}Tc-PAMA(4)-Cbl, showed a promising accumulation in tumours with a low background activity in kidneys and other vital organs in mice [75]. Although binding to TC was prohibited, the radioligand still bound to HC [75], prompting speculation for an alternative, presumably TC-independent, Cbl-uptake mechanism in tumour targeting. Although it is known that some tumours express HC in high amounts [75,115,116] no specific uptake mechanism of Cbl-HC complexes has been described so far. In addition to this, only the unspecific ASGP-R has been identified as being involved in the uptake of certain glycoforms of HC. Uptake of ^{99m}Tc-PAMA(4)-Cbl in tumours was also observed in humans in a clinical phase 0 study at the University Hospital Zürich. Cancer patients injected with ^{99m}Tc-PAMA(4)-Cbl showed tumour uptake in various cancer entities but, in contrast to the studies in mice, still exhibited high uptake in the liver and salivary glands (unpublished data).

These divergent findings in mice and humans led to the question to which extent the mouse is a suitable model for evaluation of novel Cbl derivatives. There are several differences between rodents and humans that should be taken into account when studying Cbl transport. A major difference between humans and mice is that mice lack HC. Instead, they express a single plasma Cbl transport protein that appears to display Cbl binding properties found in both human TC and HC [149]. It is unclear whether a Cbl derivative that does not bind to TC, e.g. ^{99m}Tc-PAMA(4)-Cbl, is actually binding to mouse transcobalamin (mTC). Additionally, mice are often held on a Cbl-deficient diet for biodistribution experiments in order to reduce accumulation in the kidneys. The kidneys of rodents seem to act as a storage organ of Cbl [196] whereas in humans Cbl is mainly stored in the liver [197].

Having generated recombinant HC, TC and mTC allowed us to study the possible uptake mechanism ^{99m}Tc-PAMA(4)-Cbl *in vitro* and *in vivo,* using human and mouse cancer cells.

6.2 Results

A previous study (Waibel *et al.* [75]) showed that ^{99m}Tc-PAMA(4)-Cbl (Figure 6.6A) accumulates in subcutaneous B16F1 mouse melanoma tumours. Furthermore, in a xenograft model with human melanoma MEL-CLS-1 (CLS-1) a high tumour uptake of approximately 13% and high circulating radioactivity in the blood was observed. A gel shift assay showed the ^{99m}Tc-PAMA(4)-Cbl to be associated with an unidentified protein with molecular mass of 120 to 140 kDa when circulating in the blood [75].

In order to test the hypothesis of *de novo* expression of HC by these tumours we included a cell line known to express HC: the human non-small lung cancer cell line HCC827 (Entrez Gene Expression Omnibus Profiles database, microarray experiment GDS2958).

6.2.1 mRNA and protein expression in CLS-1, HCC827 and B16F1 cells

Transcript levels of TCN1 (HC) in the cell lines were measured by qPCR (Figure 6.1A). As a positive control we used TCN1-transfected HEK293 cells (see section 2.4.4 [28]). Non transfected HEK293 cells and the mouse cell line B16F1 were included as negative controls. Both human cancer cell lines HCC827 and CLS-1 showed expression of TCN1 mRNA, although much less compared to the positive control (Figure 6.1).

We further tested the cell line supernatants for presence of HC and TC. To increase sensitivity, we performed a slot blot rather than Western Blot analysis. This allowed us to load up to 1 mL supernatant on the membrane without previous concentration steps. As expected, no HC could be detected in B16F1 supernatant (not shown) whereas a faint band was seen for the HCC827 and the CLS-1 cells (Figure 6.1B). However, further analysis using an antibody against an N-terminal peptide sequence of human/mouse TC resulted in a positive signal for HCC827 cells and even more for the B16F1 cells (Figure 6.1C).

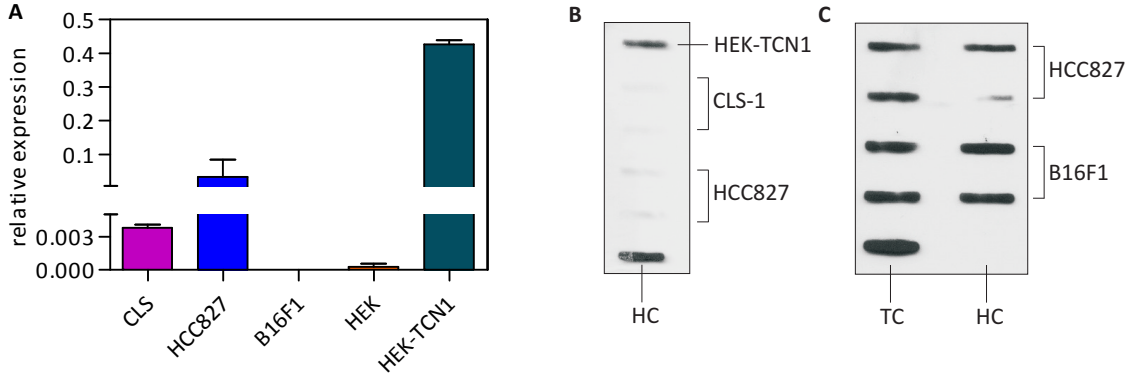

Figure 6.1 HC and TC expression of B16F1 and HCC827 cells. **A**. Total RNA was isolated from pooled cells and after synthesising first strand cDNA mRNA levels were determined using qPCR. Data represent the mean ± SD of two experiments done in triplicates of the relative fold change compared to the reference gene beta actin mRNA levels. As negative control B16F1 and HEK293 cells, as positive control TCN1 transfected HEK293 cells [28] were used. **B**. Slot blot analysis of cell culture supernatant of HEK-TCN1, CLS-1 (in duplicates) and HCC827 (in duplicates) employing anti HC antibody. Recombinant human HC was used as positive control. **C**. Slot blot analysis of cell culture supernatant of HCC827 (in quadruplicates) and B16F1 (in quadruplicates) employing anti TC antibody. 500 ng of recombinant human TC (10 pmol) and HC (8 pmol) were used as controls.

6.2.2 *In vivo* studies of Cbl derivative ^{99m}Tc-PAMA(4)-Cbl

We determined tissue distribution and tumour uptake in mice carrying CLS-1 melanoma or HCC827 non-small lung cancer xenografts or syngeneic B16F1 melanoma tumours 24 h post injection of ^{99m}Tc-PAMA(4)-Cbl (Figure 6.2 and Table 6.1). We confirmed the findings of Waibel et al. [75] for both B16F1 and CLS-1 tumours (Figure 6.2A and C). As described, the Cbl derivative cleared from the blood very rapidly in B16F1, resulting in high tumour-to-blood ratios at 24 h (Table 6.1). In contrast, the CLS-1 xenografted mice still showed a high circulating radioactivity of approximately 6% ID/g even after 24 h. (Figure 6.2A). The human HCC827 cell line revealed a very similar uptake profile to the mouse B16F1 carrying mice (Figure 6.2B and C).

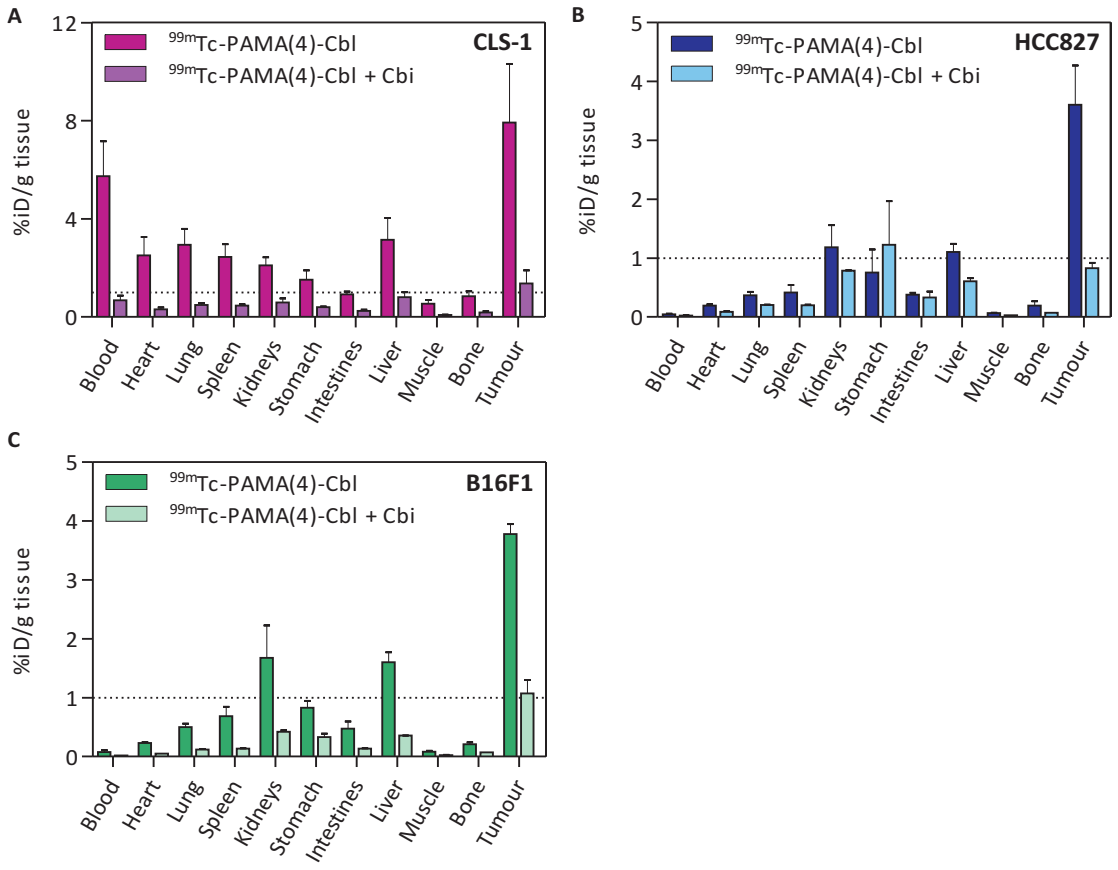

Figure 6.2 Organ distribution of ^{99m}Tc-PAMA(4)-Cbl in tumour bearing mice. The animals were intravenously injected with 6-15 ng (3-9 pmol) Cbl either with or without co-injection of 500 ng (480 pmol) Cbi per mouse and biodistribution was analysed 24 h post injection. Biodistribution was studied in xenografted nu/nu mice with (**A**) CLS-1 tumours, (**B**) HCC827 tumours and (**C**) BALB/c mice for B16F1 tumours. The results are displayed as the percentage of injected dose per gram of organ (% ID/g) ± SD for the ^{99m}Tc-PAMA(4)-Cbl group (n=3) and the results are displayed as % ID/g ± range for ^{99m}Tc-PAMA(4)-Cbl + Cbi group (n=2).

In a blocking experiment, we used Cbi, a Cbl analogue that binds to HC but not to TC. Blocking with Cbi resulted in an overall reduction of uptake in all three cell lines (Figure 6.2) whereas in the HCC827 and B16F1 bearing mice uptake in the tumour was blocked to a higher extent by Cbi than uptake in other organs such as liver and kidneys.

Table 6.1 Organ distribution of ^{99m}Tc-PAMA(4)-Cbl in tumour bearing mice

	Percentage of injected dose per gram of organ (24 h p.i.)					
Tissue	**CLS-1[a]**	**CLS-1[a] + Cbi**	**HCC827[a]**	**HCC827[a] + Cbi**	**B16F1[b]**	**B16F1[b] + Cbi**
Blood	5.74 ± 1.42	0.68 ± 0.26	0.08 ± 0.03	0.02 ± 0.01	0.04 ± 0.01	0.02 ± 0.00
Heart	2.51 ± 0.75	0.31 ± 0.12	0.23 ± 0.01	0.09 ± 0.02	0.19 ± 0.02	0.05 ± 0.00
Lung	2.94 ± 0.65	0.49 ± 0.11	0.50 ± 0.06	0.21 ± 0.00	0.37 ± 0.06	0.12 ± 0.02
Spleen	2.45 ± 0.51	0.46 ± 0.08	0.68 ± 0.16	0.20 ± 0.01	0.41 ± 0.13	0.14 ± 0.01
Kidney	2.11 ± 0.32	0.60 ± 0.24	1.68 ± 0.55	0.78 ± 0.01	1.19 ± 0.37	0.42 ± 0.04
Stomach	1.52 ± 0.37	0.40 ± 0.02	0.82 ± 0.12	1.22 ± 1.06	0.75 ± 0.39	0.33 ± 0.09
Intestine	0.92 ± 0.12	0.25 ± 0.08	0.48 ± 0.12	0.33 ± 0.14	0.38 ± 0.03	0.13 ± 0.01
Liver	3.14 ± 0.90	0.81 ± 0.29	1.60 ± 0.17	0.61 ± 0.08	1.11 ± 0.13	0.36 ± 0.01
Muscle	0.54 ± 0.16	0.08 ± 0.03	0.08 ± 0.02	0.03 ± 0.00	0.07 ± 0.00	0.03 ± 0.01
Bone	0.85 ± 0.20	0.18 ± 0.08	0.21 ± 0.03	0.07 ± 0.00	0.19 ± 0.08	0.07 ± 0.00
Tumour	7.92 ± 2.4	1.37 ± 0.75	3.78 ± 0.17	0.83 ± 0.13	3.60 ± 0.67	1.07 ± 0.32
Tumour/blood ratio	1.38	2.01	47.25	41.25	90	53.50

Biodistribution was studied 24 h after injection of the labelled Cbl derivative (3-9 pmol). The results express the mean ± SD for n = 3 animals for studies with radioligand alone, or mean ± range for n=2 for co-injection with 500 ng (480 pmol) Cbi. [a]CD-1 nu/nu mice, [b]BALB/c mice.

Ex vivo autoradiography of CLS-1 and HCC827 tumours from the *in vivo* biodistribution studies outlined above (Figure 6.2) showed good correlation of tumour tissue with the radioactivity (Figure 6.3). Thus, ^{99m}Tc-PAMA(4)-Cbl accumulates in the regions containing actively proliferating cells and not in the necrotic areas of the tumours.

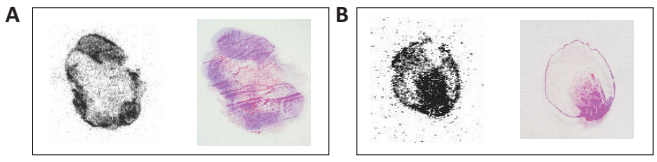

Figure 6.3 *Ex vivo* autoradiography and corresponding H&E stained sections of CLS-1 and HCC827 tumours. Autoradiograms (left) and corresponding H&E-stained sections (right) of (**A**) CLS-1 and (**B**) HCC827 tumours derived from mice 24 h after injection of ^{99m}Tc-PAMA(4)-Cbl.

6.2.3 *In vivo* biodistribution of iodinated HC

The hypothesis that ^{99m}Tc-PAMA(4)-Cbl binds to HC expressed *de novo* prompted us to study the fate of HC in mice. It is known that HC lacking terminal sialic acid is cleared by the asialoglycoprotein receptor (ASGP-R) expressed mainly in the liver [56]. This receptor is also expressed in mice and shows a 78% homology between mice and humans [198].

For the *in vivo* study, BALB/c mice and CD-1 nu/nu mice were injected intravenously with different iodinated forms of rhHC (150 pmol) (apo/holo, sialo/asialo see also 2.2.6). After 24 h the animals were sacrificed, dissected and the tissues measured in a gamma counter (Figure 6.4).

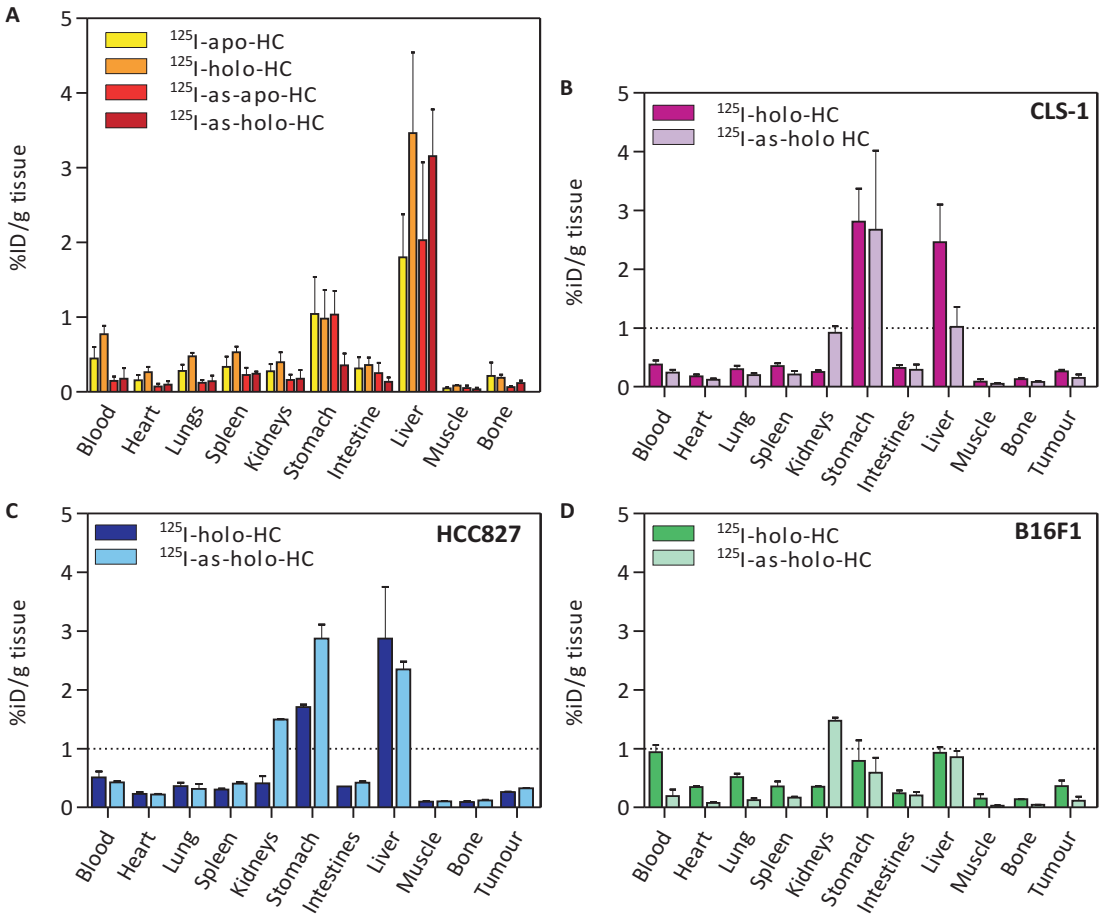

Figure 6.4 Organ distribution of ^{125}I-HC in healthy and tumour bearing mice. The animals were intravenously injected with approximately 10 µg (150 pmol) (0.1-0.6 MBq) ^{125}I-HC in either the glycosylated or the asialo-form. **A**. Distribution of iodinated HC in apo/holo- and sialo/asialo-form in BALB/c mice (n = 3). **B**. Biodistribution of iodinated holo-HC in CLS-1 bearing mice (n = 4), **C**. Biodistribution of iodinated holo-HC in HCC827 bearing mice (n = 2), **D**. Biodistribution of iodinated holo-HC in B16F1 bearing mice (n = 3). The results are displayed as the percentage of injected dose per gram of organ (% ID/g) ± SD for A, B and D and % ID/g ± range for C 24 h after injection of ^{125}I-HC.

In the healthy mice only a small difference could be seen between the normal glycosylated form and the asialo form of HC (Figure 6.4A). In all organs except for the liver, the asialo form of HC showed a slightly increased clearance (e.g. blood 0.45 ± 0.15 and 0.77 ± 0.11% ID/g versus 0.15 ± 0.06 and 0.18 ± 0.15% ID/g). The only organ showing a higher uptake of radioactivity was the liver (>1.8% ID/g) whereas both apo-forms of the protein seemed to clear faster than the holo-forms (1.81 ± 0.57 and 2.03 ± 1.04% ID/g versus 3.46 ± 1.08 and 3.16 ± 0.63% ID/g). As stated before, no difference in liver uptake was seen by comparing the normal forms to the asialoforms of the protein.

Table 6.2 Organ distribution of ^{125}I-rhHC in BALB/c mice

	Percentage of injected dose per gram of organ (24 h p.i.)			
Tissue	**^{125}I-apo-HC**	**^{125}I-holo HC**	**^{125}I-asialo-apo-HC**	**^{125}I-asialo-holo-HC**
Blood	0.45 ± 0.15	0.77 ± 0.11	0.15 ± 0.06	0.18 ± 0.15
Heart	0.16 ± 0.07	0.26 ± 0.07	0.07 ± 0.03	0.10 ± 0.05
Lung	0.28 ± 0.08	0.48 ± 0.05	0.13 ± 0.04	0.14 ± 0.08
Spleen	0.33 ± 0.14	0.53 ± 0.07	0.23 ± 0.09	0.24 ± 0.03
Kidney	0.27 ± 0.10	0.40 ± 0.13	0.16 ± 0.07	0.18 ± 0.12
Stomach	1.04 ± 0.50	0.98 ± 0.39	1.03 ± 0.32	0.36 ± 0.16
Intestine	0.31 ± 0.15	0.36 ± 0.09	0.25 ± 0.13	0.13 ± 0.06
Liver	1.81 ± 0.57	3.46 ± 1.08	2.03 ± 1.04	3.16 ± 0.63
Muscle	0.05 ± 0.02	0.08 ± 0.01	0.05 ± 0.04	0.04 ± 0.02
Bone	0.22 ± 0.18	0.19 ± 0.04	0.07 ± 0.02	0.12 ± 0.03

Biodistribution was studied 24 h after injection of the iodinated proteins approximately 10 µg (150 pmol). The results express the mean ± SD. n = 3 animals for all groups.

The biodistribution of iodinated HC in CLS-1 and HCC827 bearing mice looked similar to the healthy mice showing a positive uptake only in the liver and in the stomach. Interestingly, the asialoform of HC seemed to be actively taken up by the kidneys in contrast to the sialated form. The overall distribution in B16F1 bearing mice looked different and neither in the stomach nor in the liver could a positive uptake of the radioprotein be detected. This finding was unexpected and might be due to the age of the mice used for this experiment.

Table 6.3 Organ distribution of ^{125}I-holo-HC in tumour bearing mice

	Percentage of injected dose per gram of organ (24 h p.i.)					
	CLS-1[a]		HCC827[a]		B16F1[b]	
Tissue	^{125}I-HC	^{125}I-asialo HC	^{125}I-HC	^{125}I-asialo HC	^{125}I-HC	^{125}I-asialo HC
Blood	0.38 ± 0.06	0.24 ± 0.05	0.51 ± 0.14	0.43 ± 0.04	0.90 ± 0.11	0.19 ± 0.11
Heart	0.18 ± 0.03	0.12 ± 0.02	0.23 ± 0.04	0.22 ± 0.01	0.32 ± 0.05	0.08 ± 0.02
Lung	0.30 ± 0.05	0.20 ± 0.03	0.37 ± 0.07	0.32 ± 0.12	0.49 ± 0.06	0.12 ± 0.03
Spleen	0.36 ± 0.05	0.21 ± 0.06	0.30 ± 0.02	0.40 ± 1.49	0.33 ± 0.08	0.17 ± 0.02
Kidney	0.24 ± 0.03	0.92 ± 0.11	0.41 ± 0.17	1.49 ± 0.01	0.33 ± 0.04	1.47 ± 0.05
Stomach	3.03 ± 0.69	2.67 ± 1.35	1.71 ± 0.06	2.87 ± 0.33	0.77 ± 0.25	0.59 ± 0.26
Intestine	0.31 ± 0.05	0.29 ± 0.09	0.36 ± 0.00	0.42 ± 0.02	0.23 ± 0.04	0.20 ± 0.06
Liver	2.40 ± 0.57	1.02 ± 0.34	2.88 ± 1.24	2.35 ± 0.19	0.71 ± 0.39	0.86 ± 0.10
Muscle	0.09 ± 0.04	0.05 ± 0.01	0.10 ± 0.01	0.11 ± 0.01	0.13 ± 0.07	0.03 ± 0.00
Bone	0.12 ± 0.02	0.08 ± 0.02	0.10 ± 0.02	0.12 ± 0.01	0.13 ± 0.02	0.04 ± 0.00
Tumour	0.25 ± 0.03	0.15 ± 0.06	0.26 ± 0.01	0.32 ± 0.01	0.38 ± 0.07	0.12 ± 0.07

Biodistribution was studied 24 h after injection of the labelled HC form. The results express the mean ± SD or mean ± range when n=2, with n=4 for CLS-1, n=2 for HCC827 and n = 3 animals for B16F1 mice. [a]CD-1 nu/nu mice, [b]BALB/c mice.

6.2.4 Biodistribution of ^{125}I-antibody against human HC

Although the level of HC expression in the two human cell lines CLS-1 and HCC827 differed in the amount of expressed mRNA (Figure 6.1A), we wanted to explore whether we could detect HC expressed by these cells in tumour bearing mice using an anti-HC (Hyb335) antibody. This is a monoclonal antibody specific for deglycosylated HC and has been used for the measurement of total corrinoids in human serum [114,199]. Interestingly, the monoclonal antibody showed an equally efficient precipitation of native HC, neuraminidase treated HC and deglycosylated HC [199]. The antibody was iodinated and injected in CLS-1 and HCC827 bearing mice and after 24 h tissue distribution of the antibody was determined (Figure 6.5 and Table 6.4). With the exception of high uptake in the stomach of CLS-1 bearing mice, the distribution pattern of both groups of mice looked very similar. Both groups showed a quick blood clearance and no accumulation in the tumours.

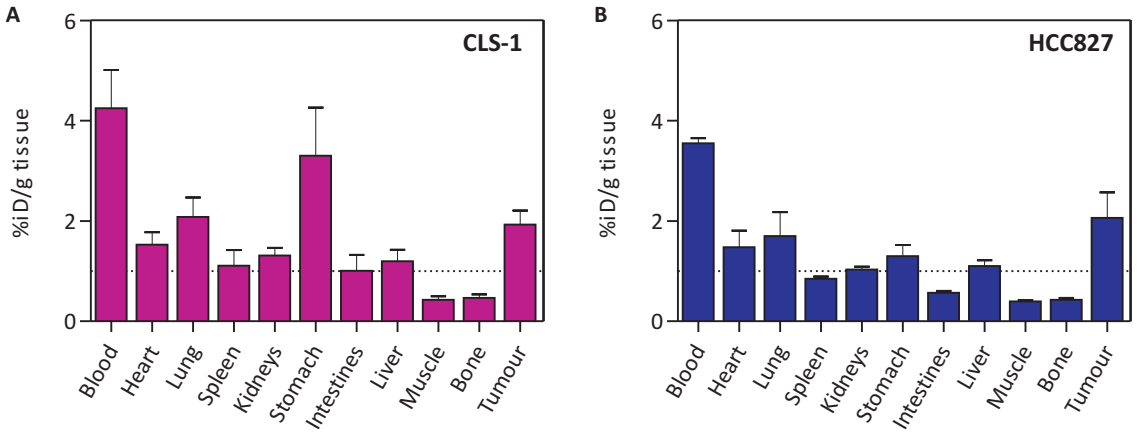

Figure 6.5 Organ distribution of ^{125}I-Hyb335 anti HC antibody in tumour bearing CD-1 nu/nu mice. The animals were intravenously injected with approximately 10 µg (83 pmol) (0.8 MBq) ^{125}I-HC. **A**. Biodistribution of iodinated anti-HC antibody in CLS-1 bearing CD-1 nu/nu mice (n = 3). **B**. Biodistribution of iodinated anti-HC antibody in HCC827 bearing CD-1 nu/nu mice (n = 3). The results are displayed as the percentage of injected dose per gram of organ (% ID/g) ± SD.

Table 6.4 Organ distribution of ^{125}I-Hyb335 anti HC antibody in xenografted CD-1 nu/nu mice

	Percentage of injected dose per gram of organ (24 h p.i.)	
Tissue	**CLS-1**	**HCC827**
Blood	4.25 ± 0.76	3.55 ± 0.10
Heart	1.53 ± 0.24	1.48 ± 0.33
Lung	2.08 ± 0.39	1.70 ± 0.48
Spleen	1.11 ± 0.31	0.85 ± 0.04
Kidney	1.31 ± 0.16	1.03 ± 0.06
Stomach	3.30 ± 0.96	1.30 ± 0.22
Intestine	1.01 ± 0.32	0.57 ± 0.04
Liver	1.20 ± 0.23	1.10 ± 0.12
Muscle	0.43 ± 0.07	0.40 ± 0.02
Bone	0.47 ± 0.07	0.43 ± 0.04
Tumour	1.93 ± 0.28	2.06 ± 0.51

Biodistribution was studied 24 h after injection of 10 µg (approximately 80 pmol) (0.8 MBq) of the iodinated proteins. The results express the mean ± SD. n = 3 animals for all groups.

6.2.5 Interaction of radioactive Cbl derivatives with the Cbl transport proteins *in vitro*

In humans two Cbl transport proteins are found in the circulation – HC and TC [14]. In mice the situation differs in that they possess only one circulating Cbl transport protein known as mouse transcobalamin (mTC) [149]. Although structurally more similar to TC (sequence identity of about 73% to human TC and only 28% to human HC) its ability to bind to different Cbl derivatives shows more resemblance to HC [149].

In order to study the transport protein-dependent uptake *in vitro* we first determined the ability of the three transport proteins to bind to ^{99m}Tc-PAMA(4)-Cbl and compared it to their binding to a Cbl derivative which retains binding to TC. While in Waibel *et al.* [75] this was done by gel shift assay we decided to perform differential scanning fluorimetry (DSF) (see section 5). This allowed us to determine the different stabilising effect of the ligands toward the transport proteins based on thermal unfolding.

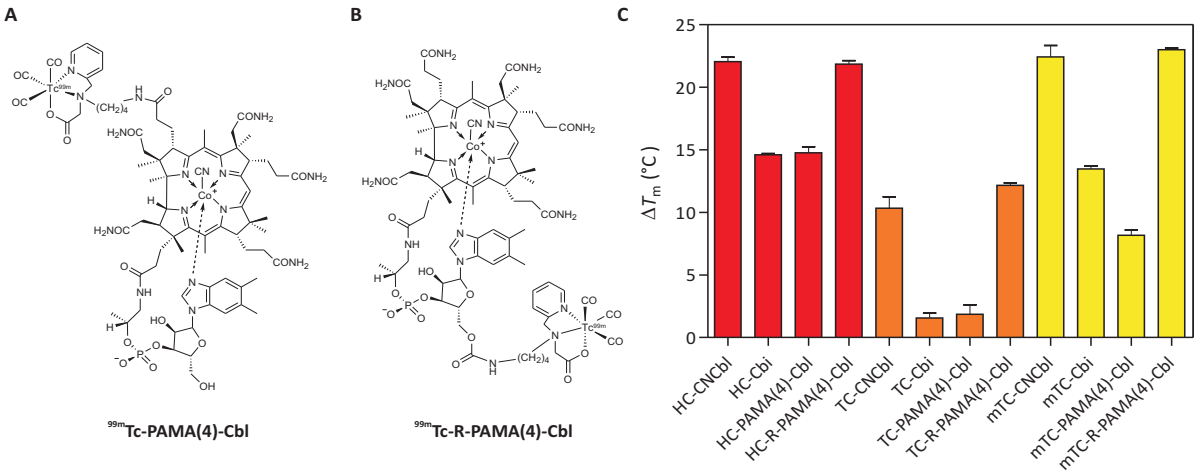

Figure 6.6 Cbl derivatives and their binding ability to the transport proteins. **A**. and **B**. Structural formula of the ^{99m}Tc-labelled PAMA(4)-Cbl derivative and the ^{99m}Tc-labelled R-PAMA-Cbl derivative. **C.** Thermal stabilisation of human Cbl transport proteins by binding to different ligands. The T_m values of HC, TC and mTC were determined either alone (300 -400 nM) or in the presence of an excess (10-20 µM) of CNCbl, Cbi, cold PAMA(4)-Cbl and cold R-PAMA(4) derivative. Here the T_m values of the ligand-protein complexes relative to the unbound proteins (ΔT_m) are presented.

The two used Cbl derivatives carry a monoanionic PAMA ligand ([pyridine-2-ylmethyl-amino]-acetic acid] [200] and could be quantitatively labelled with $[^{99m}Tc(OH_2)_3(CO)_3]^+$ [201,202]. The ^{99m}Tc-PAMA(4)-Cbl (Figure 6.6A) used in the study by Waibel *et al.* [75] carries

the PAMA ligand at the *b*-acid side chain, whereas the other Cbl derivative (^{99m}Tc-R-PAMA(4)-Cbl) was conjugated to the 5'-OH side chain of the ribose (Figure 6.6B). This site does not interfere with the binding to the different transport proteins [73]. For DSF the different proteins were incubated with an excess of ligands, after which the fluorescent dye Sypro® Orange was added and the mixture was gradually heated up. During the proteins denaturation, hydrophobic sites become available to bind to the dye, resulting in a fluorescence signal depicting a curve that allowed the calculation of the melting points (T_m). An increase in T_m (ΔT_m) indicates a stabilising effect of the ligand shown in a protein's increased resistance to thermal unfolding. By comparing the measured values to the values obtained with CNCbl and Cbi we could assume the affinity of a protein towards different ligands by comparing the ΔT_m values, representing the T_m values of the ligand protein complex relative to the unbound protein (Figure 6.6C).

Table 6.5 ΔT_m values of HC, TC and mTC with different ligands

	ΔT_m (°C)			
	CNCbl	**Cbi**	**PAMA(4)-Cbl**	**R-PAMA(4)-Cbl**
HC	22.06 ± 0.34	14.61 ± 0.09	14.77 ± 0.47	21.86 ± 0.26
TC	10.33 ± 0.92	1.55 ± 0.39	1.87 ± 0.75	12.16 ± 0.21
mTC	22.44 ± 0.90	13.16 ± 0.68	8.17 ± 0.42	23.01 ± 0.14

ΔT_m was determined as the melting points T_m of the ligand-protein complexes relative to the unbound proteins. The results express the mean ± SD for n > 4.

Both Cbl derivatives bound to HC, showing smiliar ΔT_m values for PAMA(4)-Cbl as for Cbi and similar values of R-PAMA(4)-Cbl compared to CNCbl, strongly indicating a good binding ability of both ligands. TC bound strongly to R-PAMA(4)-Cbl. In contrast, PAMA(4)-Cbl showed a shift comparable to that of Cbi and therefore indicating a much lower affinity to TC of this latter derivative. This was in agreement with the gel shift assay done by Waibel *et al*. [75]. R-PAMA(4)-Cbl exhibited strong binding to mTC, similar to that seen for CNCbl-binding to mTC, whereas ΔT_m for PAMA(4)-Cbl was smaller than for Cbi. Cbi binds to mTC, although with reduced affinity [149]. From this data, we cannot say whether PAMA(4)-Cbl would bind to mTC under physiological conditions. However, we can conclude that is has significantly lower affinity for PAMA(4)-Cbl than for R-PAMA(4)-Cbl.

6.2.6 *In vitro* uptake studies with the Cbl derivatives

To study the possible tumour uptake mechanism of Cbl *in vitro* we performed internalisation studies using the different cell lines outlined in section 6.2.1 and the ^{99m}Tc-labelled Cbl derivatives described in section 6.2.5. First, time dependent uptake of ^{99m}Tc-PAMA(4)-Cbl was tested by incubating the ligand for 1.5, 3, 6 and 24 h followed by determination of internalised radiolabelled PAMA(4)-Cbl in the lysed cells (Figure 6.7). The uptake by the human cell lines (CLS-1 and HCC827) was very low, in contrast to uptake by the B16F1 cells.

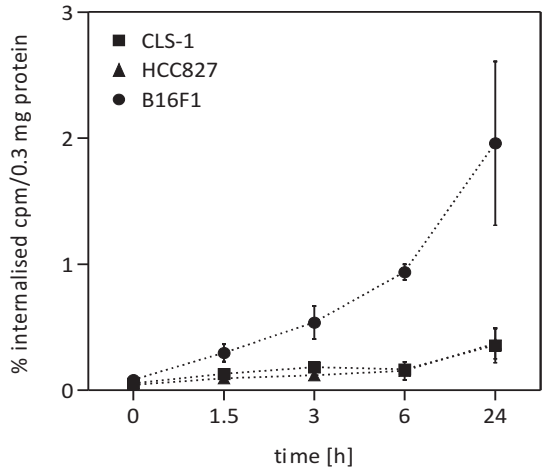

Figure 6.7 Time dependent uptake of ^{99m}Tc-PAMA(4)-Cbl in CLS-1, HCC827 and B16F1 cells. Cells were incubated with approximately 7-14 pM 0.04 MBq ^{99m}Tc-labelled PAMA(4)-Cbl after incubation for 24 h at 37°C, uptake of radiolabelled ligand in the lysed cells was determined as % measured cpm of the lysed cells relative to 0.3 mg cell protein ± SD with n = 2.

Regarding the very similar results found for CLS-1 and HCC827 cells throughout the *in vivo* studies and also in this preliminary internalisation study, in which the only difference seems to be the slow blood clearance of CLS-1 bearing mice, the following experiments were conducted using only the human cell line HCC827 and the mouse cell B16F1. The two cell lines were incubated with the radioligands and after 24 h the uptake of radioactivity in the lysed cells was determined (Figure 6.8). Furthermore, a transport protein-facilitated uptake was investigated by adding 0.1 µg of the recombinant transport proteins HC (1.5 nM), TC (2 nM) or mTC (2 nM). To avoid interference of Cbl or transport proteins in the media, cells were cultivated in Cbl-free medium and depleted of fetal calf serum for the duration of the assay.

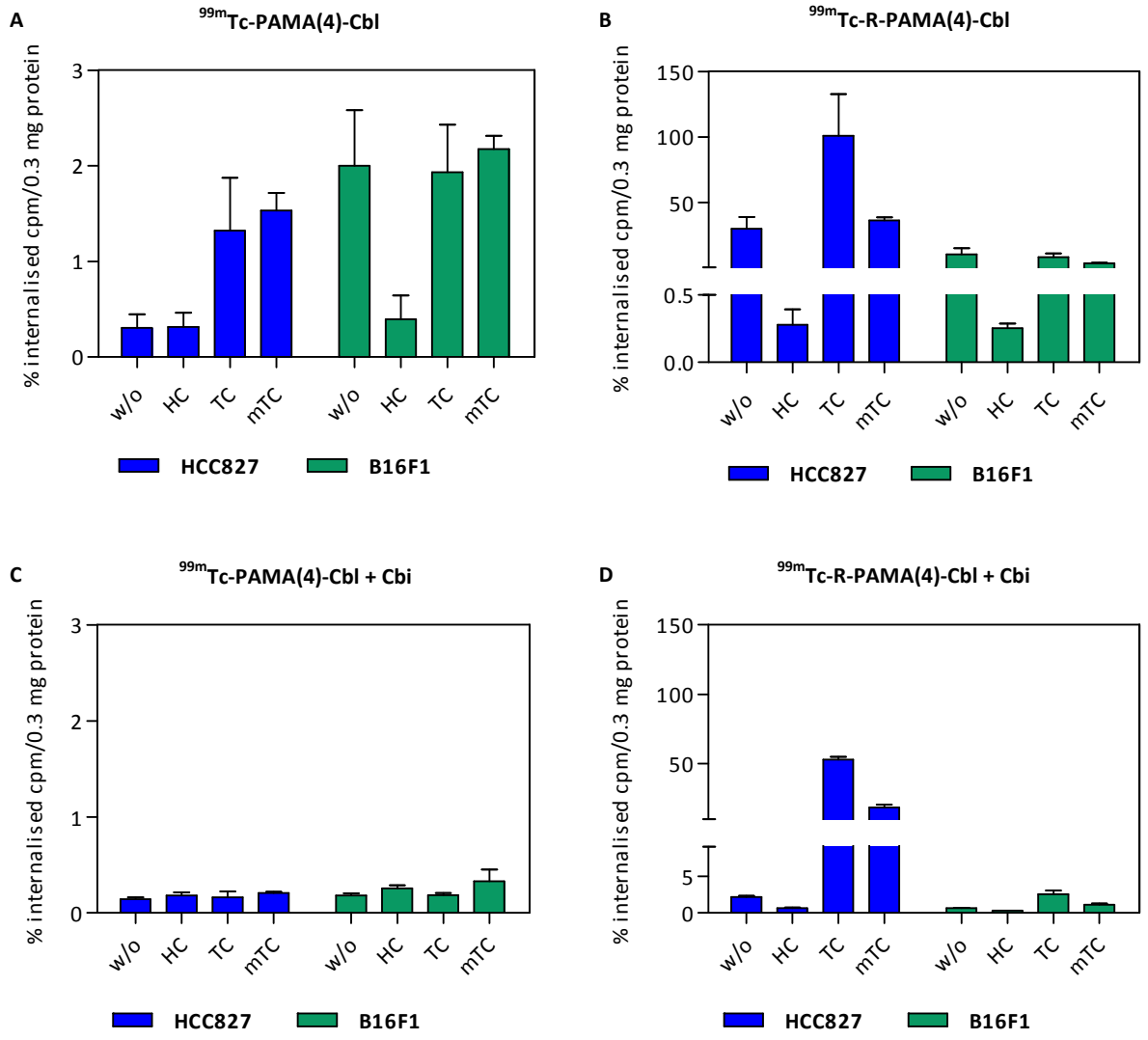

Figure 6.8 Internalisation of ^{99m}Tc-PAMA(4)-Cbl and ^{99m}Tc-R-PAMA(4)-Cbl. The Cbl derivatives were incubated for 24 h at 37°C alone or in the presence of 1.5-2 nM recombinant proteins. **A**. Internalisation of 7-14 pM 0.04 MBq ^{99m}Tc-PAMA(4)-Cbl in HCC827 and B16F1 cells without and with (**C**) co-incubation of 240 nM Cbi; **B**. Internalisation of 7-14 pM 0.04 MBq ^{99m}Tc-R-PAMA(4)-Cbl in HCC827 and B16F1 cells without and with (**D**) co-incubation of 240 nM Cbi. The results express % measured cpm of the lysed cells relative to 0.3 mg cell protein ± SD. All experiments were measured in triplicates and n ≥ 1. w/o indicates incubation with the radioligand alone.

Table 6.6 *in vitro* uptake of ^{99m}Tc-PAMA(4)-Cbl and ^{99m}Tc-R-PAMA(4)-Cbl in HCC827 and B16F1 cells

	% internalised cpm/0.3 mg protein							
	HCC827				B16F1			
Ligands	**w/o**	**HC**	**TC**	**mTC**	**w/o**	**HC**	**TC**	**mTC**
^{99m}Tc-PAMA(4)-Cbl	0.31 ± 0.14	0.32 ± 0.15	1.32 ± 0.55	1.53 ± 0.19	2.00 ± 0.58	0.40 ± 0.25	1.93 ± 0.50	2.18 0.14
+ Cbi	0.14 ± 0.02	0.22 ± 0.09	0.13 ± 0.05	0.22 ± 0.00	0.10 ± 0.01	0.16 ± 0.02	0.09 ± 0.01	0.19 ± 0.08
^{99m}Tc-R-PAMA(4)-Cbl	30.00 ± 8.97	0.28 ± 0.12	100.96 ± 31.85	36.50 ± 2.20	10.63 ± 4.59	0.25 ± 0.04	8.52 ± 2.66	3.81 ± 0.53
+ Cbi	2.20 ± 0.15	0.64 ± 0.06	53.05 ± 1.94	18.37 ± 1.99	0.65 ± 0.04	0.31 ± 0.02	2.54 0.52	1.14 0.19

Internalisation of 7-14 pM 0.04 MBq ^{99m}Tc-PAMA(4)-Cbl and ^{99m}Tc-R-PAMA(4)-Cbl after 24 h incubation at 37°C alone or in the presence of 1.5-2 nM recombinant proteins. The results express % measured cpm of the lysed cells relative to 0.3 mg cell protein ± SD. All experiments were measured in triplicates and n ≥ 1.

Adding HC resulted in an overall reduction of the internalisation of both derivatives, indicating that there is no HC mediated uptake mechanism in both cell lines. Instead, HC efficiently captures the Cbl-derivatives in the medium and prevents their uptake (Figure 6.8A and B). Although adding TC and mTC also resulted in an increased uptake of ^{99m}Tc-PAMA(4)-Cbl in the human cells, its absolute uptake value was relatively low (around 1.5%) (Figure 6.8A).

As expected, the highest uptake of approximatley 100% was seen for the ^{99m}Tc-R-PAMA(4)-Cbl derivative together with TC (Figure 6.8B). In contrast, the mouse cells showed a transport protein independent uptake that was not affected by adding TC or mTC (Figure 6.8B). The same uptake was seen for the ^{99m}Tc-R-PAMA(4)-Cbl derivative in human cells without any additional protein (Figure 6.8B).

Co-incubation with Cbi resulted in an overall inhibition of ^{99m}Tc-PAMA(4)-Cbl uptake (Figure 6.8C) while only the transport protein-independent uptake mechanism for ^{99m}Tc-R-PAMA(4)-Cbl could be blocked in HCC827 cells (Figure 6.8D) . The mouse cell line B16F1 showed an overall reduction of internalisation in a manner similar to that seen for uptake of ^{99m}Tc-PAMA(4)-Cbl.

6.3 Discussion

Our studies confirm the findings by Waibel *et al*. that certain tumours take up ^{99m}Tc-PAMA(4)-Cbl *in vivo* in a manner that can be blocked by an excess of Cbi. *Ex vivo* autoradiography suggests uptake of this radioligand in actively proliferating tumour cells and not necrotic areas. However, our data does not support the hypothesis that the uptake is HC-dependent for several reasons. First, there was no evident difference between tumour uptake of ^{99m}Tc-PAMA(4)-Cbl in a HC-producing (HCC827) and a non-producing tumour (B16F1) *in vivo*. Second, we could neither observe uptake of recombinant HC by cells in culture or tumours, nor did an anti-HC antibody specifically accumulate in tumour tissue *in vivo*. Instead, addition of HC blocked the uptake of the Cbl derivatives *in vitro*.

It is known that by binding to TC or mTC, a Cbl derivative is easily taken up via endocytosis facilitated by CD320. In contrast to the *in vivo* experiments, no significant uptake of the ^{99m}Tc-PAMA(4)-Cbl derivative could be seen in either of the two cell lines *in vitro* (Figure 6.8A). Even addition of mTC did not result in an increased uptake of the radiotracer, indicating that ^{99m}Tc-PAMA(4)-Cbl is not binding to mTC. However, exact binding affinity constants are missing for mTC in order to confirm this finding.

Although the overall uptake of ^{99m}Tc-PAMA(4)-Cbl was low for both cell lines (HCC827 and B16F1), incubation with an excess of Cbi either with or without addition of recombinant transport proteins resulted in an overall reduction in the uptake of radioactivity uptake. This is in agreement with the *in vivo* studies (see section 6.2.2) where it was shown that co-injection with Cbi resulted in an overall reduction in uptake in mouse tissues (Figure 6.2). Because TC-mediated uptake cannot be blocked by Cbi, the seen blocking in our experiments indicates a specific, saturable TC-independent uptake mechanism of the Cbl-derivative, and precludes non-specific uptake by pinocytosis, for example.

The ability of ^{99m}Tc-R-PAMA(4)-Cbl to bind to TC and mTC was useful to study the transport protein mediated uptake of tumour cells. Interestingly, only the human cells showed a protein mediated uptake in the presence of TC or mTC, confirmed by the blocking with Cbi. Although it is known that Cbi binds to mTC [149] albeit with reduced affintiy, the high affinity of ^{99m}Tc-R-PAMA(4)-Cbl to mTC seems to actively prevent binding to Cbi (Figure 6.8D). To our surprise, even the ligand itself was taken up, but in contrast to the protein mediated uptake, its entry into cells could be blocked by the presence of Cbi (Figure 6.8D).

The situation in the mouse cell line with ^{99m}Tc-R-PAMA(4)-Cbl differed from the human cell line in that its uptake seems to be completely independent of transport proteins, resulting in overall uptake blockage with Cbi (Figure 6.8D). Further studies need to be conducted in order to elucidate if the uptake of ^{99m}Tc-R-PAMA(4)-Cbl can be blocked by Cbi *in vivo*.

A different uptake mechanism for Cbl may play a role in its tumour uptake as seen *in vivo* as well as *in vitro*. The existence of such an alternative uptake mechanism for free Cbl would also be in agreement with the recent finding that CD320 knockout mice show a normal level of serum, liver and kidney Cbl [203] and that patients with congenital TC deficiency improve when receiving therapeutic doses of free Cbl [204]. Furthermore, early studies by Berliner *et al*. and Hall *et al*. showed uptake of free Cbl in human cells *in vitro*, although the amount of free Cbl internalised was only a fraction of that taken up when Cbl was bound to TC [204-206]. A recent study by Lidlballe *et al*. [207] also showed unexpectedly high tissue uptake of Cbl and Cbi in mice, far exceeding the capacity of a TC-mediated transport. To what extent such an uptake mechanism for free Cbl is physiological important remains to be clarified.

Several additional experiments should be conducted in order to determine the uptake mechanism of ^{99m}Tc-R-PAMA(4)-Cbl *in vitro* and *in vivo*. In order to clarify whether there is any degradation of the two labelled Cbl derivatives, *in vitro* and *in vivo* stability experiments of the derivatives should be performed. However, fast clearance of free ^{99m}Tc would be expected, indicating that the labelled Cbl derivatives used in our experiments were stable. The same should be considered regarding the *in vivo* experiments with iodinated HC. Metabolism studies, as well as plasma stability testing for the ^{125}I-labelled HC are not available at present, and so it is unknown whether the whole ^{125}I-HC protein is taken up, or just labelled parts of it. The high uptake of radioactivity in the stomach strongly indicates the presence of free radioiodine [100] due to deiodination of labelled HC in hepatocyte microsomes [208] and uptake of the free radioiodine by the Na^+/I^- symporters in the gastric mucosa [209]. Nevertheless, the *in vivo* biodistribution of rhHC in BALB/c mice and tumour bearing CD-1 nu/nu mice primarily showed uptake of the radioactivity in the liver of the mice and no increased uptake of radiolabelled HC in the tumours.

The results described in this section are just the beginning of a possible explanation for the high tumour uptake in addition to a low liver uptake seen in mice injected with ^{99m}Tc-PAMA(4)-Cbl. It is worth reiterating that mice possess a different Cbl transport system and translation of the effects seen in mice do not reflect the ones found in humans.

In general, tumour uptake of radiolabelled Cbl derivatives was seen for both ^{99m}Tc-PAMA(4)-Cbl (unpublished data) and the ^{111}In-DTPA-Cbl, a Cbl derivative which binds to all three transport proteins [105]. By ruling out HC as a potential mediator of specific tumour uptake, our study strongly proposes the possible involvement of an alternative Cbl uptake mechanism found in tumours, which is independent of the known transport proteins.

6.4 Materials and Methods

6.4.1 TCN1 gene expression

A TCN1 gene expression enquiry was performed using the National Center for Biotechnology Information (NCBI) website (NCB I website: http://www.ncbi.nlm.nih.gov/guide accessed 2011). The GEO Profiles database was searched using the term TCN1 (http://www.ncbi.nlm.nih.gov/geoprofiles/45055761).

6.4.2 Recombinant proteins

The recombinant proteins HC, TC and mTC were expressed and purified as described in sections 2.4.4, 2.4.5, 3.4.4 and 3.4.6.

6.4.3 Cell cultures

For the *in vitro* and *in vivo* experiments the following cell lines were cultivated: mouse melanoma cells B16F1 and human non-small lung cancer carcinoma cells, HCC827, were grown in Dulbecco's modified Eagle's medium (DMEM) containing 4.5 g/L glucose, supplemented with 10% fetal calf serum, 100 U/mL penicillin, 100 µg/mL streptomycin, 0.25 µg/mL funigzone, and 2 mM glutamine in a 5% CO_2 incubator at 37°C. All tissue culture reagents were purchased from BioConcept (Basel, Switzerland).

6.4.4 Slot blot analysis

After the cells reached 80-100% confluency, they were washed twice with PBS and serum free growth medium was added to the flask. The cells were incubated for 24 h at 37°C, 5% CO_2, and the supernatants were centrifuged to remove cell debris. 1 ml of the supernatant was used for blotting using a Bio-Dot SF apparatus (Bio-Rad Laboratories, Switzerland). Incubation with anti-Transcobalamin I (M-16) or Transcobalamin II (E-13) (Santa Cruz Biotechnology, Switzerland) was performed according to the manufacturer's protocol overnight at 4°C in TBST (20 mM Tris HCl pH 7.5, 500 mM NaCl, 0.05% Tween 20) containing 2% BSA. The secondary antibody was donkey anti-goat IgG-HRP: sc-2020 (Santa Cruz Biotechnology, Switzerland).

6.4.5 Animals

All animal experiments were approved by the Animal Ethics Committee of the Kanton Aargau (Nr. 75546 and 75528). Four to five-week-old female BALB/c mice or CD-1 nu/nu mice were purchased from Charles River Laboratories. In order to reduce interference of high Cbl levels in mice, the animals were fed with al Cbl-deficient rodent diet (Harlan) starting five weeks before the experiments.

6.4.6 Labelling procedures

1 ml Na [$^{99m}TcO_4$] eluted from a $^{99}Mo/^{99m}Tc$ generator (Mallinckrodt-Covidien, Netherlands) using 0.9% saline was added to a mixture of 4.5 mg sodium bornocarbonate, 2.9 mg borax, 9 mg potassium sodium tartrate tetrahydrate and 7-8 mg sodium carbonate. This solution was heated to 150°C for 40 s in a microwave device (System Initiator, Biotage). After cooling down to RT, the pH of the tricarbonyl solution was adjusted to 6-7 with 350 µl neutralisation buffer (62 mL HCl 25% and 15.6 g sodium dihydrogen phosphate ad 900 mL). 10-30 µg Cbl-*b*-(butyl)-PAMA-OEt or Cbl-5'OH-(butyl)-PAMA-OEt was chelated to the precursor by adding 100 µl MES buffer (1:1 MES sodium and MES hydrate) and adding $[^{99m}Tc(OH_2)_3(CO)_3]^+$ up to 1 mL. The reaction mixture was kept at 75°C for 1 to 2 h. HPLC analysis with γ-detection was perormed to verify full conversion of the ^{99m}Tc species.

In order to achieve high specific activity, the radioactive labelled Cbl derivative was separated from unlabelled cobalamin on an analytic HPLC system using a XTerra RP8 column. Buffers used were, A: acetate buffer/ethanol 10%, and B: 70% ethanol. The separation was performed with a linear gradient 86% A/14% B to 50% A/50% B for 20 min at a flow rate of 0.9mL/min. The absorbance was monitored at 360 nm. Due to HPLC purification, the specific activities of the radiotracers can be considered identical with that of ^{99m}Tc in the generator eluate, 24 h post elution (approx. $1.93 \cdot 10^4$ MBq/nmol).

6.4.7 *In vivo* biodistribution of ^{99m}Tc-PAMA(4)-Cbl

Mice were inoculated subcutaneous with the tumour cell suspension ($5 \cdot 10^6$ cells) into the subcutis of the axilla. Biodistribution studies with ^{99m}Tc-PAMA(4)-Cbl were performed 12-14 days after tumour cell inoculation. The radiotracer was administered via a lateral tail vein and after 24 h the animals were sacrificed and dissected. The selected tissues were

removed, weighed and counted for radioactivity to determine distribution of radioactivity within the animals. The results were listed as percentage of injected dose per gram (% ID/g) tissue, using a reference sample.

6.4.8 *Ex vivo* autoradiography

Frozen tumours derived from biodistribution animals were cut into sections of 10 µm (Microm Cryo-Star HM 560 M, Germany) and mounted on glass slides (Superfrost plus slides, Menzelgläser, Germany). Tumour sections were exposed to Super Resolution phosphor imaging screens (Packard Instruments Co., Meriden, CT, USA) in X-ray cassettes. After 10–15 min, screens were imaged by a Cyclone phosphor imager and analysed using the OptiQuant 03.00 image processing system.

Tumour sections were subsequently stained with H&E using standard protocols and the staining pattern was compared to the corresponding autoradiogram.

6.4.9 *In vivo* biodistribution of ^{125}I labelled proteins

Prior to the labelling procedure the proteins were deglycosylated by incubating them overnight at 37°C with 0.1 U/mg Neuraminidase from Clostridium perfringens (Sigma).

The proteins and the antibody anti-HC (Hyb335) antibody (kindly provided by Prof. Ebba Nexø, Aarhus), were labelled with ^{125}I using the Iodogen method (Pierce) and purified on a PD10 column (GE healthcare, Switzerland). Mice were injected intravenously (tail vein) with 10 µg (150 pmol)/0.1-0.4 MBq of the ^{125}I-rhHC proteins or 10µg (83 pmol)/0.8 MBq in 100 µL PBS. After 24 h the animals were sacrificed, dissected and measured in a gamma counter (Cobra II Packard, Canberra Packard GmbH, Frankfurt, Germany).

6.4.10 *In vitro* cell uptake of ^{99m}Tc-labelled Cbl derivatives

24 hours prior to the experiment HCC827 and B16F1 cells were seeded in 12-well plates in triplicates to form confluent monolayers overnight. Before adding the labelled Cbl derivatives cells were washed twice with PBS (pH 7.4). 500 µl binding medium (normal culture medium but without FCS, + HEPES 20 mM) was pipetted into each well and 500 µl of the ^{99m}Tc-labelled Cbl derivatives (7-14 pMol 0.04 MBq) with or without 100 ng (1.5 nM HC,

2 nM TC, 2 nM mTC) of the recombinant proteins were added. After 24 hours incubation at 37°C, 5% CO_2, the cells were washed twice with PBS/0.1% bovine serum albumin and then incubated for 5 min. with ice-cold acid wash buffer (50 mM Glycine-HCl, 100 mM NaCl, pH 2.8). Subsequently, cells were solubilised by incubation with 1 N NaOH for 5 min. The radioactivity in the cell medium, the acid wash (cell-surface bound) and the solubilised cells (internalised) were determined with a NaI-γ-counter (Cobra II Packard, Canberra Packard GmbH).

6.4.11 Analysis of gene transcription level - RNA extraction, cDNA synthesis and qPCR

Total RNA was isolated from cultured cells using the RNeasy Mini kit (Qiagen). Before total RNA was isolated the cells were washed with PBS, detached with PBS/EDTA 1mM and harvested in 1mL PBS. Centrifugation of the cells was done by spinning at 1000 rpm and 4°C for 5 min. The cells were lysed by adding 600 µL of Buffer RLT supplied by the kit and total RNA was extracted according to the manufacturer. About 2 µg of total RNA was used for first strand cDNA synthesis using the RevertAid H Minus First Strand cDNA Synthesis Kit (Thermo Scientifc). 1 µl of the cDNA synthesis was then directly used for qRT-PCR with QuantiTect® SYBR® Green PCR Kit (Qiagen). Primer #2 (Primer bank ID: 133987572b2): Forward 5'-ATTCCAAGCCAACTATGCGAG-3', Reverse 5'-CAGAGGTTTTAGGCGGATGTAG-3'. Primer #3 (Primer bank ID: 133987572b3): Forward 5'-CATCCGCCTAAAACCTCTGTT-3', Reverse 5'-CGCTGGTTCCCCTGTTATAGTT-3' and as internal control the beta actin primers: Forward 5'-CATGTACGTTGCTATCCAGGC-3', Reverse 5'-CTCCTTAATGTCACGCACGAT-3' (Microsynth) were used for PCR amplification and fluorescence detection on an 7900 HT Fast Real-Time PCR System (Applied Biosystems) under the following conditions: 95°C, for 10 min, followed by 40 cycles of 94°C, 15 s, 53°C, 30 s, 72°C, 30 s. The fold change was calculated by the comparative CT method ($2^{-\Delta\Delta Ct}$) of relative quantitation.

6.4.12 Differential scanning fluorimetry

A Rotor-Gene cycler (Rotor-Gene 5plex HRM, QIAGEN) was used for protein stability measurement by differential scanning fluorimetry. Stability measurements were performed in phosphate buffered saline (PBS). SYPRO® Orange (Invitrogen) was used at 5x

endconcentration. Protein concentrations of approximately 300-400 nM and excess ligand concentration of about 10-20 µM were used. HRM was programmed to increase the temperature from 25°C to 95°C, collecting the data every 0.5°C, with an equilibration time of 2 seconds (see also section 5).

.

7 Conclusion and Outlook

HC's role in Cbl transport in blood as well as structural explanations for the low ligand specificity has been obscure since the discovery of the protein. The findings that HC may play a potential role in the transport and uptake of radiolabelled Cbl derivatives to tumour cells even stressed the lack of information about this protein.

To gain a broader insight into the complex mechanism of Cbl transport and uptake, it was crucial to have milligrams of highly pure HC available, in order to study ligand binding and transport pathways more accurately. Therefore, succeeding in the development of an expression system for rhHC can be regarded as a milestone in Cbl research.

Expression of rhHC in HEK293 cells resulted in approximately 6 mg/L highly pure protein that allowed us to crystallise rhHC in complex with CNCbl and Cbi. Two major differences could be identified: First, the non-conserved amino acid residues Asn120, Asn373 and Arg357 to both the *e*- and the *f*-side chains of the corrin ring seem to be responsible for the ligand specificity, by stabilizing ligands with missing or modified DMB moieties. Secondly, Arg357 stabilises the "flip-in"-conformation of Cbi's *e*-side chain and therefore accounts for its binding ability to HC. All these observations extended our knowledge about Cbl and Cbl analogue binding and the ligand specificity among the human Cbl transport proteins and is therefore very useful to a much more rational design of new Cbl derivatives.

Having all three human transport proteins available and in order to test the binding ability of newly synthesised Cbl derivatives, we evaluated DSF as a potential technique. Despite the very high affinity constants of approximately 10^{-15} M of the three transport proteins to Cbls, DSF offers a simple, inexpensive and robust method to rank the different Cbl derivatives based on their ΔT_m values. This allows determination of a ligand's ability to bind to a given transport protein by comparing the values obtained with the values of ligands with a known binding behaviour (e.g. CNCbl or Cbi).

The promising tumour uptake of HC-specific Cbl derivative, ^{99m}Tc-PAMA(4)-Cbl, in mice (Waibel *et al*. 2008) and also in humans (unpublished data) lead to many unanswered questions concerning HC's role in tumour uptake of Cbl-derivatives. Although our *in vivo* biodistribution and *ex vivo* autoradiography data strongly indicated a specific uptake of the radiolabeled Cbl derivative, our data do not support the hypothesis that the uptake is HC-

dependent, because HC-producing (HCC827) as well as HC-nonproducing (B16F1) cells showed uptake of the HC-specific ^{99m}Tc-PAMA(4)-Cbl. Furthermore, no specific uptake of recombinant HC or accumulation of an anti-HC antibody in tumour tissue could be observed *in vivo*. *In vitro* experiments with human and mouse cell lines even indicated a blocking of uptake in the presence of recombinant HC. Overall the *in vitro* experiments strongly point toward an alternative uptake mechanism, as it has been described in literature before [203-206]. Further *in vitro* and *in vivo* studies should be conducted for a valid explanation for the high tumour uptake seen in mice.

References

1. Stubbe J (1994) Binding site revealed of nature's most beautiful cofactor. Science, 266: 1663-1664.

2. Randaccio L, Geremia S, Demitri N, Wuerges J (2010) Vitamin B12: unique metalorganic compounds and the most complex vitamins. Molecules, 15: 3228-3259.

3. Banerjee R (1999) Chemistry and biochemistry of B12; Banerjee R, editor. New York: Wiley. xxii, 921 p.

4. Minot GR, Murphy WP (1927) Treatment of pernicious (Addisonian) anaemia with a diet rich in liver. British Medical Journal, 1927: 674-676.

5. Rickes EL, Brink NG, Koniuszy FR, Wood TR, Folkers K (1948) Crystalline Vitamin B12. Science, 107: 396-397.

6. Hodgkin DC (1956) Structure of vitamin B12. Nature, 178: 64-66.

7. Maugh TH, 2nd (1973) Vitamin B12: after 25 years, the first synthesis. Science, 179: 266-267.

8. Battersby AR (1999) Biosynthesis of B12 in the aerobic organism *Pseudomonas dentrificans*. Chemistry and biochemistry of B12. New York: Wiley. pp. 507-535 p.

9. Scott AI, Roessner CA, Santader PJ (1999) B12 Biosynthesis: the anaerobic pathway Chemistry and biochemistry of B12. New York: Wiley. pp. 507-535 p.

10. Randaccio L, Geremia S, Wuerges J (2007) Crystallography of vitamin B-12 proteins. Journal of Organometallic Chemistry, 692: 1198-1215.

11. Wuerges J, Garau G, Geremia S, Fedosov SN, Petersen TE, et al. (2006) Structural basis for mammalian vitamin B12 transport by transcobalamin. Proc Natl Acad Sci USA, 103: 4386-4391.

12. Mathews FS (2007) Crystal structure of human intrinsic factor: cobalamin complex at 2.6-A resolution. Proc Natl Acad Sci USA, 104: 17311-17316.

13. Fedosov SN (2012) Physiological and molecular aspects of cobalamin transport. Subcell Biochem, 56: 347-367.

14. Nielsen MJ, Rasmussen MR, Andersen CB, Nexo E, Moestrup SK (2012) Vitamin B12 transport from food to the body's cells--a sophisticated, multistep pathway. Nat Rev Gastroenterol Hepatol, 9: 345-354.

15. Roth JR, Lawrence JG, Bobik TA (1996) Cobalamin (coenzyme B12): synthesis and biological significance. Annu Rev Microbiol, 50: 137-181.

16. Kräutler B (2007) B12-Coenzymes, the Central Theme. Vitamin B12 and B12-Proteins: Wiley-VCH Verlag GmbH. pp. 1-2.

17. Lerner-Ellis JP (2006) Identification of the gene responsible for methylmalonic aciduria and homocystinuria, cblC type. Nat Genet, 38: 93-100.

18. Kim J, Gherasim C, Banerjee R (2008) Decyanation of vitamin B12 by a trafficking chaperone. Proc Natl Acad Sci USA, 105: 14551-14554.

19. Hannibal L (2009) Processing of alkylcobalamins in mammalian cells: a role for the MMACHC (cblC) gene product. Mol Genet Metab, 97: 260-266.

20. Pratt JM (1972) Inorganic chemistry of vitamin B12. London, New York,: Academic Press.

21. Banerjee R, Ragsdale SW (2003) The many faces of vitamin B12: catalysis by cobalamin-dependent enzymes. Annu Rev Biochem, 72: 209-247.

22. Carmel R, Green R, Rosenblatt DS, Watkins D (2003) Update on cobalamin, folate, and homocysteine. Hematology Am Soc Hematol Educ Program: 62-81.

23. Fedosov SN, Petersen TE, Nexo E (1996) Transcobalamin from cow milk: isolation and physico-chemical properties. Biochim Biophys Acta, 1292: 113-119.

24. Ortigues-Marty I, Micol D, Prache S, Dozias D, Girard CL (2005) Nutritional value of meat: the influence of nutrition and physical activity on vitamin B12 concentrations in ruminant tissues. Reprod Nutr Dev, 45: 453-467.

25. Allen RH (1975) Human vitamin B12 transport proteins. Prog Hematol, 9: 57-84.

26. Nexø E (1998) Cobalamin Binding Proteins. Vitamin B12 and B12-Proteins: Wiley-VCH Verlag GmbH. pp. 461-475.

27. Moestrup SK (2006) New insights into carrier binding and epithelial uptake of the erythropoietic nutrients cobalamin and folate. Curr Opin Hematol, 13: 119-123.

28. Furger E, Fedosov SN, Lildballe DL, Waibel R, Schibli R, et al. (2012) Comparison of recombinant human haptocorrin expressed in human embryonic kidney cells and native haptocorrin. PLoS One, 7: e37421.

29. Morkbak AL, Hvas AM, Lloyd-Wright Z, Sanders TA, Bleie O, et al. (2006) Effect of vitamin B12 treatment on haptocorrin. Clin Chem, 52: 1104-1111.

30. Gordon MM, Hu C, Chokshi H, Hewitt JE, Alpers DH (1991) Glycosylation is not required for ligand or receptor binding by expressed rat intrinsic factor. Am J Physiol, 260: G736-G742.

31. Alpers DH, Russell-Jones G (1999) Intrinsic factor, Haptocorrin, and their Receptors. Chemistry and biochemistry of B12. New York: Wiley. pp. 411-440 p.

32. Allen RH, Seetharam B, Podell E, Alpers DH (1978) Effect of proteolytic enzymes on the binding of cobalamin to R protein and intrinsic factor. In vitro evidence that a failure to partially degrade R protein is responsible for cobalamin malabsorption in pancreatic insufficiency. J Clin Invest, 61: 47-54.

33. Gueant JL, Djalali M, Aouadj R, Gaucher P, Monin B, et al. (1986) In vitro and in vivo evidences that the malabsorption of cobalamin is related to its binding on haptocorrin (R binder) in chronic pancreatitis. Am J Clin Nutr, 44: 265-277.

34. Moestrup SK (1998) The intrinsic factor/vitamin B12 receptor and target of teratogenic antibodies is a megalin-binding peripheral membrane protein with homology to developmental proteins. J Biol Chem, 273: 5235-5242.

35. Fyfe JC, Madsen M, Hojrup P, Christensen EI, Tanner SM, et al. (2004) The functional cobalamin (vitamin B12)-intrinsic factor receptor is a novel complex of cubilin and amnionless. Blood, 103: 1573-1579.

36. He Q (2005) Amnionless function is required for cubilin brush-border expression and intrinsic factor-cobalamin (vitamin B12) absorption in vivo. Blood, 106: 1447-1453.

37. Birn H, Verroust PJ, Nexo E, Hager H, Jacobsen C, et al. (1997) Characterization of an epithelial approximately 460-kDa protein that facilitates endocytosis of intrinsic factor-vitamin B12 and binds receptor-associated protein. J Biol Chem, 272: 26497-26504.

38. Kozyraki R (1998) The human intrinsic factor-vitamin B12 receptor, cubilin: molecular characterization and chromosomal mapping of the gene to 10p within the autosomal recessive megaloblastic anemia (MGA1) region. Blood, 91: 3593-3600.

39. Fedosov SN, Berglund L, Nexo E, Petersen TE (1999) Sequence, S-S bridges, and spectra of bovine transcobalamin expressed in Pichia pastoris. J Biol Chem, 274: 26015-26020.

40. Quadros EV, Nakayama Y, Sequeira JM (2009) The protein and the gene encoding the receptor for the cellular uptake of transcobalamin-bound cobalamin. Blood, 113: 186-192.

41. Amagasaki T, Green R, Jacobsen DW (1990) Expression of transcobalamin II receptors by human leukemia K562 and HL-60 cells. Blood, 76: 1380-1386.

42. Cho W (2008) Expression of CD320 in human B cells in addition to follicular dendritic cells. BMB Rep, 41: 863-867.

43. Jiang W, Sequeira JM, Nakayama Y, Lai SC, Quadros EV (2010) Characterization of the promoter region of TCblR/CD320 gene, the receptor for cellular uptake of transcobalamin-bound cobalamin. Gene, 466: 49-55.

44. Arendt JF, Quadros EV, Nexo E (2012) Soluble transcobalamin receptor, sCD320, is present in human serum and relates to serum cobalamin - establishment and validation of an ELISA. Clin Chem Lab Med, 50: 515-519.

45. Quadros EV, Nakayama Y, Sequeira JM (2005) The binding properties of the human receptor for the cellular uptake of vitamin B12. Biochem Biophys Res Commun, 327: 1006-1010.

46. Moestrup SK (1996) Megalin-mediated endocytosis of transcobalamin-vitamin-B12 complexes suggests a role of the receptor in vitamin-B12 homeostasis. Proc Natl Acad Sci USA, 93: 8612-8617.

47. Zheng G, Bachinsky DR, Stamenkovic I, Strickland DK, Brown D, et al. (1994) Organ distribution in rats of two members of the low-density lipoprotein receptor gene family, gp330 and LRP/alpha 2MR, and the receptor-associated protein (RAP). J Histochem Cytochem, 42: 531-542.

48. Kounnas MZ, Haudenschild CC, Strickland DK, Argraves WS (1994) Immunological localization of glycoprotein 330, low density lipoprotein receptor related protein and 39 kDa receptor associated protein in embryonic mouse tissues. In Vivo, 8: 343-351.

49. Leheste JR (1999) Megalin knockout mice as an animal model of low molecular weight proteinuria. Am J Pathol, 155: 1361-1370.

50. Morkbak AL, Poulsen SS, Nexo E (2007) Haptocorrin in humans. Clin Chem Lab Med, 45: 1751-1759.

51. Hurlimann J, Zuber C (1969) Vitamin B12-binders in human body fluids. I. Antigenic and physico-chemical characteristics. Clin Exp Immunol, 4: 125-140.

52. Rachmilewitz B, Rachmilewitz M, Gross J (1974) A vitamin B12 binder with transcobalmin I characteristics synthesized and released by human granulocytes in vitro. Br J Haematol, 26: 557-567.

53. Waxman S, Gilbert HS (1973) A tumor-related vitamin B12 binding protein in adolescent hepatoma. N Engl J Med, 289: 1053-1056.

54. Nexo E, Olesen H, Christensen JM, Thomsen J, Kristiansen K (1975) Characterization of a cobalamin-binding plasma protein from a patient with hepatoma. Scand J Clin Lab Invest, 35: 683-690.

55. Yang SY, Coleman PS, Dupont B (1982) The biochemical and genetic basis for the microheterogeneity of human R-type vitamin B12 binding proteins. Blood, 59: 747-755.

56. Burger RL, Schneider RJ, Mehlman CS, Allen RH (1975) Human plasma R-type vitamin B12-binding proteins. II. The role of transcobalamin I, transcobalamin III, and the normal granulocyte vitamin B12-binding protein in the plasma transport of vitamin B12. J Biol Chem, 250: 7707-7713.

57. Bider MD, Cescato R, Jeno P, Spiess M (1995) High-affinity ligand binding to subunit H1 of the asialoglycoprotein receptor in the absence of subunit H2. Eur J Biochem, 230: 207-212.

58. Hom BL, Olesen HA (1969) Plasma clearance of 57cobalt-labelled vitamin B12 bound in vitro and in vivo to transcobalamin I and II. Scand J Clin Lab Invest, 23: 201-211.

59. Kolhouse JF, Kondo H, Allen NC, Podell E, Allen RH (1978) Cobalamin analogues are present in human plasma and can mask cobalamin deficiency because current

radioisotope dilution assays are not specific for true cobalamin. N Engl J Med, 299: 785-792.

60. Stupperich E, Nexo E (1991) Effect of the cobalt-N coordination on the cobamide recognition by the human vitamin B12 binding proteins intrinsic factor, transcobalamin and haptocorrin. Eur J Biochem, 199: 299-303.

61. Del Corral A, Carmel R (1990) Transfer of cobalamin from the cobalamin-binding protein of egg yolk to R binder of human saliva and gastric juice. Gastroenterology, 98: 1460-1466.

62. Allen RH, Seetharam B, Allen NC, Podell ER, Alpers DH (1978) Correction of cobalamin malabsorption in pancreatic insufficiency with a cobalamin analogue that binds with high affinity to R protein but not to intrinsic factor. In vivo evidence that a failure to partially degrade R protein is responsible for cobalamin malabsorption in pancreatic insufficiency. J Clin Invest, 61: 1628-1634.

63. Froese DS, Gravel RA (2010) Genetic disorders of vitamin B12 metabolism: eight complementation groups - eight genes. Expert Rev Mol Med, 12: e37.

64. Banerjee R, Gherasim C, Padovani D (2009) The tinker, tailor, soldier in intracellular B12 trafficking. Curr Opin Chem Biol, 13: 484-491.

65. Beedholm-Ebsen R, van de Wetering K, Hardlei T, Nexo E, Borst P, et al. (2010) Identification of multidrug resistance protein 1 (MRP1/ABCC1) as a molecular gate for cellular export of cobalamin. Blood, 115: 1632-1639.

66. Hogenkamp HPC, Collins DA, Grissom CB, West FG (1999) Diagnostic and therapeutic analogues of cobalamin. Chemistry and biochemistry of B12. New York: Wiley. pp. 385-410 p.

67. Zhou K (2012) Vitamin B12 derivatives with peptide backbones. Zürich: Dissertation University Zürich.

68. Fedosov SN, Fedosova NU, Berglund L, Moestrup SK, Nexo E, et al. (2004) Assembly of the intrinsic factor domains and oligomerization of the protein in the presence of cobalamin. Biochemistry, 43: 15095-15102.

69. Fedosov SN, Fedosova NU, Berglund L, Moestrup SK, Nexo E, et al. (2005) Composite organization of the cobalamin binding and cubilin recognition sites of intrinsic factor. Biochemistry, 44: 3604-3614.

70. Wuerges J, Geremia S, Randaccio L (2007) Structural study on ligand specificity of human vitamin B12 transporters. Biochem J, 403: 431-440.

71. Fedosov SN, Grissom CB, Fedosova NU, Moestrup SK, Nexo E, et al. (2006) Application of a fluorescent cobalamin analogue for analysis of the binding kinetics. A study employing recombinant human transcobalamin and intrinsic factor. FEBS J, 273: 4742-4753.

72. Fedosov SN, Fedosova NU, Krautler B, Nexo E, Petersen TE (2007) Mechanisms of discrimination between cobalamins and their natural analogues during their binding to the specific B12-transporting proteins. Biochemistry, 46: 6446-6458.

73. Clardy SM, Allis DG, Fairchild TJ, Doyle RP (2011) Vitamin B12 in drug delivery: breaking through the barriers to a B12 bioconjugate pharmaceutical. Expert Opin Drug Deliv, 8: 127-140.

74. Pathare PM, Wilbur DS, Heusser S, Quadros EV, McLoughlin P, et al. (1996) Synthesis of cobalamin-biotin conjugates that vary in the position of cobalamin coupling. Evaluation of cobalamin derivative binding to transcobalamin II. Bioconjug Chem, 7: 217-232.

75. Waibel R, Treichler H, Schaefer NG, van Staveren DR, Mundwiler S, et al. (2008) New derivatives of vitamin B12 show preferential targeting of tumors. Cancer Res, 68: 2904-2911.

76. Vlahov IR, Leamon CP (2012) Engineering folate-drug conjugates to target cancer: from chemistry to clinic. Bioconjug Chem, 23: 1357-1369.

77. Müller C (2012) Folate based radiopharmaceuticals for imaging and therapy of cancer and inflammation. Curr Pharm Des, 18: 1058-1083.

78. Bagnato JD, Eilers AL, Horton RA, Grissom CB (2004) Synthesis and characterization of a cobalamin-colchicine conjugate as a novel tumor-targeted cytotoxin. J Org Chem, 69: 8987-8996.

79. Howard WA, Jr., Bayomi A, Natarajan E, Aziza MA, el-Ahmady O, et al. (1997) Sonolysis promotes indirect Co-C bond cleavage of alkylcob(III)alamin bioconjugates. Bioconjug Chem, 8: 498-502.

80. Siega P, Wuerges J, Arena F, Gianolio E, Fedosov SN, et al. (2009) Release of toxic Gd3+ ions to tumour cells by vitamin B12 bioconjugates. Chemistry, 15: 7980-7989.

81. Mundwiler S, Spingler B, Kurz P, Kunze S, Alberto R (2005) Cyanide-bridged vitamin B12-cisplatin conjugates. Chemistry, 11: 4089-4095.

82. Ruiz-Sánchez P (2010) Vitamin B12: A Potential Targeting Molecule for Therapeutic Drug Delivery. Ideas in Chemistry and Molecular Sciences: Wiley-VCH Verlag GmbH & Co. KGaA. pp. 93-115.

83. Ruiz-Sanchez P, Mundwiler S, Spingler B, Buan NR, Escalante-Semerena JC, et al. (2008) Syntheses and characterization of vitamin B12-Pt(II) conjugates and their adenosylation in an enzymatic assay. J Biol Inorg Chem, 13: 335-347.

84. Ruiz-Sanchez P, Konig C, Ferrari S, Alberto R (2011) Vitamin B12 as a carrier for targeted platinum delivery: in vitro cytotoxicity and mechanistic studies. J Biol Inorg Chem, 16: 33-44.

85. Bauer JA, Morrison BH, Grane RW, Jacobs BS, Dabney S, et al. (2002) Effects of interferon beta on transcobalamin II-receptor expression and antitumor activity of nitrosylcobalamin. J Natl Cancer Inst, 94: 1010-1019.

86. Bauer JA, Lupica JA, Schmidt H, Morrison BH, Haney RM, et al. (2007) Nitrosylcobalamin potentiates the anti-neoplastic effects of chemotherapeutic agents via suppression of survival signaling. PLoS One, 2: e1313.

87. Russell-Jones GJ, Westwood SW, Habberfield AD (1995) Vitamin B12 mediated oral delivery systems for granulocyte-colony stimulating factor and erythropoietin. Bioconjug Chem, 6: 459-465.

88. Russell-Jones GJ, Westwood SW, Farnworth PG, Findlay JK, Burger HG (1995) Synthesis of LHRH antagonists suitable for oral administration via the vitamin B12 uptake system. Bioconjug Chem, 6: 34-42.

89. Petrus AK, Fairchild TJ, Doyle RP (2009) Traveling the Vitamin B-12 Pathway: Oral Delivery of Protein and Peptide Drugs. Angewandte Chemie-International Edition, 48: 1022-1028.

90. McEwan JF, Veitch HS, Russell-Jones GJ (1999) Synthesis and biological activity of ribose-5'-carbamate derivatives of vitamin B12. Bioconjug Chem, 10: 1131-1136.

91. Petrus AK, Vortherms AR, Fairchild TJ, Doyle RP (2007) Vitamin B12 as a carrier for the oral delivery of insulin. ChemMedChem, 2: 1717-1721.

92. Chalasani KB, Russell-Jones GJ, Yandrapu SK, Diwan PV, Jain SK (2007) A novel vitamin B12-nanosphere conjugate carrier system for peroral delivery of insulin. J Control Release, 117: 421-429.

93. Chalasani KB, Russell-Jones GJ, Jain AK, Diwan PV, Jain SK (2007) Effective oral delivery of insulin in animal models using vitamin B12-coated dextran nanoparticles. J Control Release, 122: 141-150.

94. Viola-Villegas N, Rabideau AE, Bartholoma M, Zubieta J, Doyle RP (2009) Targeting the cubilin receptor through the vitamin B12 uptake pathway: cytotoxicity and mechanistic insight through fluorescent Re(I) delivery. J Med Chem, 52: 5253-5261.

95. Vortherms AR, Kahkoska AR, Rabideau AE, Zubieta J, Andersen LL, et al. (2011) A water soluble vitamin B12-ReI fluorescent conjugate for cell uptake screens: use in the confirmation of cubilin in the lung cancer line A549. Chem Commun (Camb), 47: 9792-9794.

96. Anderson RC, Delabarre Y (1951) The Preparation of Radioactive Vitamin-B12 by Direct Neutron Irradiation. Journal of the American Chemical Society, 73: 4051-4052.

97. Smith EL (1952) Tracer Studies with the Vitamins-B12 .1. Neutron Irradiation of Vitamin-B12. Biochem J, 52: 384-387.

98. Smith EL, Hockenhull DJD, Quilter ARJ (1952) Tracer Studies with the Vitamins-B12 .2. Biosynthesis of Vitamin-B12 Labelled with Co-60 and P-32. Biochem J, 52: 387-388.

99. Flodh H, Ullberg S (1968) Accumulation of labelled vitamin B12 in some transplanted tumours. Int J Cancer, 3: 694-699.

100. Wilbur DS, Hamlin DK, Pathare PM, Heusser S, Vessella RL, et al. (1996) Synthesis and nca-Radioiodination of Arylstannyl−Cobalamin Conjugates. Evaluation of Aryliodo−Cobalamin Conjugate Binding to Transcobalamin II and Biodistribution in Mice. Bioconjugate Chemistry, 7: 461-474.

101. Kunze S, Zobi F, Kurz P, Spingler B, Alberto R (2004) Vitamin B12 as a ligand for technetium and rhenium complexes. Angew Chem Int Ed Engl, 43: 5025-5029.

102. van Staveren DR, Mundwiler S, Hoffmanns U, Pak JK, Spingler B, et al. (2004) Conjugation of a novel histidine derivative to biomolecules and labelling with $[^{99m}Tc(OH_2)_3(CO)_3]^+$. Org Biomol Chem, 2: 2593-2603.

103. Collins DA, Hogenkamp HP (1997) Transcobalamin II receptor imaging via radiolabeled diethylene-triaminepentaacetate cobalamin analogs. J Nucl Med, 38: 717-723.

104. Yang JQ, Li Y, Lu J, Wang XB (2005) Preparation and biodistribution in mice of Tc-99m-DTPA-b-cyanocobalamin. Journal of Radioanalytical and Nuclear Chemistry, 265: 467-472.

105. Collins DA, Hogenkamp HP, O'Connor MK, Naylor S, Benson LM, et al. (2000) Biodistribution of radiolabeled adenosylcobalamin in patients diagnosed with various malignancies. Mayo Clin Proc, 75: 568-580.

106. Collins DA, Hogenkamp HP, Gebhard MW (1999) Tumor imaging via indium 111-labeled DTPA-adenosylcobalamin. Mayo Clin Proc, 74: 687-691.

107. Smeltzer CC, Cannon MJ, Pinson PR, Munger JD, Jr., West FG, et al. (2001) Synthesis and characterization of fluorescent cobalamin (CobalaFluor) derivatives for imaging. Organic Letters, 3: 799-801.

108. McGreevy JM, Cannon MJ, Grissom CB (2003) Minimally invasive lymphatic mapping using fluorescently labeled vitamin B12. J Surg Res, 111: 38-44.

109. Russell-Jones G, McTavish K, McEwan J (2011) Preliminary studies on the selective accumulation of vitamin-targeted polymers within tumors. J Drug Target, 19: 133-139.

110. van Dam GM, Themelis G, Crane LM, Harlaar NJ, Pleijhuis RG, et al. (2011) Intraoperative tumor-specific fluorescence imaging in ovarian cancer by folate receptor-alpha targeting: first in-human results. Nat Med, 17: 1315-1319.

111. Chawla-Sarkar M, Bauer JA, Lupica JA, Morrison BH, Tang Z, et al. (2003) Suppression of NF-kappa B survival signaling by nitrosylcobalamin sensitizes neoplasms to the anti-tumor effects of Apo2L/TRAIL. J Biol Chem, 278: 39461-39469.

112. Bauer JA, Frye G, Bahr A, Gieg J, Brofman P (2010) Anti-tumor effects of nitrosylcobalamin against spontaneous tumors in dogs. Invest New Drugs, 28: 694-702.

113. Moestrup SK, Verroust PJ (1999) Mammalian Receptors of Vitamin B12-Binding Proteins. Chemistry and biochemistry of B12. New York: Wiley. pp. 475-488 p.

114. Hardlei TF, Nexo E (2009) A new principle for measurement of cobalamin and corrinoids, used for studies of cobalamin analogs on serum haptocorrin. Clin Chem, 55: 1002-1010.

115. Lildballe DL, Nguyen KQ, Poulsen SS, Nielsen HO, Nexo E (2011) Haptocorrin as marker of disease progression in fibrolamellar hepatocellular carcinoma. Eur J Surg Oncol, 37: 72-79.

116. Nexo E, Olesen H, Norredam K, Schwartz M (1975) A rare case of megaloblastic anaemia caused by disturbances in the plasma cobalamin binding proteins in a patient with hepatocellular carcinoma. Scand J Haematol, 14: 320-327.

117. Gruvberger SK, Ringner M, Eden P, Borg A, Ferno M, et al. (2003) Expression profiling to predict outcome in breast cancer: the influence of sample selection. Breast Cancer Res, 5: 23-26.

118. Fedosov SN, Laursen NB, Nexo E, Moestrup SK, Petersen TE, et al. (2003) Human intrinsic factor expressed in the plant Arabidopsis thaliana. Eur J Biochem, 270: 3362-3367.

119. Gordon M, Chokshi H, Alpers DH (1992) In vitro expression and secretion of functional mammalian intrinsic factor using recombinant baculovirus. Biochim Biophys Acta, 1132: 276-283.

120. Quadros EV, Sai P, Rothenberg SP (1993) Functional human transcobalamin II isoproteins are secreted by insect cells using the baculovirus expression system. Blood, 81: 1239-1245.

121. Nexo E (1978) Transcobalamin I and other human R-binders: purification, structural, spectral and physiological studies. Scand J Haematol, 20: 221-236.

122. Henning S, Peter-Katalinic J, Pohlentz G (2009) Structure analysis of N-glycoproteins. Methods Mol Biol, 492: 181-200.

123. Gupta R, Brunak S (2002) Prediction of glycosylation across the human proteome and the correlation to protein function. Pac Symp Biocomput: 310-322.

124. Julenius K, Molgaard A, Gupta R, Brunak S (2005) Prediction, conservation analysis, and structural characterization of mammalian mucin-type O-glycosylation sites. Glycobiology, 15: 153-164.

125. Fedosov SN, Berglund L, Fedosova NU, Nexo E, Petersen TE (2002) Comparative analysis of cobalamin binding kinetics and ligand protection for intrinsic factor, transcobalamin, and haptocorrin. J Biol Chem, 277: 9989-9996.

126. Nexo E, Olesen H (1976) Changes in the ultraviolet and circular dichroism spectra of aquo-, hydroxy-, azido-, and cyanocobalamin when bound to human intrinsic factor or human transcobalamin I. Biochim Biophys Acta, 446: 143-150.

127. Burger RL, Allen RH (1974) Characterization of vitamin B12-binding proteins isolated from human milk and saliva by affinity chromatography. J Biol Chem, 249: 7220-7227.

128. Burger RL, Waxman S, Gilbert HS, Mehlman CS, Allen RH (1975) Isolation and characterization of a novel vitamin B12-binding protein associated with hepatocellular carcinoma. J Clin Invest, 56: 1262-1270.

129. Nexo E (1975) A new principle in biospecific affinity chromatography used for purification of cobalamin-binding proteins. Biochim Biophys Acta, 379: 189-192.

130. Pace CN, Vajdos F, Fee L, Grimsley G, Gray T (1995) How to measure and predict the molar absorption coefficient of a protein. Protein Sci, 4: 2411-2423.

131. Park JH, Cho EW, Shin SY, Lee YJ, Kim KL (1998) Detection of the asialoglycoprotein receptor on cell lines of extrahepatic origin. Biochem Biophys Res Commun, 244: 304-311.

132. Sandig V, Rose T, Winkler K, Brecht R (2005) Mammalian Cells. Production of Recombinant Proteins: Wiley-VCH Verlag GmbH & Co. KGaA. pp. 233-252.

133. Nexo E, Hansen MR, Konradsen L (1988) Human salivary epidermal growth factor, haptocorrin and amylase before and after prolonged exercise. Scand J Clin Lab Invest, 48: 269-273.

134. Grunberg J, Knogler K, Waibel R, Novak-Hofer I (2003) High-yield production of recombinant antibody fragments in HEK-293 cells using sodium butyrate. Biotechniques, 34: 968-972.

135. Morkbak AL, Pedersen JF, Nexo E (2005) Glycosylation independent measurement of the cobalamin binding protein haptocorrin. Clin Chim Acta, 356: 184-190.

136. Fedosov SN, Berglund L, Nexø E, Petersen TE (2007) Tetrazole derivatives and matrices as novel cobalamin coordinating compounds. J Organomettallic Chem, 692: 1234-1242.

137. Elder JH, Alexander S (1982) endo-beta-N-acetylglucosaminidase F: endoglycosidase from Flavobacterium meningosepticum that cleaves both high-mannose and complex glycoproteins. Proc Natl Acad Sci USA, 79: 4540-4544.

138. Chang VT, Crispin M, Aricescu AR, Harvey DJ, Nettleship JE, et al. (2007) Glycoprotein structural genomics: solving the glycosylation problem. Structure, 15: 267-273.

139. Nexo E, Christensen AL, Petersen TE, Fedosov SN (2000) Measurement of transcobalamin by ELISA. Clin Chem, 46: 1643-1649.

140. Allen RH, Majerus PW (1972) Isolation of vitamin B12-binding proteins using affinity chromatography. III. Purification and properties of human plasma transcobalamin II. J Biol Chem, 247: 7709-7717.

141. Van Kapel J, Loef BG, Lindemans J, Abels J (1981) An improved method for large scale purification of human holo-transcobalamin II. Biochim Biophys Acta, 676: 307-313.

142. Quadros EV, Rothenberg SP, Pan YC, Stein S (1986) Purification and molecular characterization of human transcobalamin II. J Biol Chem, 261: 15455-15460.

143. Platica O, Geneczko R, Regec A, Quadros EV, Rothenberg SP (1989) Isolation of the complementary DNA for human transcobalamin II. Proc Soc Exp Biol Med, 192: 95-97.

144. Seetharam S, Dahms N, Li N, Seetharam B (1991) Functional expression of transcobalamin II cDNA in Xenopus laevis oocytes. Biochem Biophys Res Commun, 181: 1151-1155.

145. Coffey JW, Hansen HJ, Miller ON (1965) Studies on the Interaction of Vitamin B12: Intrinsic Factor and Receptors. 3. Chemical and Biological Properties of Vitamin B12 Combining Substances from the Stomach, Serum, and Ascites Fluid of the Mouse. Arch Biochem Biophys, 110: 117-123.

146. Green PD, Savage CR, Jr., Hall CA (1976) Mouse transcobalamin II: biosynthesis and uptake by L-929 cells. Arch Biochem Biophys, 176: 683-689.

147. Hippe E, Schonau Jorgensen F, Olesen H (1977) Cobalamin binding proteins in stomach and serum from various animal species data for B12 binding capacities and molecular sizes of the binding proteins. Comp Biochem Physiol B, 56: 305-309.

148. Frater-Schroder M, Haller O, Gmur R, Kierat L, Anastasi S (1982) Allelic forms of mouse transcobalamin 2. Biochem Genet, 20: 1001-1014.

149. Hygum K (2011) Mouse transcobalamin has features resembling both human transcobalamin and haptocorrin. PLoS One, 6: e20638.

150. Tan CH, Blaisdell SJ, Hansen HJ (1973) Mouse transcobalamin II metabolism: the effects of antibiotics on the clearance of vitamin B12 from the serum transcobalamin II-vitamin B12 complex and the reappearance of free serum transcobalamin II in the mouse. Biochim Biophys Acta, 320: 469-477.

151. Platica O, Janeczko R, Quadros EV, Regec A, Romain R, et al. (1991) The cDNA sequence and the deduced amino acid sequence of human transcobalamin II show homology with rat intrinsic factor and human transcobalamin I. J Biol Chem, 266: 7860-7863.

152. Yamada R, Mizutani S, Kurauchi O, Okano K, Imaizumi H, et al. (1988) Purification and characterization of human placental aminopeptidase A. Enzyme, 40: 223-230.

153. Hirel PH, Schmitter MJ, Dessen P, Fayat G, Blanquet S (1989) Extent of N-terminal methionine excision from Escherichia coli proteins is governed by the side-chain length of the penultimate amino acid. Proc Natl Acad Sci USA, 86: 8247-8251.

154. Rothenberg SP, Quadros EV, Regec A (1999) Transcobalamin II. Chemistry and biochemistry of B12. New York: Wiley. pp. 441-473 p.

155. Allen RH, Majerus PW (1972) Isolation of vitamin B12-binding proteins using affinity chromatography. II. Purification and properties of a human granulocyte vitamine B12-binding protein. J Biol Chem, 247: 7702-7708.

156. Chen VB, Arendall WB, 3rd, Headd JJ, Keedy DA, Immormino RM, et al. (2010) MolProbity: all-atom structure validation for macromolecular crystallography. Acta Crystallogr D Biol Crystallogr, 66: 12-21.

157. Fedosov SN, Fedosova NU, Nexo E, Petersen TE (2000) Conformational changes of transcobalamin induced by aquocobalamin binding. Mechanism of substitution of the cobalt-coordinated group in the bound ligand. J Biol Chem, 275: 11791-11798.

158. Arnold K, Bordoli L, Kopp J, Schwede T (2006) The SWISS-MODEL workspace: a web-based environment for protein structure homology modelling. Bioinformatics, 22: 195-201.

159. Davis SJ, Davies EA, Barclay AN, Daenke S, Bodian DL, et al. (1995) Ligand binding by the immunoglobulin superfamily recognition molecule CD2 is glycosylation-independent. J Biol Chem, 270: 369-375.

160. Sievers F, Wilm A, Dineen D, Gibson TJ, Karplus K, et al. (2011) Fast, scalable generation of high-quality protein multiple sequence alignments using Clustal Omega. Mol Syst Biol, 7: 539.

161. Laskowski RA, Chistyakov VV, Thornton JM (2005) PDBsum more: new summaries and analyses of the known 3D structures of proteins and nucleic acids. Nucleic Acids Res, 33: D266-268.

162. Zhou K, Oetterli RM, Brandl H, Lyatuu FE, Buckel W, et al. (2012) Chemistry and bioactivity of an artificial adenosylpeptide B12 cofactor. Chembiochem, 13: 2052-2055.

163. Andersen CB, Madsen M, Storm T, Moestrup SK, Andersen GR (2010) Structural basis for receptor recognition of vitamin-B12-intrinsic factor complexes. Nature, 464: 445-448.

164. Kabsch W (2010) Xds. Acta Crystallogr D Biol Crystallogr, 66: 125-132.

165. McCoy AJ, Grosse-Kunstleve RW, Adams PD, Winn MD, Storoni LC, et al. (2007) Phaser crystallographic software. J Appl Crystallogr, 40: 658-674.

166. Adams PD, Afonine PV, Bunkoczi G, Chen VB, Davis IW, et al. (2010) PHENIX: a comprehensive Python-based system for macromolecular structure solution. Acta Crystallogr D Biol Crystallogr, 66: 213-221.

167. Emsley P, Cowtan K (2004) Coot: model-building tools for molecular graphics. Acta Crystallogr D Biol Crystallogr, 60: 2126-2132.

168. Davis IW, Murray LW, Richardson JS, Richardson DC (2004) MOLPROBITY: structure validation and all-atom contact analysis for nucleic acids and their complexes. Nucleic Acids Res, 32: W615-619.

169. Karplus PA, Diederichs K (2012) Linking crystallographic model and data quality. Science, 336: 1030-1033.

170. Gouet P, Robert X, Courcelle E (2003) ESPript/ENDscript: Extracting and rendering sequence and 3D information from atomic structures of proteins. Nucleic Acids Res, 31: 3320-3323.

171. Kolhouse JF, Allen RH (1977) Absorption, plasma transport, and cellular retention of cobalamin analogues in the rabbit. Evidence for the existence of multiple mechanisms that prevent the absorption and tissue dissemination of naturally occurring cobalamin analogues. J Clin Invest, 60: 1381-1392.

172. Velazquez-Campoy A, Freire E (2006) Isothermal titration calorimetry to determine association constants for high-affinity ligands. Nat Protocols, 1: 186-191.

173. Perozzo R, Folkers G, Scapozza L (2004) Thermodynamics of protein-ligand interactions: history, presence, and future aspects. J Recept Signal Transduct Res, 24: 1-52.

174. Brada N, Gordon MM, Wen JP, Alpers DH (2001) Transfer of cobalamin from intrinsic factor to transcobalamin II. Journal of Nutritional Biochemistry, 12: 200-206.

175. Marchaj A, Jacobsen DW, Savon SR, Brown KL (1995) Kinetics and Thermodynamics of the Interaction of Cyanocobalamin (Vitamin-B-12) with Haptocorrin - Measurement of the Highest Protein-Ligand Binding Constant yet Reported. Journal of the American Chemical Society, 117: 11640-11646.

176. Nexø E, Olesen H (1982) Quantitation of Cobalamins in Human Serum. In: Dolphin D, editor. B12. New York: Wiley. pp. 88-103.

177. Pantoliano MW, Petrella EC, Kwasnoski JD, Lobanov VS, Myslik J, et al. (2001) High-density miniaturized thermal shift assays as a general strategy for drug discovery. J Biomol Screen, 6: 429-440.

178. Park J, Kim J (2012) Glutathione and vitamin B12 cooperate in stabilization of a B12 trafficking chaperone protein. Protein J, 31: 158-165.

179. Niesen FH, Berglund H, Vedadi M (2007) The use of differential scanning fluorimetry to detect ligand interactions that promote protein stability. Nat Protoc, 2: 2212-2221.

180. Fedosov SN (2003) Human intrinsic factor expressed in the plant Arabidopsis thaliana. Eur J Biochem, 270: 3362-3367.

181. Layton CJ, Hellinga HW (2010) Thermodynamic analysis of ligand-induced changes in protein thermal unfolding applied to high-throughput determination of ligand affinities with extrinsic fluorescent dyes. Biochemistry, 49: 10831-10841.

182. Matulis D, Kranz JK, Salemme FR, Todd MJ (2005) Thermodynamic stability of carbonic anhydrase: measurements of binding affinity and stoichiometry using ThermoFluor. Biochemistry, 44: 5258-5266.

183. Vedadi M, Niesen FH, Allali-Hassani A, Fedorov OY, Finerty PJ, Jr., et al. (2006) Chemical screening methods to identify ligands that promote protein stability, protein crystallization, and structure determination. Proc Natl Acad Sci USA, 103: 15835-15840.

184. Hippe E, Olesen H (1971) Nature of vitamin B 12 binding. 3. Thermodynamics of binding to human intrinsic factor and transcobalamins. Biochim Biophys Acta, 243: 83-88.

185. Holdgate GA, Ward WH (2005) Measurements of binding thermodynamics in drug discovery. Drug Discov Today, 10: 1543-1550.

186. Zhou K, Zelder F (2010) Vitamin B12 mimics having a peptide backbone and tuneable coordination and redox properties. Angew Chem Int Ed Engl, 49: 5178-5180.

187. Cannon MJ, Myszka DG, Bagnato JD, Alpers DH, West FG, et al. (2002) Equilibrium and kinetic analyses of the interactions between vitamin B12 binding proteins and cobalamins by surface plasmon resonance. Anal Biochem, 305: 1-9.

188. Brandts JF, Lin LN (1990) Study of strong to ultratight protein interactions using differential scanning calorimetry. Biochemistry, 29: 6927-6940.

189. Lo MC, Aulabaugh A, Jin G, Cowling R, Bard J, et al. (2004) Evaluation of fluorescence-based thermal shift assays for hit identification in drug discovery. Anal Biochem, 332: 153-159.

190. DiGirolamo PM, Huennekens FM (1975) Transport of vitamin B12 into mouse leukemia cells. Arch Biochem Biophys, 168: 386-393.

191. Jacobsen DW, Montejano YD, Vitols KS, Huennekens FM (1980) Adherence of L1210 murine leukemia cells to sephacryl-aminopropylcobalamin beads treated with transcobalamin-II. Blood, 55: 160-163.

192. Takahashi K, Tavassoli M, Jacobsen DW (1980) Receptor binding and internalization of immobilized transcobalamin II by mouse leukaemia cells. Nature, 288: 713-715.

193. Birn H (2002) Megalin is essential for renal proximal tubule reabsorption and accumulation of transcobalamin-B12. Am J Physiol Renal Physiol, 282: F408-F416.

194. Newmark P, Newman GE, O'Brien JR (1970) Vitamin B12 in the rat kidney. Evidence for an association with lysosomes. Arch Biochem Biophys, 141: 121-130.

195. Russell-Jones G, McTavish K, McEwan J, Rice J, Nowotnik D (2004) Vitamin-mediated targeting as a potential mechanism to increase drug uptake by tumours. J Inorg Biochem, 98: 1625-1633.

196. Birn H, Nexo E, Christensen EI, Nielsen R (2003) Diversity in rat tissue accumulation of vitamin B12 supports a distinct role for the kidney in vitamin B12 homeostasis. Nephrol Dial Transplant, 18: 1095-1100.

197. Hsu JM, Kawin B, Minor P, Mitchell JA (1966) Vitamin B12 Concentrations in Human Tissues. Nature, 210: 1264-1265.

198. Sanford JP, Doyle D (1990) Mouse asialoglycoprotein receptor cDNA sequence: Conservation of receptor genes during mammalian evolution. Biochimica et Biophysica Acta (BBA) - Gene Structure and Expression, 1087: 259-261.

199. Hardlei TF, Morkbak AL, Nexo E (2007) Enzymatic extraction of cobalamin from monoclonal antibody captured haptocorrin and transcobalamin. Clin Biochem, 40: 1392-1397.

200. Stichelberger A, Waibel R, Dumas C, Schubiger PA, Schibli R (2003) Versatile synthetic approach to new bifunctional chelating agents tailor made for labeling with the fac-$[M(CO)_3]^+$ core (M = Tc, ^{99m}Tc, Re): synthesis, in vitro, and in vivo behavior of the model complex $[M(APPA)(CO)_3]$ (APPA = [(5-amino-pentyl)-pyridin-2-yl-methyl-amino]-acetic acid). Nucl Med Biol, 30: 465-470.

201. Alberto R, Schibli R, Egli A, Schubiger AP, Abram U, et al. (1998) A novel organometallic aqua complex of technetium for the labeling of biomolecules: Synthesis of [Tc-99m$(OH_2)_3(CO)_3]^+$ from $[(TcO_4)$-Tc-99m$]^-$ in aqueous solution and its reaction with a bifunctional ligand. Journal of the American Chemical Society, 120: 7987-7988.

202. Waibel R, Alberto R, Willuda J, Finnern R, Schibli R, et al. (1999) Stable one-step technetium-99m labeling of His-tagged recombinant proteins with a novel Tc(I)-carbonyl complex. Nature Biotechnology, 17: 897-901.

203. Quadros EV (2012) Blood transport and tissue distribution of cobalamins: The role of transcobalamin and the receptor for transcobalamin-bound cobalamin. Vitamin B12 Symposium. Nancy France.

204. Hall C, Hitzig W, Green P, Begley J (1979) Transport of therapeutic cyanocobalamin in the congenital deficiency of transcobalamin II (TC II). Blood, 53: 251-263.

205. Berliner N, Rosenberg LE (1981) Uptake and metabolism of free cyanocobalamin by cultured human-fibroblasts from controls and a patient with transcobalamin-II deficiency. Metabolism-Clinical and Experimental, 30: 230-236.

206. Hall CA, Colligan PD (1989) The function of cellular transcobalamin II in cultured human cells. Experimental Cell Research, 183: 159-167.

207. Lildballe DL, Mutti E, Birn H, Nexo E (2012) Maximal load of the vitamin B12 transport system: a study on mice treated for four weeks with high-dose vitamin B12 or cobinamide. Plos One, 7: e46657.

208. Hennemann G (2005) Notes on the history of cellular uptake and deiodination of thyroid hormone. Thyroid, 15: 753-756.

209. Vayre L, Sabourin JC, Caillou B, Ducreux M, Schlumberger M, et al. (1999) Immunohistochemical analysis of Na+/I- symporter distribution in human extra-thyroidal tissues. Eur J Endocrinol, 141: 382-386.